

1 **In vivo single cell transcriptomics reveals *Klebsiella pneumoniae* rewiring of lung**  
2 **macrophages to promote infection**

3 Amy Dumigan<sup>1</sup>, Oisin Cappa<sup>1</sup>, Brenda Morris<sup>1</sup>, Joana Sá Pessoa<sup>1</sup>, Ricardo Calderon-  
4 Gonzalez<sup>1</sup>, Grant Mills<sup>1</sup>, Rebecca Lancaster<sup>1</sup>, David Simpson<sup>1</sup>, Adrien Kissenpfennig<sup>1</sup>, Jose  
5 A. Bengoechea<sup>1\*</sup>

6 <sup>1</sup>Wellcome-Wolfson Institute for Experimental Medicine. School of Medicine, Dentistry and  
7 Biomedical Sciences, Queen's University Belfast, 97 Lisburn Road, Belfast

8 \* Corresponding author: [j.bengoechea@qub.ac.uk](mailto:j.bengoechea@qub.ac.uk)

9

10

11 The authors have declared that no conflict of interest exists.

12

13

14

15

16

17

18

19

20

21

22

23

24

25 ***Abstract***

26 The strategies deployed by antibiotic resistant bacteria to counteract host defences are poorly  
27 understood. Here, we elucidate a novel host-pathogen interaction that results in the control of  
28 lung macrophage polarisation by the human pathogen *Klebsiella pneumoniae*. We identify  
29 interstitial macrophages (IMs) as the main population of lung macrophages associated with  
30 *Klebsiella*. Single cell transcriptomics and trajectory analysis of cells uncover that type I IFN  
31 and IL10 signalling, and macrophage polarization are characteristic of infected IMs, whereas  
32 Toll-like receptor (TLR) and Nod-like receptor signalling are features of infected alveolar  
33 macrophages. *Klebsiella*-induced macrophage polarization is a singular M2-type we termed  
34 M(Kp). To rewire macrophages towards M(Kp), *K. pneumoniae* hijacks a hitherto unknown  
35 TLR-type I IFN-IL10-STAT6 innate axis. Absence of STAT6 limits the intracellular survival  
36 of *Klebsiella* whereas the inhibition of STAT6 facilitates the clearance of the pathogen in  
37 vivo. Glycolysis characterises M(Kp) metabolism, and inhibition of glycolysis results in  
38 clearance of intracellular *Klebsiella*. We demonstrate the capsule polysaccharide is the  
39 *Klebsiella* factor governing M(Kp). *Klebsiella* also skews human macrophage polarization  
40 towards M(Kp) in a type I IFN-IL10-STAT6-dependent manner. Altogether, our work  
41 demonstrates that *Klebsiella* induction of M(Kp) represents a hitherto unknown strategy to  
42 overcome host restriction during pneumonia.

43

44

45

46

47

48

49

50

51

52

## 53 **Introduction**

54 Antibiotic resistance is a pandemic claiming more than 750,000 deaths per year.  
55 *Klebsiella pneumoniae* exemplifies the threat of this pandemic by the increasing number of  
56 strains resistant to fluoroquinolones, third-generation cephalosporins, aminoglycosides, and  
57 even carbapenems (1). These infections are associated with high mortality rates and  
58 prolonged hospitalization (2). Not surprisingly, the World Health Organization includes *K.*  
59 *pneumoniae* in the “critical” group of pathogens for which new therapeutics are urgently  
60 needed.

61 Less obvious but critical for pathogenesis are *K. pneumoniae* adaptations to the  
62 human immune system allowing the pathogen to flourish in human tissues such as the  
63 airways. This is an aspect often overlooked because *K. pneumoniae* is not considered a  
64 pathogen able to manipulate the host cells because it does not encode type III or IV secretion  
65 systems known to deliver effectors into immune cells, or any of the toxins affecting cell  
66 biology. Of particular interest is to understand whether *K. pneumoniae* deploys any strategy  
67 to manipulate macrophage function. These cells are crucial in host defence against infection  
68 by eliminating the invading pathogen via phagocytosis and the subsequent degradation in a  
69 phagolysosomal compartment, and by producing cytokines and chemokines following  
70 recognition of the pathogen to orchestrate the activation of other immune cells.

71 Macrophages show a remarkable plasticity allowing them to adapt to different  
72 microenvironments. Signals such as tissue damage, presence of a pathogen, and the presence  
73 of cytokines and other immune cells dictate different polarization states of macrophages.  
74 Depending on the stimuli, macrophages broadly differentiate into type M1, pro-inflammatory  
75 showing potent microbicidal activity, M2 with immunomodulatory role to limit tissue  
76 damage and to control inflammation, M3 or “switch” state (3), and M4 which is mediated by  
77 CXCL4 and observed in differentiated atherosclerotic plaque-associated macrophages (4).  
78 Different subsets of M2 macrophages have been identified, from M2a to M2d; all of them  
79 have in common the high-level expression of IL10 compared to M1 macrophages (5).  
80 Interestingly, increasing the number of M2 macrophages in the lungs as result of alcohol  
81 abuse or trauma is associated with increased susceptibility to *K. pneumoniae* infections (6-8).  
82 On the contrary, there is an improvement in bacterial clearance when the M2 macrophage  
83 population is eliminated (6-8), or after skewing macrophages towards an M1 state (9). These  
84 clinical observations suggest a role for macrophage polarization in *K. pneumoniae* infection

85 biology, although this has not been investigated yet. The manipulation of macrophage  
86 polarization is emerging as an important virulence strategy of intracellular pathogens.  
87 However, and contrary to the conventional wisdom, there is no clear pattern of macrophage  
88 polarization induced by intracellular pathogens (10, 11). Furthermore, there are few cases in  
89 which this has been studied *in vivo*. Therefore, it remains an open question whether the  
90 polarization state induced by a pathogen is a host protective mechanism or represents a  
91 virulence strategy.

92 This work was designed to provide a comprehensive understanding of the *K.*  
93 *pneumoniae*-macrophage interface *in vivo*. We identify interstitial macrophages (IMs) as the  
94 main population of lung macrophages associated with *K. pneumoniae*. Single cell  
95 transcriptomics uncover the programme induced by *K. pneumoniae* in infected and bystander  
96 alveolar macrophages (AMs) and IMs. Pathway analysis reveal a network involved in  
97 macrophage polarization, and mechanistic studies demonstrate that *K. pneumoniae* exploits  
98 the immune effectors IL10 and type I IFNs to trigger a singular macrophage polarization  
99 governed by the signal transducer and activator of transcription (STAT6) following the  
100 activation of TLR signalling. Inhibition of this pathway results in clearance of *K.*  
101 *pneumoniae*, illustrating the importance of macrophage polarization in *K. pneumoniae*  
102 infection biology. Altogether, our work describes a new polarization state induced by a  
103 human pathogen to overcome host restriction during pneumonia.

104

## 105 **Results**

### 106 ***K. pneumoniae is associated with interstitial macrophages and alveolar macrophages.***

107 In the mouse lungs, and similarly to the human lungs, two main populations of  
108 macrophages have been identified: AMs, with an embryonic origin, and IMs, originating  
109 mainly from hematopoietic stem cells (12-14). A population of circulating monocytes (MNs)  
110 can be also found in the lungs (12-14). To determine to which macrophage subpopulations *K.*  
111 *pneumoniae* associates in the lungs of infected mice, C57BL/6 mice were infected  
112 intranasally with the clinical isolate *K. pneumoniae* CIP52.145 (hereafter Kp52145) (15).  
113 This strain clusters within the KpI group that includes the strains associated with human  
114 infections (16, 17). Moreover, Kp52145 encodes all the loci found in those strains associated  
115 with invasive community acquired infections (16, 17). To facilitate the detection of *K.*

116 *pneumoniae* in vivo, Kp52145 was tagged with mCherry. 24 h and 48 h post-infection, lungs  
117 were processed and stained for cytometric analysis of MNs (Ly6C<sup>+</sup>CD11b<sup>+</sup>CD11c<sup>-</sup>), IMs  
118 (Ly6C<sup>+</sup>CD11b<sup>+</sup>CD11c<sup>-</sup>SiglecF<sup>-</sup>), and AMs (Ly6C<sup>+</sup>CD11b<sup>-</sup>CD11c<sup>+</sup>Siglec F<sup>+</sup>). The gating  
119 strategy is shown in Supplementary data figure 1. The number of MNs, AMs and IMs did  
120 not change over time in PBS-treated mice (Fig 1A). The number of MNs was higher in  
121 Kp52145-infected mice at 48 h post infection than at 24 h (Fig 1A). The number of AMs was  
122 not significantly different between non-infected and infected mice (Fig 1A) which is  
123 consistent with previous findings (18). In contrast, the number of IMs was significantly  
124 higher in infected mice than in PBS control animals (Fig 1A). However, the number of IMs  
125 was not significantly different 48 and 24 h post infection (Fig 1A). Flow cytometric detection  
126 of mCherry-tagged Kp52145 showed that at 24 h post infection, 31% of IMs were associated  
127 with Kp52145 whereas 1% of MNs and 5% AMs were positive (Fig 1B). At 48 h post  
128 infection, MNs remained negative for *Klebsiella* whereas there was a significant increase in  
129 the percentage of AMs associated with Kp52145 reaching 15% (Fig 1B). The percentage of  
130 IMs associated with Kp52145 at 48 h was not significantly different to that at 24 h post  
131 infection (Fig 1B). Collectively, these results demonstrate that in vivo *K. pneumoniae* is  
132 associated with two ontogenetically distinct macrophage lineages, namely IMs and AMs.

133 ***Single cell RNA-seq reveals distinct transcriptomes in IM and AM populations during K.***  
134 ***pneumoniae infection in vivo.***

135 We sought to characterize the transcriptomes of infected IMs and AMs in comparison  
136 to those of bystander IMs and AMs from infected mice, and to those of IMs and AMs from  
137 PBS-mock infected mice. Mice were infected with mCherry-tagged Kp52145, and the IMs  
138 and AMs populations with and without associated bacteria were separated by FACS sorting  
139 (Fig 2A). The gating strategy for cell sorting is outlined in Supplementary Figure 1. Single  
140 cell mRNA sequencing (scRNA-seq) technology using the 10 x Genomics platform was  
141 utilised to determine the transcriptome of the different populations of macrophages. The  
142 resulting dataset was curated using the Immgen20 open-source reference database (19) to  
143 remove any non-macrophage cells from the data set, resulting in a total of 7,462  
144 macrophages. 512 and 1113 AM and IMs, respectively from PBS-treated mice, 3080 AMs  
145 from infected mice, 2281 with associated Kp52145 and 758 bystander AMs, and 2797 IMs  
146 from infected mice, 2273 with associated *Klebsiella* and 524 bystander cells. After  
147 normalisation of the samples, uniform manifold approximation and projection (UMAP)  
148 dimensionality reduction analysis of the combined samples revealed two clusters. One of the

149 clusters comprised the IMs, characterised by the expression of the IM marker *cx3cr1*,  
150 whereas the other comprised the AMs, characterised by the expression of the marker *siglecF*  
151 (Fig 2B). In the case of the IM cluster, it was possible to distinguish the cluster of cells from  
152 non-infected mice from those from infected mice which were further separated between  
153 bystander cells and those with associated bacteria (Fig 2C). In contrast, there was no clear  
154 separation between the different populations of macrophages in the AM cluster.

155 Differential gene expression analysis revealed that 1,083 genes were differentially  
156 expressed in IMs from infected mice versus PBS-mock infected mice. Of those, 393 genes  
157 were common between bystander and infected IMs, whereas 126 and 171 were only found in  
158 bystander cells and infected IMs, respectively. We compared the transcriptome of the  
159 different populations of IMs to identify signatures of infected and bystander cells. 890 and  
160 979 genes were differentially expressed in bystander and infected IMs versus PBS-mock  
161 infected IMs, respectively (Supplementary Table 1). Of them, 518 and 564 genes were  
162 upregulated whereas 372 and 415 were down regulated in bystander and infected IMs versus  
163 PBS-mock infected IMs, respectively (Supplementary Table 1). To acquire insights into the  
164 biological processes of significance that characterize infected IMs and bystander cells, we  
165 performed gene set enrichment analysis (gProfiler) and then constructed network enrichment  
166 maps. When considering the downregulated genes, bystander and Kp52145-infected IMs  
167 shared an enrichment of networks related to translation (Supplementary Fig 2A and B).  
168 Pathways related to TGF $\beta$  signalling and ErbB4-Notch signalling were specific of bystander  
169 and Kp52145-infected IMs, respectively (Supplementary Fig 2A and B). In the case of the  
170 upregulated genes, there was an enrichment of pathways related to immune signalling in IMs  
171 from infected mice (Fig 2D and E). It is notable the over representation of gene networks  
172 related to interferon signalling in bystander and infected IMs (Fig 2D and 2E). This finding is  
173 consistent with an enrichment of motifs for transcriptional factors of the Irf family, and  
174 STAT1 in the promoter regions of the upregulated genes of IMs from infected mice as  
175 detected interrogating the TRANSFAC database (20). Only in Kp52145-infected IMs, we  
176 found gene networks involved in response to oxidative stress, starvation, iron uptake, and  
177 macrophage polarization, (*nos2*, *arg1*, *mrc1/cd206*) (Fig 2D). Interestingly, TRANSFAC-  
178 based analysis revealed an enrichment of the motif recognized by the transcriptional factor  
179 GKLF/Klf4 only in infected IMs. This transcriptional factor regulates M2 macrophage  
180 polarization (21). In contrast, networks found only in bystander IMs included those related to  
181 TNF signalling, inflammasome activation and IL1 signalling, and C-type lectin receptors (Fig

182 2E). Altogether, these results uncover that upregulation of IFN signalling and downregulation  
183 of translation are features of IMs following *K. pneumoniae* infection. The signature of  
184 infected IMs is the activation of networks connected to cellular stress and macrophage  
185 polarization whereas networks connected to antimicrobial defence and sensing of infections  
186 are specific of bystander IMs.

187 Within the AM population, 218 genes were differentially expressed in Kp52145-  
188 associated AMs versus PBS-mock infected whereas only 63 genes were differentially  
189 expressed in bystander AMs. (Supplementary Table 1). No networks were enriched within  
190 the downregulated genes of Kp52145-infected AMs whereas supplementary Figure 3 shows  
191 the network enrichment maps corresponding to the upregulated genes. Four clusters were  
192 identified, receptor signalling cluster having the most nodes. Gene networks within this  
193 cluster are related to Toll-like receptor (TLR) and Nod-like receptor (NLR) signalling.  
194 TRANSFAC-based analysis showed that the motif recognized by the NF- $\kappa$ B transcriptional  
195 factor is enriched in the promoter region of the genes within this cluster. Connected to this  
196 cluster are the clusters of TNF signalling, and antigen presentation. Networks related to  
197 immune signalling include cytokines and chemokines, *il1b*, *tnfa*, *cxclc2*, *cxcl3*, and calcium-  
198 dependent inflammatory proteins, *s100A9*, *s100A8*. No pathways were enriched in bystander  
199 AMs. Collectively, these results demonstrate a reduced activation of AMs following infection  
200 compared to IMs. The transcriptional pattern of infected AMs is related to TLR and NLR  
201 signalling-governed inflammation in an NF- $\kappa$ B-dependent manner.

202 To establish whether it is possible to construct a trajectory from non-infected to  
203 infected cells, we utilised Monocle analysis to determine the temporal pattern of gene  
204 expression over pseudotime. Whereas no distinct trajectory was observed in AMs  
205 (Supplementary Fig 4), Monocle analysis revealed a clear trajectory in IMs from non-infected  
206 cells to bystander cells to Kp52145-infected cells (Fig 3A). Seven modules of genes showing  
207 similar pattern of expression were identified (Supplementary Table 2). Heat map analysis  
208 revealed that genes included in modules 3, 4 and 6 were upregulated in IMs from infected  
209 mice, whereas the expression of genes in modules 3 and 4 were higher in Kp52145-infected  
210 IMs than in bystander cells (Fig 3B). Genes in module 6 were upregulated in bystander cells  
211 (Fig 3B). In contrast, genes in modules 1 and 7 were upregulated in IMs from non-infected  
212 mice (Fig 3B). Enrichment map analysis of modules 1 and 7 using gProfiler revealed one  
213 cluster related to regulation of translation (Supplementary Fig 5). Pathway analysis of  
214 modules 3 and 4, characteristic of *K. pneumoniae*-infected IMs, revealed an enrichment in



215 pathways related to immune signalling, particularly type I IFN stimulated genes (ISGs)  
216 (*isg15, cxc10, ifit1, uspl8, irgm1, irg1*) and IL10 signalling (*ptgs2, csf1, ptafr*), and IL4  
217 signalling and macrophage polarization (*nos2, arg1, lcn2, socs1, socs3*) (Fig 3C). STRING  
218 analysis seeking functional interactions between the 234 genes revealed two clusters (Fig  
219 3D). One cluster includes 39 genes associated with IFN signalling, and the other one  
220 encompasses 74 genes related to cytokine signalling and macrophage polarization (Fig 3D).  
221 TRANSFAC analysis showed that the regulatory regions of genes within modules 3 and 4 are  
222 characterized by motifs for transcriptional factors of the Irf family, and for the p65 subunit of  
223 NF- $\kappa$ B. Module 6, characteristic of bystander cells, is enriched with genes related to immune  
224 signalling, and IFN signalling (Fig 3E). This module is characterized by the presence of  
225 binding motifs for Irf5 and Irf8 in the regulatory regions of the genes. Figure 3F shows the  
226 changes over pseudotime of selected top expressed genes within the modules 3, 4 and 6. Data  
227 demonstrates the increase in transcription of ISGs IFN (*isg15, cxcl10, irg1, ifi203, mmdA,*  
228 *ifi205*), IL10 signalling (*ptgs2, ptafr*), IL4 signalling and macrophage polarization (*nos2,*  
229 *arg1, lcn2, socs1, socs3*) from non-infected to bystander to infected cells. In contrast, there is  
230 a decrease in transcription from non-infected cells to bystander to infected cells of genes  
231 related to translation (*rnas6, rpsA, rps21*) and some others related to migration of immune  
232 cells and activation (*pparg, ifngr1, cytip, lsp1*). Altogether, this analysis revealed that IFN  
233 and IL10 signalling governed by Irf and NF- $\kappa$ B transcriptional factors is characteristic of *K.*  
234 *pneumoniae* infected IMs whereas Irf-controlled IFN signalling is characteristic of bystander  
235 IMs. Furthermore, our data suggested that *K. pneumoniae* infection skews macrophage  
236 polarization.

237 ***K. pneumoniae induces a singular polarization state in interstitial and alveolar***  
238 ***macrophages.***

239 The fact that one of the features of Kp52145-infected macrophages was the  
240 upregulation of genes associated with macrophage polarization led us to interrogate further  
241 the scRNA-seq data set to assess the expression of genes associated with macrophage  
242 polarization. Heat map analysis revealed an upregulation of several M1 related genes in  
243 bystander and infected IMs including *il1b, il12b, cd38, cxcl10, cxcl2, and nos2* (Fig 4A).  
244 However, the expression of M2 related genes was higher than that of M1 genes (Fig 4A). M2  
245 upregulated genes included *msr1, cxcl16, egr2, arg1, il1rn, mmp14, ccr1, ccr2, clec4b* and  
246 *parp14* (Fig 4A). Remarkably, Kp52145-induced polarization has features of several of M2  
247 subsets. *Arg1, il1rn, il10* and *fizz1* are found in M2a cells, *il10, tnfa, il6* and *il12* are typical of



248 M2b cells, *cd163*, *cd206*, *il10* and *arg1* are characteristic of M2c macrophages, whereas *il10*  
249 and *nos2* are found in M2d cells (5). A similar picture was observed in AMs (Supplementary  
250 Figure 6) although the number of upregulated genes was reduced compared to IMs.

251 Next, we carried out flow cytometry experiments interrogating infected and bystander  
252 IMs and AMs to confirm the scRNA-seq observations. iNOS was upregulated only in  
253 Kp52145-associated AMs but not on the IM population (Fig 4B). The M2 markers Arg1,  
254 Fizz1, and CD163 were upregulated in Kp52145-infected IMs and AMs but not in bystander  
255 cells (Fig 4C-E), uncovering the importance of macrophage-*Klebsiella* contact for  
256 macrophage polarization.

257 Altogether, these results suggest that *K. pneumoniae* induces a singular polarization in  
258 IMs and AMs consistent with M2 polarization state. We term this macrophage polarization as  
259 M(Kp) because it cannot be ascribed to any of the known M2 subsets. scRNA-seq data,  
260 including pathway analysis and pseudotime data, and the flow cytometry experiments showed  
261 that M(Kp) is characterized by the increased expression of Arg1, Fizz1, iNOS, CD163,  
262 *cd206*, type I IFN and IL10 signalling-regulated genes, and the decreased expression of  
263 *ppary*, and inflammatory markers.

#### 264 ***K. pneumoniae*-induced M(Kp) polarization is STAT6 dependent.**

265 We next sought to provide mechanistic insights into the signalling pathway(s)  
266 governing M(Kp) polarization. To facilitate this research, we questioned whether *K.*  
267 *pneumoniae* triggers M(Kp) polarization in immortalized bone marrow derived macrophages  
268 (iBMDMs). These cells have been widely used to investigate immune signalling and  
269 macrophage polarization. Consistent with the in vivo scRNA-seq results, infection of  
270 iBMDMs resulted in the upregulation of *arg1* and Arg1 (Supplementary Figure 7A), *fizz1* and  
271 Fizz1 ((Supplementary Figure 7B), *ppary*, *nos2*, *il12*, *il6* and *tnfa* (Supplementary Figure 7C-  
272 G). *Il10* levels were also upregulated in infected iBMDMs (Supplementary Figure 7H). The  
273 increased expression of *il10* was consistent with the increased phosphorylation of the IL10-  
274 governed transcriptional factor STAT3 in Kp52145-infected macrophages (Supplementary  
275 Figure 7I). We have previously demonstrated the upregulation of type I IFN-dependent genes  
276 in *Klebsiella*-infected iBMDMs (18). Altogether, these results demonstrate that infection of  
277 iBMDMs recapitulates the in vivo *K. pneumoniae*-induced macrophage polarization.

278 M2 macrophage polarization involves the activation of STAT6 that controls the  
279 transcription of M2-specific genes (22, 23). Therefore, we sought to determine whether

280 STAT6 governs *K. pneumoniae*-induced M(Kp) polarization. We first investigated whether  
281 Kp52145 induced the phosphorylation of STAT6 because this is a prerequisite for nuclear  
282 localization and DNA binding of STAT6 (24). Immunoblotting experiments confirmed that  
283 Kp52145 induced STAT6 phosphorylation (Fig 5A). *K. pneumoniae* strains NJST258-1,  
284 NJST258-2 and SHG10 also induced the phosphorylation of STAT6 (Fig 5B), indicating that  
285 *K. pneumoniae* activation of STAT6 is not strain dependent. NJST258-1 and NJST258-2  
286 cluster within the epidemic clonal group ST258 producing the *K. pneumoniae*  
287 carbapenemase, and SGH10 belongs to the clonal group CG23 causing liver abscesses (25,  
288 26). STAT6 cooperates with KLF4 to regulate M2 macrophage (21). Kp52145 also increased  
289 the expression of *klf4* and KLF4 in macrophages (Fig 5C). To connect mechanistically  
290 STAT6 activation and *K. pneumoniae*-induced M(Kp) polarization, we infected *stat6*<sup>-/-</sup>  
291 macrophages and assessed the expression of M(Kp) markers. Figure 5D shows that *arg1* and  
292 Arg1 levels were decreased in infected *stat6*<sup>-/-</sup> macrophages compare to infected wild-type  
293 cells. Furthermore, Kp52145 did not upregulate the expression of *il10*, *klf4*, *pparg* and *fizz1*  
294 in *stat6*<sup>-/-</sup> macrophages (Fig 5 E-H). In contrast, the expressions of *nos2*, *tnfa*, *il12*, *il6* were  
295 higher in infected *stat6*<sup>-/-</sup> macrophages than in wild-type cells (Fig 5I-K). The levels of *isg15*  
296 were not significantly between infected wild-type and *stat6*<sup>-/-</sup> macrophages (Fig 5L). Flow  
297 cytometry experiments using mCherry-tagged Kp52145 demonstrated that neither Arg1 nor  
298 CD206 were upregulated in infected *stat6*<sup>-/-</sup> macrophages in contrast to wild-type cells with  
299 associated bacteria (Fig 5M-N). In contrast, the levels of MHC-II, a well-established M1  
300 marker, were significantly upregulated in *stat6*<sup>-/-</sup> infected macrophages compare to wild-type  
301 cells (Fig 5O). Similar results were obtained when *K. pneumoniae*-induced STAT6 activation  
302 was suppressed using the STAT6 inhibitor AS1517499 (27). When infections were performed  
303 in the presence of AS1517499, Kp52145 did not upregulate the expression of *arg1*, *il10*, and  
304 *fizz1* (Supplementary Figure 8A-C). In contrast, the expression of *nos2*, and *il12* were  
305 upregulated following infection (Supplementary Figure 8D-E). AS1517499 did not affect  
306 *Klebsiella*-induced *isg15* (Supplementary Figure 8F) in line with *stat6*<sup>-/-</sup>-infected cells.

307 Collectively, these results demonstrate that STAT6 acts as a key regulator of *K.*  
308 *pneumoniae*-induced M(Kp) polarization. Furthermore, in the absence of STAT6 *K.*  
309 *pneumoniae* induces a macrophage phenotype consistent with M1 polarization.

310

### 311 ***K. pneumoniae* activation of STAT6 promotes infection.**

312 To establish the importance of *K. pneumoniae*-induced activation of STAT6 on *K.*  
313 *pneumoniae* infection biology, we first investigated whether STAT6 contributes to *K.*

314 *pneumoniae* subversion of cell-intrinsic immunity. We asked whether absence of STAT6  
315 impairs *K. pneumoniae* intracellular survival. While no differences were observed in the  
316 adhesion of Kp52145 to *stat6*<sup>-/-</sup> and wild-type macrophages (Fig 6A), the phagocytosis of  
317 Kp52145 was reduced in *stat6*<sup>-/-</sup> macrophages compared to wild-type cells (Fig 6B). Time  
318 course experiments showed that the intracellular survival of Kp52145 was diminished in  
319 *stat6*<sup>-/-</sup> macrophages (Fig 6C). Previously, we have demonstrated that *K. pneumoniae*  
320 manipulates the traffic of the phagosome following phagocytosis to create a vacuole that does  
321 not fuse with lysosomes, the KCV, allowing the intracellular survival of *Klebsiella* (28). We  
322 then sought to determine whether the reduced intracellular survival observed in *stat6*<sup>-/-</sup> cells  
323 was due to an increase colocalization of lysosomes with the KCV. Lysosomes were labelled  
324 with the membrane-permeant fluorophore cresyl violet (29), and cells were infected with  
325 GFP-labelled Kp52145 to assess the KCV at the single cell level by immunofluorescence.  
326 Confocal microscopy experiments revealed that the majority of the KCVs from wild-type  
327 macrophages did not colocalize with cresyl violet (Fig 6D and Fig 6E), corroborating our  
328 previous work (28). In contrast, there was an increase of colocalization of the KCV from  
329 *stat6*<sup>-/-</sup> macrophages with the marker cresyl violet (Fig 6D and Fig 6E), demonstrating that  
330 the absence of STAT6 results in the fusion of the KCV with lysosomes with a concomitant  
331 reduction in the numbers of intracellular bacteria.

332 To obtain a global view of the role of STAT6 in *K. pneumoniae* infection biology, we  
333 examined the effect of the STAT6 inhibitor AS1517499 on the ability of wild-type mice to  
334 control *K. pneumoniae* infection. At 24 h post infection, the bacterial loads in the lungs of  
335 mice pre-treated with AS1517499 were significantly lower than those of mice pre-treated  
336 with the vehicle solution (Fig 6F). Bacterial loads in the spleens were not significantly  
337 different between the two groups of mice (Fig 6G). The expression of M2 polarisation  
338 markers *arg1*, *il10* and *pparg* were significantly reduced in whole lungs from infected  
339 animals treated with AS1517499 compared to DMSO controls (Fig 6H and Fig 6J). These  
340 results establish the importance of STAT6 activation for *K. pneumoniae* survival *in vivo*.

341

### 342 ***K. pneumoniae*-induced M(Kp) polarization is governed by TLR2 and TLR4 signalling.**

343 We next sought to identify the signalling pathway(s) utilized by *K. pneumoniae* to  
344 activate STAT6 to induce M(Kp) polarization. Previous work of our laboratory demonstrates  
345 that *K. pneumoniae* manipulates pattern recognition receptors (PRRs) as a virulence strategy  
346 to control inflammation (30). We then asked whether *K. pneumoniae* may exploit TLR  
347 signalling to activate STAT6 to induce M(Kp). Kp52145 did not induced the phosphorylation

348 of STAT6 in *tlr2*<sup>-/-</sup>, *tlr4*<sup>-/-</sup>, and *tlr2/tlr4*<sup>-/-</sup> macrophages (Fig 7A). Consistent with the lack of  
349 activation of STAT6 in macrophages lacking TLR2 and TLR4, Kp52145 did not increase the  
350 levels of Arg1 (Fig 7B), *arg1* (Fig 7C), and *fizz1* (Fig 7D) in *tlr2*<sup>-/-</sup>, *tlr4*<sup>-/-</sup>, and *tlr2/4*<sup>-/-</sup>  
351 macrophages. The expressions of *il10*, *nos2* and the ISGs *isg15*, and *mx1* were only  
352 upregulated in *tlr2*<sup>-/-</sup> macrophages following infection (Fig 7E-H), indicating that TLR4  
353 controls the levels of these M(Kp) markers. In contrast, TLR2 controls the expression of  
354 *ppary* because Kp52145 did not upregulate *ppary* in *tlr2*<sup>-/-</sup> and *tlr2/tlr4*<sup>-/-</sup> macrophages (Fig  
355 7I). Altogether, these results demonstrate that *K. pneumoniae*-induced M(Kp) polarization is  
356 TLR2 and TLR4 dependent.

357

### 358 ***The TLR adaptors MyD88, TRAM, and TRIF govern K. pneumoniae-induced M(Kp)*** 359 ***polarization.***

360 TLR signalling involves a series of different adaptors. Myeloid-Differentiation factor-  
361 88 (MyD88) is a universal adaptor used by all TLRs except TLR3, Toll/IL-1R domain-  
362 containing adaptor-inducing IFN-β (TRIF) is used by TLR3 and TLR4, whereas TRIF-related  
363 adaptor molecule (TRAM) is recruited by endosomal located TLR and TLR4 (31). Therefore,  
364 we asked whether MyD88, TRAM, and TRIF are required to induce the M(Kp) polarization.  
365 Phosphorylation of STAT6 was not detected in infected *myd88*<sup>-/-</sup>, and *tram/trif*<sup>-/-</sup> macrophages  
366 (Fig 8A). As anticipated Arg1 (Fig 8B) and *arg1* (Fig 8C) were not upregulated in infected  
367 *myd88*<sup>-/-</sup>, and *tram/trif*<sup>-/-</sup> macrophages. Kp52145 induction of *il10* was MyD88-dependent  
368 because Kp52145 upregulated *il10* only in *tram/trif*<sup>-/-</sup> macrophages (Fig 8D). The expressions  
369 of *pparg* and *fizz1* were abrogated in the absence of Myd88 and TRAM/TRIF (Fig 8E-F). In  
370 addition, *isg15* and *mx1* were not upregulated in infected *tram/trif*<sup>-/-</sup> macrophages (Fig 8G-H),  
371 which is consistent with our recent evidence demonstrating that *K. pneumoniae* induces type I  
372 IFNs and ISGs in a TRAM-TRIF-dependent manner (18). Kp52145 did not upregulate *nos2*  
373 in *tram/trif*<sup>-/-</sup> macrophages (Fig 8I) which is in agreement with *nos2* being an ISG (32). In  
374 contrast, *nos2* levels were upregulated in infected *myd88*<sup>-/-</sup> macrophages (Fig 8I). This result  
375 is consistent with the facts that MyD88 signalling is needed for *K. pneumoniae* induction of  
376 *il10* (Fig 8D) and IL10 reduces the levels of *nos2* in *K. pneumoniae*-infected macrophages  
377 (Fig 10H). Altogether, these findings establish that *K. pneumoniae*-induced M(Kp) is  
378 MyD88, TRAM and TRIF dependent.

379

### 380 ***K. pneumoniae exploits type I IFN signalling to induce M(Kp) polarization.***

381           Given that TLR4-TRAM-TRIF pathway is essential for M(Kp) activation, that this  
382 pathway controls type I IFN signalling in *K. pneumoniae* infections (18), and that type I IFN  
383 signalling is a feature of IMs following infection, we decided to elucidate whether *K.*  
384 *pneumoniae* exploits type I IFN to induce M(Kp) polarization. To address this question, we  
385 infected type I IFN receptor-deficient (*ifnar1*<sup>-/-</sup>) macrophages and assessed M(Kp) markers.  
386 Kp52145 did not induce the phosphorylation of STAT6 in *ifnar1*<sup>-/-</sup> macrophages (Fig 9A). As  
387 expected, Arg1 and *arg1* were not upregulated in Kp52145-infected *ifnar1*<sup>-/-</sup> cells (Fig 9B).  
388 Similar result was observed for *nos2*, *pparγ* and *fizz1* (Fig 9 C-E). In contrast, Kp52145 still  
389 upregulated *il10* in *ifnar1*<sup>-/-</sup> macrophages (Fig 9F). Flow cytometry experiments showed that  
390 Kp52145 did not upregulate the expression of Arg1 (Fig 9G), and CD206 in *ifnar1*<sup>-/-</sup> cells  
391 (Fig 9H) whereas the expression of MHC-II was higher in *ifnar1*<sup>-/-</sup> macrophages than in wild-  
392 type cells following infection (Fig 9I). Type I IFN stimulation alone did not induce STAT6  
393 phosphorylation nor upregulate Arg1 in wild-type cells (Supplementary Figure 9A-B).

394           Because Irf3 controls type I IFN production in *K. pneumoniae* in vitro and in vivo  
395 (18), we postulated that Irf3 is required for *K. pneumoniae* induction of M(Kp). Indeed,  
396 Kp52145 did not phosphorylate STAT6 or induced Arg1 in *irf3*<sup>-/-</sup> macrophages (Fig 9J-K).  
397 As anticipated, *arg1* (Fig 9B), *pparγ* (Fig 9D), and *fizz1* (Fig 9E) levels were not increase in  
398 *irf3*<sup>-/-</sup> cells following infection whereas the levels of *il10* were similar that those found in  
399 infected wild-type cells (Fig 9F). The fact that *nos2* levels were upregulated in infected *irf3*<sup>-/-</sup>  
400 macrophages (Fig 9C) indicates that Irf3 does not control the transcription of this gene.

401           Collectively, these experiments demonstrate that *K. pneumoniae* leverages the  
402 immunomodulatory properties of type I IFN to induce M(Kp) polarization.

403

#### 404 ***IL10 is required for K. pneumoniae-governed M(Kp).***

405           Our findings indicate that IL10 is one of the signatures of M(Kp). Therefore, we  
406 sought to identify the signalling pathways governing *K. pneumoniae*-induction of IL10. Our  
407 previous results revealed that TLR4-MyD88 signalling controls IL10 production following  
408 Kp52145 infection (Fig 7E and Fig 8D). The fact that the transcriptional factor CREB  
409 controls IL10 production in macrophages following TLR stimulation (33) led us to ascertain  
410 whether CREB governs *K. pneumoniae*-induced IL10 production. The phosphorylation of  
411 CREB is a key event regulating its transcriptional activity (34). Immunoblotting experiments  
412 confirmed that Kp52145 triggered the phosphorylation of CREB in wild-type macrophages  
413 (Fig 10A and Fig 10B). However, CREB phosphorylation was reduced in infected *tlr4*<sup>-/-</sup> (Fig  
414 10A) and *myd88*<sup>-/-</sup> (Fig 10B) macrophages. To connect CREB activation and IL10 production



415 in *K. pneumoniae* infected cells, we used a siRNA-based approach to knockdown CREB in  
416 macrophages. The efficiency of CREB knockdown in wild-type macrophages is shown in  
417 (Supplementary Figure 10). Kp52145 induction of *il10* was abrogated in CREB knockdown  
418 macrophages (Fig 10C), demonstrating the role of CREB activation in *K. pneumoniae*  
419 induction of IL10. Collectively, these experiments uncover that a TLR4-MyD88-CREB  
420 signalling pathway mediates *K. pneumoniae* induction of IL10.

421 To determine whether *K. pneumoniae* exploits the immunomodulatory properties of  
422 IL10 to skew macrophage polarization, we infected *il10*<sup>-/-</sup> macrophages and assessed different  
423 M(Kp) markers. We did not detect the phosphorylation of STAT6 in infected *il10*<sup>-/-</sup>  
424 macrophages (Fig 10D). Consistent with the lack of activation of STAT6, the levels of *arg1*,  
425 *Arg1* were not upregulated in infected *il10*<sup>-/-</sup> macrophages (Fig 10E). The expressions of  
426 *pparγ* (Fig 10F) and *fizz1* (Fig 10G) were not upregulated in infected *il10*<sup>-/-</sup> macrophages. In  
427 contrast, the levels of *nos2*, *tnfa*, *mx1* and *isg15* were significantly increased in infected *il10*<sup>-/-</sup>  
428 macrophages compared to wild-type controls (Fig 10H and Fig 10K). Flow cytometric  
429 analysis showed that Kp52145 did not increase *Arg1* (Fig 10L) and CD206 (Fig 10M) in *il10*<sup>-/-</sup>  
430 macrophages whereas the levels of MHC-II were higher in *il10*<sup>-/-</sup> macrophages, with and  
431 without bacteria, than in the wild-type ones (Fig 10N). Recombinant IL10 neither alone nor  
432 in combination with type I IFN induced the phosphorylation of STAT6 or the upregulation of  
433 *Arg1* in wild-type macrophages (Supplementary Figure 9A-B). Altogether, these data  
434 indicate that IL10 is necessary for *K. pneumoniae*-induction of M(Kp).

435 Given the importance of IL10 in *K. pneumoniae*-macrophage interplay, we asked  
436 whether IL10 is required for *K. pneumoniae* intracellular survival. No differences were  
437 observed in the adhesion (Fig 10O) and phagocytosis (Fig 10P) of Kp52145 between wild-  
438 type and *il10*<sup>-/-</sup> macrophages. Assessment of the numbers of intracellular bacteria over time  
439 showed a 50% decrease of Kp52145 survival in *il10*<sup>-/-</sup> macrophages (Fig 10Q). Confocal  
440 microscopy experiments showed an increase in the colocalization of the KCV from *il10*<sup>-/-</sup>  
441 macrophages with cresyl violet (Fig 10R and Fig 10S), demonstrating that the lack of IL10  
442 results in the fusion of the KCV with lysosomes with a concomitant reduction in the numbers  
443 of intracellular bacteria.

444 In summary, our data demonstrates that *K. pneumoniae* exploits IL10 following the  
445 activation of a TLR4-MyD88-CREB pathway to induce M(Kp) polarization. IL10 is crucial  
446 for *K. pneumoniae*-governed control of the phagosome maturation to survive inside  
447 macrophages.

448

449 **Glycolysis characterizes the M(Kp) metabolism.**

450 Metabolic reprogramming is a key aspect in the regulation of macrophage polarisation  
451 and function (35, 36). Therefore, we sought to characterize the metabolism associated with *K.*  
452 *pneumoniae*-induced M(Kp) polarization. Depending on the stimuli received, macrophages  
453 can switch between an aerobic metabolism, based on oxidative phosphorylation, to an  
454 anaerobic one, based on glycolysis. M1 macrophages display enhanced glycolysis whereas  
455 M2 macrophages utilize fatty acid oxidation (FAO) and mitochondrial oxidative  
456 phosphorylation (OXPHOS) to obtain energy (36). We interrogated the scRNA-seq data to  
457 reveal whether *K. pneumoniae* infection is associated with changes in the expression of  
458 metabolic genes. It has been established that metabolic changes in macrophages are  
459 associated with changes in the transcription of genes governing the different metabolic  
460 pathways (35). Dot plot analysis showed an upregulation of genes related to glycolysis in  
461 Kp52145-associated and bystander IMs including *Pfkp*, *Hif1a*, *HK3*, *gapdh* and *Ldha* (Fig  
462 11A). In contrast, the expression of genes related to FAO and OXPHOS was downregulated  
463 (Fig 11A). In AMs, the glycolysis related genes *pgaml*, *HK3*, and *hif1a* were also upregulated  
464 in bystander and infected cells (Supplementary Figure 11). Taken together, these data suggest  
465 that glycolysis may characterize *K. pneumoniae*-triggered M(Kp) polarization.

466 To provide experimental evidence on the metabolism linked to M(Kp), we monitored  
467 glycolysis parameters (glycolysis and glycolytic reserve) and mitochondrial function  
468 characteristics (basal mitochondrial respiration, ATP production, maximal respiration, and  
469 spare respiratory capacity) in infected macrophages by measuring the extracellular  
470 acidification rate (ECAR) and the oxygen consumption rate (OCR) using a Seahorse XFe96  
471 analyser. Infection of wild-type macrophages with Kp52145 resulted in an increase in ECAR  
472 (Fig 11B), representing the glycolysis rate. Inhibition of the mitochondrial  $F_1F_0$ -ATPase with  
473 oligomycin resulted in a modest increase in ECAR (Fig 11B). The lack of increase in ECAR  
474 following the addition of the ionophore FCCP, that uncouples mitochondrial respiration by  
475 increasing  $H^+$  transport across the inner mitochondrial membrane, and rotenone and  
476 antimycin A, inhibitors of mitochondrial complex I and III, respectively, indicates that the  
477 maximal glycolytic capacity was already reached (Fig 11B). This result suggests that ATP  
478 production is mostly dependent on glycolysis in Kp52145-infected macrophages because  
479 carbon flux is coupled to glycolytic ATP production. The increase of OCR following  
480 Kp52145 infection reflected an increase in mitochondrial basal respiration (Fig 11C and Fig  
481 11D). Addition of oligomycin triggered a decrease of cellular OCR, however the OCR was



482 still significantly higher in Kp52145 infected cells compared to non-infected ones indicating  
483 that not all oxygen consumption is used for ATP production in *K. pneumoniae*-infected cells  
484 (Fig 11C). Subsequent addition of FCCP, which stimulates respiration, showed that the  
485 maximal respiration capacity was higher in Kp52145-infected macrophages than in non-  
486 infected ones (Fig 11C and Fig 11E). However, the spare respiratory capacity was not  
487 significantly different between Kp52145-infected macrophages and non-infected ones (Fig  
488 11F), indicating that *K. pneumoniae* infection does not deplete the cellular energy via an  
489 increased OXPHOS. No differences were found in ATP production between non-infected and  
490 Kp52145-infected cells (Fig 11G). The fact that OCR was higher in Kp52145-infected cells  
491 as compared to non-infected ones after the addition of rotenone and antimycin A indicates  
492 that the non-mitochondrial respiration is increased in *K. pneumoniae*-infected macrophages  
493 (Fig 11H). When ECAR and OCR analysis following infection were done in the presence of  
494 the STAT6 inhibitor AS1517499, we observed a reduction in both measurements  
495 (Supplementary Figure 12A-B), connecting *Klebsiella*-induced metabolism with STAT6  
496 activation. Altogether, these results are consistent with the model in which glycolysis is  
497 characteristic of *K. pneumoniae*-induced M(Kp) without impairment of mitochondrial  
498 bioenergetics.

499 To determine the effect of *K. pneumoniae*-induced metabolism on *Klebsiella*-  
500 macrophage interface, we used 2-deoxyglucose (2DG) to inhibit glycolysis, and oligomycin  
501 and etomoxir to inhibit OXPHOS. Control experiments showed that the drugs did not affect  
502 the growth of Kp52145 (Supplementary Figure 13A). The drugs did not affect the adhesion  
503 of Kp52145 to macrophages (Supplementary Figure 13B). Oligomycin and etomoxir pre-  
504 treatments had no effect on the phagocytosis of Kp52145 whereas inhibition of glycolysis  
505 using 2DG resulted in an increase of phagocytosis (Supplementary Figure 13C). Time course  
506 experiments revealed that oligomycin and etomoxir pre-treatments did not impair Kp52145  
507 intracellular survival (Fig 11I). In stark contrast, 2DG pre-treatment significantly reduced the  
508 survival of Kp52145 (Fig 11I). Moreover, 2DG pre-treatment increased the colocalization of  
509 the KCV with cresyl violet, indicating that inhibition of glycolysis results in an increased  
510 fusion of the KCV with lysosomes (Fig 11J and Fig 10K). Interestingly, oligomycin and  
511 etomoxir pre-treatments had no effect on the activation of NF- $\kappa$ B and Irf3 following infection  
512 whereas 2DG pre-treatment resulted in a significant decrease in NF- $\kappa$ B and Irf3 activation  
513 after Kp52145 infection (Supplementary Figure 13D-E). The latter result is consistent with  
514 the importance of glycolysis to mount inflammatory responses following infection (37).

515 Altogether, these experiments demonstrate that glycolysis is associated with *K.*  
516 *pneumoniae*-induced M(Kp) polarization. Moreover, our results highlight the importance of  
517 host cell glycolysis for *K. pneumoniae* survival while OXPPOS seems dispensable.

518 ***K. pneumoniae*-governed M(Kp) is dependent on the capsule polysaccharide.**

519 We next sought to identify the *K. pneumoniae* factor(s) governing M(Kp)  
520 polarization. Given that TLR4 governs M(Kp) and that the *K. pneumoniae* capsule  
521 polysaccharide (CPS) and the LPS O-polysaccharide are recognized by TLR4 (38, 39), we  
522 asked whether these polysaccharides mediate *K. pneumoniae* induction of the M(Kp)  
523 polarization. The LPS-O-polysaccharide mutant, strain 52145- $\Delta$ *glf* (30), induced the  
524 phosphorylation of STAT6 (Fig 2A). The mutant also upregulated the levels of the M(Kp)  
525 marker CD206 to the same levels as Kp52145-infected macrophages (Fig 12B). In contrast,  
526 the *cps* mutant, strain 52145-  $\Delta$ *wcaK2* (40), did not trigger the phosphorylation of STAT6 (Fig  
527 12C), and did not induce *arg1* (Fig 12D). Single cell experiments using flow cytometry  
528 demonstrated that the levels of Arg1, and CD206 were significantly lower in macrophages  
529 infected with the *cps* mutant than in those infected with the wild-type strain (Fig 12E and  
530 Fig12F). The opposite was found for the M1 marker MHC-II (Fig 12G). Taken together, this  
531 evidence supports the notion that *K. pneumoniae* CPS controls M(Kp) polarization.

532 ***K. pneumoniae* induces M(Kp) polarization in human macrophages.**

533 We next focused to extend the work performed in mice to humans to determine  
534 whether *K. pneumoniae* also triggers M(Kp) polarization in human macrophages. To address  
535 this question, we infected macrophages generated from human PBMCs from six different  
536 healthy donors. Violin plots show that Kp52145 infection increased the levels of the M(Kp)  
537 markers *arg1*, *ill10*, *chi311*, *ppary*, *mrc1*, *nos2* and *isg56* (Fig 13A-G). Kp52145 also  
538 upregulated the levels of *illrn* and *ido*, indoleamine 2,3-dioxygenase (Fig 13H-I). *illrn* and  
539 *ido* are two of the markers often associated with M2 polarization in human macrophages (41).  
540 These results suggest that *K. pneumoniae* also skews macrophage polarization in human  
541 macrophages towards M(Kp).

542 To ascertain whether *K. pneumoniae* exploits the same molecular mechanisms in  
543 human macrophages than in mouse macrophages to induce M(Kp) polarization, we switched  
544 to PMA-differentiated THP-1 human macrophages. This cell line derived from a patient with  
545 acute monocytic leukaemia and it is used commonly to model the activation of human  
546 macrophages. Immunoblotting experiments confirmed that Kp52145 induced the

547 phosphorylation of STAT6 (Fig 13J). RT-qPCR experiments showed that Kp52145 infection  
548 increased the levels of the M(Kp) markers *arg1*, *ill10*, *nos2*, the ISG *isg56*, and *ido* in THP-1  
549 cells in a STAT6-dependent manner because the STAT6 inhibitor AS1517499 abrogated  
550 *Klebsiella*-mediated upregulation of these M(Kp) markers (Fig 13K-O). Collectively, these  
551 results demonstrate that *K. pneumoniae* triggers M(Kp) polarization in THP-1 cells in a  
552 STAT6-dependent manner.

553 To determine whether *K. pneumoniae*-induced type I IFN and IL10 would also govern  
554 the induction of M(Kp) polarization in human macrophages, cells were infected in the  
555 presence of blocking antibodies against human IFNAR1 receptor, and IL10. Figure 13P-Q  
556 shows that Kp52145 did not upregulate the expression of *arg1* and *ido* when infections were  
557 done in the presence of IFNAR1 blocking antibody (Fig 13P and Fig 13Q). Similar results  
558 were obtained following IL10 suppression (Fig 13R and Fig 13S). Together, these results  
559 demonstrate that type I IFN and IL10 signalling are crucial for *K. pneumoniae* induction of  
560 M(Kp) polarization in human macrophages.

561 To establish whether *K. pneumoniae* CPS also controls M(Kp) polarization in human  
562 macrophages, PMA-differentiated THP-1 cells were infected with the *cps* mutant, strain  
563 Kp52145  $\Delta wca_{K2}$ . Immunoblotting experiments showed that the *cps* mutant did not induce  
564 the phosphorylation of STAT6 in THP-1 cells (Fig 13T). As anticipated, single cell analysis  
565 by flow cytometry revealed that infection with the *cps* mutant did not increase the levels of  
566 Arg1 (Fig 13U) and CD206 (Fig 13V). Taken together, these results demonstrate that *K.*  
567 *pneumoniae* CPS also governs M(Kp) polarization in human macrophages.

568

## 569 **Discussion**

570 *K. pneumoniae* is one of the pathogens sweeping the World in the antibiotic resistant  
571 pandemic. Although, there is a wealth of knowledge on how *K. pneumoniae* develops  
572 resistance to different antibiotics, we still lack a complete understanding of what makes *K.*  
573 *pneumoniae* a successful pathogen. Of particular interest is to uncover whether *K.*  
574 *pneumoniae* has evolved strategies to overcome macrophages. These cells are an integral  
575 component of the tissue immune surveillance, response to infection and the resolution of  
576 inflammation. Therefore, pathogens such as *Klebsiella* cannot avoid innate immune responses  
577 if they are not able to overcome macrophages. Macrophages are a diverse population of

578 immune cells of different ontogenic origins that undergo differentiation according to  
579 molecular cues provided by the microenvironment. In this work, we demonstrate that *K.*  
580 *pneumoniae* induces a singular polarization state, termed M(Kp), in ontogenically distinct  
581 populations of macrophages, AMs and IMs. Our findings demonstrate the central role of  
582 STAT6 in *K. pneumoniae*-governed M(Kp). Mechanistic studies revealed that *K. pneumoniae*  
583 hijacks the immune effectors type I IFN and IL10 following the activation of TLR-controlled  
584 pathways to activate STAT6-controlled M(Kp). These results illustrate how the co-evolution  
585 of *K. pneumoniae* with the immune system has resulted in the pathogen exploiting immune  
586 effectors and receptors sensing infections to thwart innate immune defences. We establish  
587 that STAT6 is necessary for *K. pneumoniae* intracellular survival whereas inhibition of  
588 STAT6 in vivo facilitates the clearance of the pathogen, revealing that STAT6-governed  
589 macrophage polarization plays an integral role in *K. pneumoniae* infection biology.

590 Despite four decades of extensive investigation, our knowledge of the interface  
591 between macrophages and bacterial pathogens still relies on interrogating cellular models in  
592 vitro. Therefore, we have a poor understanding of the *in vivo* molecular dynamics of the  
593 interface between pathogens and the populations of tissue resident macrophages. Our results  
594 establish that lung IMs are the main target of *K. pneumoniae*. This population of  
595 macrophages is derived from postnatal blood monocytes (42, 43), and they exhibit a distinct  
596 gene expression pattern than that of AMs in the murine lung at steady state (42, 43). IMs  
597 show marked upregulation of gene sets related to reactive oxygen species (ROS)  
598 biosynthesis, high levels of nitric oxide, iron sequestration, and inflammatory responses (42,  
599 43). Therefore, IMs are considered to show increased microbicidal activity. Consistent with  
600 this role, infection triggers the recruitment of IMs (this work and (44, 45)) and, for example,  
601 they control *Mycobacterium tuberculosis* in vivo (46). This is in agreement with our results  
602 showing an enrichment of pathways related to sensing infections and antimicrobial defence in  
603 bystander IMs from *K. pneumoniae*-infected mice. It was not surprising that *K. pneumoniae*-  
604 infected IMs also showed some of these features including the enrichment of pathways  
605 related to cellular stress. *K. pneumoniae* also targeted AMs, although compared to IMs the  
606 number of genes differentially expressed was lower. Pathway analysis revealed an  
607 enrichment in gene networks related to TLR and NLR signalling, and inflammation in  
608 infected AMs. The fact that similar networks were found in AMs infected with *M.*  
609 *tuberculosis* (47) suggests that this transcription programme is part of a common AM  
610 response to bacterial pathogens. However, a distinct feature of the interaction between *K.*

611 *pneumoniae* and IMs and AMs was the upregulation of networks related to an M2-like anti-  
612 inflammatory polarization state. The markers characteristic of *K. pneumoniae*-controlled  
613 macrophage polarization were Arg1, Fizz1, iNOS, CD163, *cd206*, type I IFN and IL10  
614 signalling-regulated genes, and the decreased expression of *ppary*, and inflammatory  
615 markers. The fact that this macrophage polarization resembled an M2-like state but cannot be  
616 ascribed to any of the M2 subtypes (5) led us to name it as M(Kp) following international  
617 guidelines on macrophage polarization (5). To the best of our knowledge, *K. pneumoniae* is  
618 the first pathogen skewing the polarization of lung macrophages. Our results are consistent  
619 with a scenario in which rewiring macrophage polarization is a *K. pneumoniae* virulence  
620 strategy to survive in the lungs.

621 Interestingly, *K. pneumoniae*-induced macrophage polarization is species independent  
622 because similar findings were obtained in mouse, human and porcine macrophages (this work  
623 and (48)). The fact that there are significant differences between macrophages from different  
624 species (49) suggests that *K. pneumoniae* cellular targets should be conserved throughout  
625 evolution. Indeed, our results demonstrate that *K. pneumoniae* targets STAT6 across species  
626 to induce M(Kp) polarization (this work and (48)). This transcriptional factor arose early  
627 during the evolution of vertebrates (50) and belongs to the STAT family which is conserved  
628 through evolution from the first single cell organisms (50). Remarkably, and despite the role  
629 of STAT6 governing macrophage polarization, this transcriptional factor is not a common  
630 target of pathogens to control macrophage biology, being *Klebsiella* the first bacterial  
631 pathogen doing so.

632 It was intriguing to determine how *K. pneumoniae* manipulates the polarization of  
633 macrophages because it does not encode any type III or IV secretion systems known to  
634 deliver effectors into immune cells, or any of the toxins affecting cell biology. Our work  
635 demonstrates that *K. pneumoniae*-controlled STAT6 activation was dependent on type I IFN  
636 and IL10 following the activation of TLR4-governed signalling pathway. Type I IFNs, IL10,  
637 and TLR4 also appeared early during the evolution of vertebrates (51, 52). Therefore, *K.*  
638 *pneumoniae* has evolved to manipulate an innate axis conserved during evolution formed by  
639 TLR4-type I IFN-IL10-STAT6 to rewire macrophages. This is a previously unknown axis  
640 exploited by a human pathogen to manipulate immunity. This underappreciated anti-immune  
641 strategy is radically different from that employed by other pathogens, such as *Listeria*,  
642 *Salmonella*, *Shigella*, or *Mycobacterium*, who deliver bacterial proteins into host cells to  
643 manipulate the host. However, we believe that indeed it is an emerging theme in the infection

644 biology of bacterial pathogens. Providing further support to this notion, TLR-controlled  
645 signalling is exploited by *S. Typhimurium* to survive in macrophages (53), and *L.*  
646 *monocytogenes* leverages type I IFN for intracellular survival (54, 55).

647 Our work sheds new light into the role of IL10 on *K. pneumoniae* infection biology.  
648 The importance of IL10 *in vivo* is marked by the fact that neutralization of the cytokine  
649 enhances the clearance of the *K. pneumoniae* (56). However, it remained an open question  
650 the exact role of IL10 in *K. pneumoniae*-host interaction beyond the well-known role of IL10  
651 to downregulate inflammation. In this work, we establish that IL10 is essential to skew  
652 macrophage polarization and, in fact, IL10 is one of the signatures of M(Kp). In addition, our  
653 results demonstrate that IL10 is essential for the intracellular survival of *Klebsiella*. How *K.*  
654 *pneumoniae* induces IL10 was unknown. Our results demonstrate that *K. pneumoniae*-  
655 induced IL10 is controlled by TLR4-MyD88-CREB signalling pathway. This is a well-  
656 established pathway governing the expression of IL10 (33). The facts that CREB affects the  
657 activation of host defence responses independently of IL10, and that CREB regulates T cells  
658 (57) suggest that *K. pneumoniae* may leverage the immunomodulatory roles of CREB beyond  
659 IL10 production. Current efforts of the laboratory are devoted to investigate the role of CREB  
660 during *K. pneumoniae* infection.

661 Another novel finding of our work is the importance of glycolysis in *Klebsiella*-  
662 macrophage interface. Although reports indicate that OXPHOS is the metabolic signature of  
663 M2 macrophages (36), our results demonstrate that glycolysis characterises M(Kp). This  
664 finding is not totally unprecedented and, for example, the M2 tumour-associated  
665 macrophages are metabolically distinct from conventional M2 polarized subset in prioritizing  
666 usage of glycolysis as a key metabolic pathway (58). Notably, glycolysis is required for  
667 optimal survival of *K. pneumoniae* in macrophages. At present we can only speculate why  
668 glycolysis benefits *K. pneumoniae* survival. It is possible that glycolysis yields metabolites  
669 that *Klebsiella* needs as nutrients when residing in the KCV. These metabolites may also  
670 result in the regulation of the virulence factors governing the intracellular lifestyle of  
671 *Klebsiella*. Supporting this possibility, inhibition of glycolysis resulted in an increased  
672 colocalization of the KCV with lysosomes. Future studies are warranted to ascertain the  
673 effect of glycolysis and glycolysis-derived metabolites on *K. pneumoniae* virulence.  
674 Intriguingly, recent evidence suggest that this could be a general phenotype as Rosenberg and  
675 colleagues have shown that the glycolysis metabolite succinate activates *Salmonella*  
676 virulence during intracellular infection (59).



677 We were keen to identify the *K. pneumoniae* factor(s) governing the STAT6-mediated  
678 M(Kp) polarization. We first focused on the CPS and the LPS- O-polysaccharide because  
679 both polysaccharides are sensed by TLR4 that governs *Klebsiella*-induced activation of  
680 STAT6. Our results establish that only the CPS induced the activation of STAT6-controlled  
681 M(Kp). Importantly, the CPS is essential for *K. pneumoniae* survival in mice (pneumonia  
682 model) (60), underlining the importance of M(Kp) induction as a *K. pneumoniae* virulence  
683 trait since this process is abrogated in this mutant strain. Previous studies from the laboratory  
684 and others demonstrate the role of the CPS limiting the engulfment by phagocytes (61-64),  
685 illustrating the contribution of the CPS to *K. pneumoniae* stealth behaviour (65). However,  
686 the results of this work and our study demonstrating that the CPS activates an EGF receptor  
687 pathway to blunt inflammatory responses in epithelial cells (66) support that *K. pneumoniae*  
688 CPS is also one of the virulence factors of *K. pneumoniae* devoted to manipulate cell  
689 signalling.

690 *K. pneumoniae* exemplifies the global threat posed by antibiotic resistant bacteria. *K.*  
691 *pneumoniae*-triggered pulmonary infection has a high mortality rate reaching 50% even with  
692 antimicrobial therapy and may approach 100% for patients with alcoholism and diabetes. Not  
693 surprisingly, the World Health Organization includes *K. pneumoniae* among those pathogens  
694 for which new therapeutics are urgently needed. Absence of STAT6 resulted in macrophages  
695 consistent with M1 polarization with increased ability to clear intracellular *Klebsiella*. In vivo  
696 experiments probing a pre-clinical pneumonia mouse model demonstrated increased  
697 clearance of *K. pneumoniae* following the inhibition of STAT6. Altogether, these results  
698 strongly support that STAT6 is a target to boost human defence mechanisms against *K.*  
699 *pneumoniae*. Host-directed therapeutics aiming to interfere with host factors required by  
700 pathogens to counter the immune system are emerging as untapped opportunities that are  
701 urgently needed in the face of the global pandemic of antibiotic resistant infections. There is  
702 research to develop STAT6 inhibitors due to the implication of STAT6 signalling in  
703 colorectal cancer, melanoma, and allergic lung diseases. Based on our novel results, we  
704 propose that these drugs shall show a beneficial effect to treat *K. pneumoniae* infections alone  
705 or as a synergistic add-on to antibiotic treatment. Future studies shall confirm whether this is  
706 the case.

707

708 ***Materials and methods***



709 *Study approval*

710 All animal procedures were performed in compliance with the UK Home Office and  
711 approved by the Queen's University Belfast Animal Welfare and Ethical Review Body  
712 (AWERB). The work described in this work was carried out under project licences PPL2778  
713 and PPL2910.

714 Ethical approval for the use of blood from healthy volunteers was approved by the Research  
715 Ethics Committee of the Faculty of Medicine, Health and Life Sciences of Queen's  
716 University Belfast (approval reference MHLS 20\_136). Whole blood was obtained from the  
717 Northern Ireland Blood Transfusion Service.

718 *Animals and infection model*

719 C57BL/6 mice were purchased from Charles River Laboratories. *Ifnar1*<sup>-/-</sup> and *stat6*<sup>-/-</sup> animals  
720 were used to generate iBMDM cell lines in this study. *Ifnar1*<sup>-/-</sup> mice are maintained in  
721 Queen's University Belfast animal facility whereas *stat6*<sup>-/-</sup> animals were purchased from The  
722 Jackson Laboratory (Stock reference 005977). Mice were housed under standard laboratory  
723 conditions (12/12 h light/dark cycle with a room temperature of 21 °C and water and food  
724 available *ad libitum*). Mice used for experiments were aged between 8-12 weeks old and sex  
725 matched. For in vivo infections, bacteria in the stationary phase, were sub-cultured and grown  
726 at 37°C with agitation to reach mid log phase. Subsequently, bacteria were harvested by  
727 centrifugation (20 min, 2500 x g, 24°C), resuspended in PBS and adjusted to 5 x 10<sup>4</sup>–1 x 10<sup>5</sup>  
728 colony forming units (CFU) per 30 µl as determined by plating serial dilutions on LB plates.  
729 Mice were anesthetized with isoflurane, and infected intranasally with *K. pneumoniae* in 30  
730 µl PBS or mock-infected with PBS. In the experiments probing the STAT6 inhibitor  
731 AS1517499, mice were treated 24 h prior to infection intraperitoneally with 10mg/kg  
732 AS1517499 (AXON) or DMSO vehicle control in 200 µl volume. 6 h post-infection, mice  
733 received intranasally an additional dose of AS1517499 or DMSO (5 mg/kg in 30 µl volume).  
734 After 24 h post infection, mice were euthanized and lungs, and spleen isolated for assessment  
735 of bacterial load (CFU), or lungs processed for flow cytometry or RNA. CFUs were  
736 determined by homogenising organs in 1 mL sterile PBS and plating serial dilutions on  
737 *Salmonella-Shigella* agar plates (SIGMA). Plates were incubated overnight at 37°C before  
738 counting of colonies.

739 *Generation of stat6*<sup>-/-</sup> and *ifnar1*<sup>-/-</sup> iBMDMs.

740 Tibias and femurs were obtained from *ifnar1<sup>-/-</sup>* and *stat6<sup>-/-</sup>* mice (C57BL/6 background) and  
741 the bone marrow extracted under sterile conditions flushing bones with complete medium  
742 (DMEM, GlutaMAX, supplemented with 10% heat-inactivated foetal calf serum (FCS) and  
743 1% penicillin-streptomycin). Red blood cells were lysed via incubation with ammonium-  
744 chloride-potassium (ACK) lysis buffer (A1049201; Gibco) for 5 min at room temperature.  
745 Cells were then washed in 10 ml of complete medium and passed through a 70-mm cell  
746 strainer (2236348; Fisherbrand) prior to centrifugation. Cell pellet was dislodged before  
747 plating on 20-cm petri dishes (Sarstedt) in complete medium supplemented with 20%  
748 syringe-filtered L929 supernatant, as source of macrophage colony-stimulating factor, and  
749 maintained at 37°C in a humidified atmosphere of 5% CO<sub>2</sub>. Medium was replaced with fresh  
750 medium supplemented with L929 after 1 day of culture. After 5 days, BMDMs were  
751 immortalized by exposing them to the J2 CRE virus (carrying v-myc and v-Raf/v-Mil  
752 oncogenes, kindly donated by Avinash R. Shenoy, Imperial College London) for 24 h. This  
753 step was repeated 2 days later (day 7), followed by continuous culture in DMEM  
754 supplemented with 20% (vol/vol) filtered L929 cell supernatant for 4 to 6 weeks. The  
755 presence of a homogeneous population of macrophages was assessed by flow cytometry  
756 using antibodies for CD11b (clone M1/70; catalogue number 17-0112-82; eBioscience) and  
757 CD11c (clone N418; catalogue number 48-0114-82; eBioscience).

#### 758 *Culture of iBMDMs*

759 *Wild-type, Tlr2<sup>-/-</sup>, Tlr4<sup>-/-</sup>, Tlr2/4<sup>-/-</sup>, Myd88<sup>-/-</sup>, Tram/Trif<sup>-/-</sup>* immortalised bone marrow-derived  
760 macrophages (iBMDMs) were obtained from BEI Resources (NIAID, NIH) (repository  
761 numbers NR-9456, NR-9457, NR-9458, NR-19975, NR-15633 and NR-9568, respectively).  
762 *Ill10<sup>-/-</sup>* iBMDMs were described previously (67). iBMDMs were maintained in DMEM (Gibco  
763 41965) supplemented with 10% heat-inactivated FCS, 100 U/mL penicillin, and 0.1 mg/mL  
764 streptomycin (Sigma-Aldrich) at 37 °C in a humidified 5% CO<sub>2</sub> incubator. Cells were  
765 routinely tested for *Mycoplasma* contamination.

#### 766 *Human PBMCs*

767 PBMCs were isolated using density gradient media Ficoll-Paque PLUS (Cytiva) after  
768 centrifugation at 790 x g for 30 minutes. Resulting buffy coats were extracted and treated  
769 with ACK Lysis buffer (Gibco) to remove red blood cells, prior to freezing cells at a density  
770 of 1 x 10<sup>6</sup> per cryovial and stored at -80°C. Cells were broken out via rapid thawing in 37°C  
771 water bath before removal of DMSO via suspension in complete medium and centrifugation.  
772 Cells were then plated at a density of 3x10<sup>5</sup>/well in 12-well tissue culture plates (Sarstedt) in

773 DMEM (Gibco 41965) supplemented with 10% FCS, 100 U/ml penicillin, and 0.1 mg/mL  
774 streptomycin (Sigma–Aldrich ) supplemented with 10 ng/ml human M-CSF (Cat: 75057,  
775 Stemcell) at 37 °C in a humidified 5% CO<sub>2</sub> incubator for 5 days to allow differentiation of  
776 macrophages.

#### 777 *Culture and differentiation of THP-1 cells*

778 Human THP-1 monocytes (ATCC TIB-202) were maintained in complete medium (RPMI,  
779 supplemented with 10% FCS and 5% penicillin/streptomycin) before seeding for  
780 differentiation in the presence of PMA (5 ng/mL) for 48 h prior to infection at a density of 3  
781 x 10<sup>5</sup> cells/well in 24- well plates (Sarstedt).

#### 782 *Bacterial strains and culture conditions.*

783 Kp52145 is a clinical isolate (serotype O1:K2) previously described (15, 17). 52145- $\Delta wca_{K2}$   
784 is an isogenic mutant of Kp52145 lacking the capsule polysaccharide which has been  
785 previously described (40). 52145- $\Delta glf$  lacks the LPS O-polysaccharide and expresses similar  
786 levels of CPS than Kp52145 (30). mCherry expressing strains were generated by  
787 electroporation of pUC18T-mini-Tn7T-Apr-mCherry plasmid (68) to Kp52145, 52145-  
788  $\Delta wca_{K2}$  and 52145- $\Delta glf$ . mCherry expression was confirmed by confocal microscopy and  
789 flow cytometry. pFPV25.1Cm plasmid (61) was conjugated to Kp52145 to generate bacteria  
790 expressing GFP constitutively. Strains were grown in LB medium at 37°C on an orbital  
791 shaker (180 rpm). When appropriate, the following antibiotics were added to the growth  
792 medium at the indicated concentrations: carbenicillin, 50 µg/ml; chloramphenicol, 25 µg/ml.

#### 793 *Growth curve analysis.*

794 For growth kinetics analysis, 5 µl of overnight cultures were diluted in 250 µl of LB  
795 containing DMSO vehicle control or metabolic inhibitors, and incubated at 37°C with  
796 continuous, normal shaking in a Bioscreen Automated Microbial Growth Analyzer (MTX  
797 Lab Systems, Vienna, VA, USA). Optical density (OD; 600 nm) was measured and recorded  
798 every 20 min.

#### 799 *Macrophage infections*

800 iBMDMs were seeded into 24-well plates (1.6 x 10<sup>5</sup> cells/well) for microscopy, 12-well  
801 dishes (5 x 10<sup>5</sup> cells/well) for immunoblotting, and for assessing intracellular survival, and 6-  
802 wells (1 x 10<sup>6</sup> cells/well) for RNA and flow cytometry in complete media and allowed to  
803 adhere overnight. THP-1 cells were differentiated with PMA in 12-well dishes (3 x 10<sup>5</sup>  
804 cells/well). On the day of infection, cells were washed with 1ml PBS, and 1 ml of antibiotic

805 free media was added to the wells. To prepare the inoculum for infections, bacteria were  
806 grown until mid-exponential phase in 5 ml LB medium, supplemented with the appropriate  
807 antibiotics when required, at 37°C on an orbital shaker (180 rpm). Bacteria were recovered  
808 by centrifugation ( $3,220 \times g$ , 20 min, 22°C), washed once with PBS, and diluted in PBS to an  
809 OD<sub>600</sub> of 1.0, which corresponds to approximately  $5 \times 10^8$  CFU/ml. A multiplicity of  
810 infection of 70 bacteria per cell was used in 1 ml of appropriate medium without antibiotics.  
811 To synchronise infection, plates were centrifuged at  $200 \times g$  for 5 min. After 1 h post  
812 infection, media was removed, cells washed with 1ml 1 PBS, and 1 ml of antibiotic free  
813 media supplemented with 100 µg/mL gentamicin (Sigma-Aldrich) were added to the wells.  
814 At the indicated time points, supernatants were removed, and cells processed for  
815 immunoblotting, RNA extraction, or flow cytometry.

816 *Blocking antibodies, cytokines stimulations, and treatment with inhibitors.*

817 For cytokine stimulation experiments, cells were treated with recombinant mouse IFNβ  
818 (1000 U/ml, Stratech) or IL-10 (250 ng/ml, catalogue 210-10 Peprotech) 3 h prior to  
819 collection for immunoblotting.

820 To inhibit STAT6, cells incubated with the chemical STAT6 inhibitor AS 1517499 (50  
821 µg/ml, 919486-40-1, AXON) or DMSO as vehicle control for 2 h prior to infection and  
822 maintained throughout.

823 To inhibit cellular metabolism, macrophages were treated with DMSO vehicle control, or  
824 Cells were treated with DMSO vehicle, or 2-deoxyglucose (2DG, 3 µM), oligomycin (3 µM),  
825 etomoxir (50 µM) 2 h before infection and maintained thought. All of them were purchased  
826 from Sigma-Aldrich.

827 For IL-10 neutralisation experiments, PMA differentiated THP-1 cells were incubated 2 h  
828 prior to infection and maintained throughout with either, 1 µg/mL mouse monoclonal anti-  
829 human IL-10 antibody (R&D Systems. Ref: AF-217-NA), or equivalent concentrations of  
830 human IgG (Invitrogen) as control. To target IFNAR1/2, PMA differentiated THP-1 cells  
831 were treated with 10 µg/mL mouse monoclonal anti-human IFNAR2 (ThermoFisher  
832 Scientific, MMHAR-2), or human IgG (Invitrogen) as control. After 1 h of contact with  
833 bacteria, cells were washed once with PBS and complete medium without antibiotics  
834 supplemented with 100 µg/ml gentamicin (Sigma–Aldrich) and with the relevant antibodies.

835 *RNA extraction, and RT-qPCR*

836 Lung tissue was homogenised using a VDI 12 tissue homogeniser (VWR) in 1 ml of TRizol  
837 reagent (Ambion) and incubated at room temperature for 5 min before storage at -80°C. Total

838 RNA was extracted according to manufacturer's instructions. 5 µg of total RNA were treated  
839 with recombinant DNase I (Roche Diagnostics Ltd) at 37°C for 30 min and then purified  
840 using a standard phenol–chloroform method. The RNA was precipitated with 20 µl 3 M  
841 sodium acetate (pH 5.2) and 600 µl 98% (v/v) ethanol at -20°C, washed twice in 75% (v/v)  
842 ethanol, dried and then resuspended in RNase-free H<sub>2</sub>O.

843 To purify RNA from cells, they were washed once with 1 ml PBS before lysis in TRIzol  
844 reagent (Ambion) according to the manufacturer's instructions.

845 Duplicate cDNA preparations from each sample were generated from 1 µg of RNA using  
846 Moloney murine leukaemia virus (M-MLV) reverse transcriptase (Sigma–Aldrich) according  
847 to the manufacturer's instructions. qPCR analysis of gene expression was undertaken using  
848 the KAPA SYBR FAST qPCR kit and the Rotor-Gene Q5Plex qPCR system (Qiagen).  
849 Thermal cycling conditions were as follows: 95°C for 3 min for enzyme activation, 40 cycles  
850 of denaturation at 95°C for 10 s and annealing at 60°C for 20 s. Primers used in qPCRs are  
851 listed in Supplementary Table 3. cDNA samples were tested in duplicates, and relative  
852 mRNA quantity was determined by the comparative threshold cycle ( $\Delta\Delta CT$ ) method, using  
853 hypoxanthine phosphoribosyl transferase 1 gene normalization for mouse and human  
854 samples.

#### 855 *Flow cytometry*

856 Lung tissue was homogenised using a VDI 12 tissue homogeniser (VWR) in 1 m sterile PBS  
857 and filtered through a 70 µm cell strainer (2236348 Fisherbrand) to generate single cell  
858 suspension. Suspensions were centrifuged and red cells lysed using ACK lysis buffer  
859 (A1049201, Gibco), and washed once with 1 ml PBS. Cell lines were washed once with 1 ml  
860 ice cold PBS 5 h post infection and dislodged by scraping in a further 1 m PBS. Murine  
861 samples were treated with Fc block (clone 93, Ref: 101302, BioLegend) at 4°C for 15 min at  
862 4°C.  $\sim 5 \times 10^5$  cells per tube were washed prior to incubation with combinations of the  
863 following rat anti-mouse antibodies: against cell surface markers Ly6C APC/Cy7 (clone  
864 HK1.4, Ref: 128026), CD11b APC (Ref: 101212), CD11c Pacific Blue (Ref: 117322),  
865 SiglecF FITC (Ref: 155504, BioLegend) or SiglecF APCCy7 (Ref: 565527, Thermofisher),  
866 CD163 purified antibody (Ref: 155302) conjugated with FITC conjugation kit (Ref:  
867 ab102884, Abcam), CD206 FITC (Ref: 141704). Cells were incubated with antibodies for 15  
868 min at 4°C prior to wash with 1 ml per tube FACS buffer (PBS with 2% FCS) prior to  
869 analysis by flow cytometry.

870 For experiments including the intracellular targets this protocol was extended to include 10  
871 min incubation at room temperature in 100 µl of fixative (eBiosciences FOXP3/Transcription  
872 factor staining buffer set, ref: 00-5523-00) followed by wash in 1 ml permeabilization buffer  
873 (eBiosciences FOXP3/Transcription factor staining buffer set, ref: 00-5523-00) before  
874 incubation overnight with Arg1 FITC (Ref: 53-3697-82, Thermofisher), and iNOS PE (Ref:  
875 12-3920-82, Thermofisher) antibodies in 100 µl permeabilization buffer at 4°C. Cells were  
876 then washed once more in 1ml permeabilization buffer before flow cytometric analysis using  
877 the Canto II (BD).

878 THP-1 human macrophages were treated with mouse anti-human Fc block (Ref: 422302,  
879 BioLegend), for 15 min at 4°C prior to wash in 1 ml PBS and centrifugation at 1600 rpm for  
880 5 min and surface molecule staining with CD206 APCCy7 (BioLegend), and intracellular  
881 staining of anti-human Arginase1 FITC (Ref: 53-3697-82, Thermofisher). Cell surface  
882 markers were stained directly while intracellular staining required additional processing using  
883 a cell fixation and permeabilization kit as described above (eBiosciences  
884 FOXP3/Transcription factor staining buffer set, ref: 00-5523-00). Cell suspensions were  
885 analysed using CANTO-II analyser (BD). FlowJo V10 (Tree Star) software was used for data  
886 analysis and graphical representation.

#### 887 *Cell Sorting and single-cell RNA - seq*

888 C57BL/6 age and sex matched animals (15 per group) were infected intranasally under  
889 isoflurane anaesthesia with mCherry expressing Kp52145 or PBS. After 24 h, lungs were  
890 homogenized, pooled and red cells lysed using ACK buffer (Gibco) for 5 min at room  
891 temperature. Cells were then washed in 10 ml PBS before centrifugation at 1600 x rpm for 5  
892 min. Supernatants were aspirated and cells were then treated with Fc block (clone 93, Ref:  
893 101302, BioLegend, 1:1000) at 4°C for 15 min. Cells were washed again prior to incubation  
894 with combinations of the following rat anti-mouse antibodies: against cell surface markers  
895 Ly6C APC/Cy7 (clone HK1.4, Ref: 128026), CD11b APC (Ref: 101212), CD11c Pacific  
896 Blue (Ref: 117322), SiglecF FITC (Ref: 155504, BioLegend). Using the FACS Aria II (BD  
897 Biosciences) Ly6C+CD11b+CD11c+SiglecF- IMs and Ly6C+CD11b-CD11c+Siglec F+  
898 AMs were sorted from PBS control mice. From infected animals, four separate populations  
899 were retrieved namely IMs infected with Kp52145 (Ly6C+CD11b+CD11c+SiglecF-  
900 mCherry+), bystander IMs (Ly6C+CD11b+CD11c+SiglecF-mCherry-), Kp52145-infected  
901 AMs (Ly6C+CD11b-CD11c+Siglec F+mCherry+) and bystander AMs (Ly6C+CD11b-  
902 CD11c+Siglec F+-mCherry-) populations. Cells were collected into sterile 1 x PBS and



903 viability of all six populations was confirmed by trypan blue staining (Sigma-Aldrich) and  
904 found to be at or above 95% viable. Cells were sequenced using 10x Genomics by the  
905 Genomics Core Technology Unit, Queen's University Belfast.

#### 906 *ScRNA-seq analysis*

907 The data has been deposited to the NCBI Gene Expression Omnibus repository with the  
908 accession number GSE184290.

909 Cell Ranger (version 3.0.2) was used to process raw sequencing data. Using Mkfastq, Bcl  
910 files were converted to fastq format and demultiplexed into 6 libraries corresponding to the  
911 individual samples. Reads were quantitatively aligned to *Mus musculus* reference  
912 transcriptome (mm10) with Count. Cell Ranger was used to distinguish between data from  
913 viable cells and background signal, providing filtered gene-cell count matrices for  
914 downstream analysis.

915 QC and Clustering: filtered count matrices were analysed in R (3.6.2) using Seurat 3.1.3 (69).  
916 For each library, a further QC step was performed to remove genes expressed in less than 3  
917 cells, and cells with fewer than 200 genes or with >25% counts mapping to mitochondrial  
918 genes. The libraries were then merged resulting in a dataset of 7,462 cells with 15,547 genes.  
919 Strong overlap of replicates within the alveolar and interstitial samples indicated the absence  
920 of batch effect, therefore library integration with batch correction was not required.

921 After log normalisation, SingleR 1.4.0 (70) was used to predict cell type in comparison to  
922 Immunological Genome Project (71) reference data, based on gene expression correlation.  
923 Predicted cell type was used to achieve in silico purification, keeping only those cells  
924 identified as macrophages/monocytes. After this step, the combined dataset contained 5,677  
925 cells, with the libraries ranging between 422 and 1927 cells. All other libraries were  
926 randomly down sampled to the lowest total (repeated x3 for robustness), resulting in a final  
927 dataset of six libraries at 422 cells each, totalling 2,532 cells.

928 The resulting data was scaled to regress out cell variation attributed to mitochondrial and  
929 ribosomal gene expression and total counts per cell. The top 2,000 variable genes were  
930 identified and used as input for principal component analysis; 50 principal components (PCs)  
931 were tested in Seurat's JackStraw function, from which the first 38 PCs were identified as



932 explaining more variability than expected by chance. These 38 PCs were used as input to  
933 SNN clustering (repeated at resolutions between 0.3 and 1.2) and UMAP generation.

934 Differential Expression Analysis: Marker gene detection and differential expression testing  
935 was performed in Seurat using the MAST package (version 1.12.0) (72). Genes expressed in  
936 at least 10% of cells in either group being tested, with log fold-change >0.25, and with  
937 adjusted P-value <0.05 were considered significantly differentially expressed. Differentially  
938 expressed genes were displayed as volcano plots using EnhancedVolcano 1.4.0.

939 Pseudotime Analysis: Purified data was exported to Monocle 3.0 (73) for pseudotime  
940 analysis to model expression changes in pseudotime between control and infected cells.  
941 Inferred cell trajectories were calculated on UMAP embeddings as generated in Seurat,  
942 resulting in several distinct trajectory branches. Where possible, nodes relating to control  
943 cells were considered the ‘start’ of each trajectory, with each terminal node in the Bystander  
944 and Kp52145+ groups considered distinct endpoints. Each distinct trajectory was tested  
945 separately, with correlation between gene expression and pseudotime trajectory calculated  
946 using the Moran’s I test in Monocle, filtered for significance on P- and Q-value <0.05, and  
947 Moran’s I test statistic >0.2.

948 Pathway analysis and gene networks: Pathway enrichment analysis was performed using  
949 gProfiler. For each comparison, we created a list of genes as query, selecting only those genes  
950 where adjusted P value <0.05. The analysis was performed using the g:SCS method for  
951 multiple testing correction, the Reactome database as a data source, and the default settings  
952 for the other parameters in g:Profiler. Results were exported to Cytoscape (version 3.8.2) and  
953 visualized using the AutoAnnotate application. The enrichment of transcriptional factors,  
954 their genomic binding sites and DNA binding profiles were analysed using TRANSFAC (20)  
955 included within g:Profiler. STRING database was used to predict protein-protein interactions  
956 using the clustering algorithm MCL with default parameters.

#### 957 *Seahorse analysis*

958 iBMDMs were seeded in Seahorse XF Cell Culture Microplates at a density of  $2 \times 10^4$  per  
959 well and allowed to adhere overnight in complete media at 37 °C in a humidified 5% CO<sub>2</sub>  
960 incubator overnight. Seahorse cartridge was hydrated overnight in Seahorse XF Calibrant  
961 solution (Ref: 100840-000, Agilent) at 37°C overnight in a non-CO<sub>2</sub> incubator. iBMDMs  
962 were washed once with warmed PBS and maintained in 200 µl of complete media without

963 antibiotics. When indicated, cells were treated with DMSO or STAT6 inhibitor AS1715499  
964 (50 nM/mL, 919486-40-1; AXON Medchem) 2 h prior to infection and maintained  
965 throughout. iBMDMs were infected at 70:1 multiplicity of infection. The infection was  
966 synchronised by centrifugation at 200 x g for 5 min. After 1 h contact, cells were washed  
967 with PBS, and replenished with 180 µl XF base medium (Ref 103334-100, Agilent) pH 7.4  
968 supplemented with 1 mM pyruvate, 2 mM glutamine, 10 mM glucose and 30 µg/mL  
969 gentamicin to eliminate extracellular bacteria. Metabolic activity of cells was assessed using  
970 the Seahorse Mito Stress Test Kit (Ref: 103015-100, Agilent) according to manufacturer's  
971 instructions, and results were analysed with the Seahorse XFe96 analyser. Eight wells were  
972 used per condition in three independent experiments.

### 973 *Immunoblotting*

974 Macrophages were infected with *K. pneumoniae* strains for time points indicated in the figure  
975 legends. Cells were then washed in 1 ml of ice-cold PBS and lysed in 90 µl Laemmli buffer  
976 (4% SDS, 10% 2-mercaptoethanol, 20% glycerol, 0.004% bromophenol blue, 0.125 M Tris-  
977 HCl pH 6.8). The cell lysates were sonicated for 10 s at 10% amplitude (Branson Sonifier),  
978 boiled at 95°C for 5 min, and centrifuged at 12,000 x g for 1 min. 10 µl of the cell lysates  
979 were resolved by standard 10% SDS-PAGE gel and electroblotted onto 0.2 mm nitrocellulose  
980 membrane (Biotrace, VWR) using a semi-dry transfer unit (Bio-Rad). Membranes were  
981 blocked with 3% bovine serum albumin in Tris-buffered saline with Tween 20 (TBST).

982

983 Primary antibodies used were: p-Stat6 (Tyr641) (D8S9Y) (1:2000, Ref. 56554), p-STAT1  
984 (T701) (58D6) (1:2000, Ref: 9167), p-STAT3 (Y705) (1:2000, Ref. 9145), Total STAT3  
985 (1:2000, Ref. 12640), Arginase-1 (D4E3M) XP<sup>®</sup> (1:2000, Ref: 93668), KLF4 (1:2000, Ref:  
986 4038) all from Cell Signalling Technologies. FIZZ-1/RELM (1:1000, Ref. AF1523, R&D  
987 Systems), pCREB (1:1000, Ref: sc-7978-R, Santa Cruz BT), Tubulin (1:4000, Ref, T6074.  
988 Sigma-Aldrich). Immunoreactive bands were visualized by incubation with horseradish  
989 peroxidase-conjugated goat anti-rabbit immunoglobulins (1:5,000, Bio-Rad 170-6515) or  
990 goat anti-mouse immunoglobulins (1:5,000, Bio-Rad 170-6516). Protein bands were  
991 visualised using chemiluminescence reagents and a G:BOX Chemi XRQ chemiluminescence  
992 imager (Syngene).

993 To assess loading, membranes were stripped of previously used antibodies using a pH 2.2  
994 glycine-HCl-SDS buffer and reprobed for tubulin (1:5,000, Sigma–Aldrich 6074).

### 995 *Knock-down of CREB using siRNA*

996 Transfection of siRNAs was performed at the time of cell seeding in a 96-well plate format (2  
997  $\times 10^4$  cells/well). Lipofectamine 2000 transfection reagent (Invitrogen) was used following  
998 the manufacturer's instructions. Transfection experiments were carried out in Opti-MEM  
999 reduced serum medium (Invitrogen). siRNAs were used at a concentration of 20 nM, and  
1000 experiments were carried out 48 h after transfection. The knockdown efficiency of the siRNA  
1001 targeting murine CREB1 (Dharmacon, Ref: SO-2681745G) was quantified using RT-qPCR  
1002 using conditions described above.

### 1003 *Adhesion, phagocytosis, and intracellular survival assay*

1004 Intracellular survival experiments were carried out as previously described with minor  
1005 modifications (28). Briefly, macrophages were seeded in 12-well tissue culture and allowed  
1006 to adhere overnight at 37 °C in a humidified 5% CO<sub>2</sub> incubator. Cells were infected at an  
1007 MOI of 70:1 in a final volume of 500  $\mu$ l antibiotic free complete medium. To synchronize  
1008 infection, plates were centrifuged at 200  $\times g$  for 5 minutes. Plates were incubated at 37 °C in  
1009 a humidified 5% CO<sub>2</sub> atmosphere. After 1 hour of contact, cells were washed twice with PBS  
1010 and incubated for additional 30 minutes with 500  $\mu$ l complete medium containing gentamicin  
1011 (100  $\mu$ g/ml) to eliminate extracellular bacteria. For time course experiments, after 90 min,  
1012 cells were washed with PBS and incubated with 500  $\mu$ L complete medium containing  
1013 gentamicin (5 $\mu$ g/ml). To determine intracellular bacterial load, cells were  
1014 washed twice with prewarmed PBS and lysed with 300  $\mu$ l of 0.05% saponin (Sigma-  
1015 Aldrich) in PBS for 5 minutes at 37 °C. Adhesion was determined at 60 minutes post  
1016 infection, phagocytosis at 90 minutes post infections, and survival at 330 minutes post  
1017 infection. Serial dilutions were plated on LB to quantify the number of intracellular  
1018 bacteria. All experiments were carried out in duplicate on at least three independent  
1019 occasions.

### 1020 *Confocal microscopy*

1021 iBMDMs were seeded in 24-well plates on 13 mm glass coverslips (VWR). Infections were  
1022 performed at a multiplicity of infection of 100 bacteria per iBMDM in a final volume of 500  
1023  $\mu$ l complete medium. To synchronize infection, cells were centrifuged (200  $\times g$  for 5  
1024 min). After 60 minutes contact, cells were washed with sterile PBS and incubated in 500  $\mu$ L  
1025 complete medium containing gentamicin (100  $\mu$ g/ml). Lysosomes were stained using  
1026 cresyl violet (Ostrowski et al., 2016). 15 minutes before the end of the experiment,  
1027 cresyl violet (Sigma-Aldrich) was added to the coverslips to achieve 5  $\mu$ M final

1028 concentration. Coverslips were washed in PBS and fixed with 4% paraformaldehyde  
1029 (PFA) (Sigma-Aldrich) for 20 min at room temperature. Coverslips were mounted  
1030 with ProLong Gold antifade mountant (Invitrogen). Coverslips were visualised  
1031 on a Leica SP5 Confocal microscope with the appropriate filter sets. Experiments were  
1032 carried out in duplicate on three independent occasions.

### 1033 *Assessment of NF- $\kappa$ B and Irf3 activation*

1034 To quantify the activation of the NF- $\kappa$ B signalling pathway, we probed Raw-Blue cells  
1035 (InvivoGen) derived from Raw 264.7 macrophages containing a chromosomal integration of  
1036 a secreted embryonic alkaline phosphatase (SEAP) reported inducible by NF- $\kappa$ B and AP-1.  
1037 Cells were maintained in DMEM supplemented with 10% heat-inactivated FBS, 50 U/ml  
1038 penicillin, 50  $\mu$ g/ml streptomycin, 200  $\mu$ g/ml Zeocin were added in alternate passages to  
1039 maintain the reporter plasmid. Cells were seeded at a density of  $\sim$ 50,400 cells per well in a  
1040 96-well plate with complete medium without antibiotics, incubated overnight at 37 °C in a  
1041 humidified 5% CO<sub>2</sub> incubator. Cells were then infected at a multiplicity of infection  
1042 of 100:1 in a final volume of 190  $\mu$ l antibiotic free complete medium. To synchronize  
1043 infection, plates were centrifuged at 200  $\times$  g for 5 min. Plates were incubated at 37 °C in a  
1044 humidified 5% CO<sub>2</sub> atmosphere. After 1 h of contact, cells were washed twice with PBS and  
1045 incubated for 5 h with 180  $\mu$ l complete medium containing gentamicin (100  $\mu$ g/ml) to  
1046 eliminate extracellular bacteria. Supernatants were then transferred to a new 96-well plate,  
1047 and QUANTI-Blue (InvivoGen) was added in a 1:9 v/v ratio for 40 min. Absorbance was  
1048 measured at 620nm (POLARstar Omega).

1049 To quantify the activation of Irf3 signalling pathway, Raw-Lucia ISG cells were probed.  
1050 These cells are derived from Raw 264.7 macrophages after stable integration of an interferon  
1051 regulatory factor (irf)-inducible Lucia luciferase reporter construct. Cells were cultured in  
1052 DMEM supplemented with 10% heat-inactivated FBS, 50 U/ml penicillin, 50  $\mu$ g/ml  
1053 streptomycin, 200  $\mu$ g/ml Zeocin were added in alternate passages to maintain the reporter  
1054 plasmid. Cells were seeded and infected as described for Raw-Blue cells. At the end of the  
1055 experiment, 20  $\mu$ l of media were transferred to flat, white bottom luminometer plates  
1056 (LUMITRAC, Greiner), 50  $\mu$ l QUANTI-Luc (Invivogen) were added to the wells, and  
1057 luminescence was read immediately (Promega GloMax).

### 1058 *Statistics*

1059 Statistical analyses were performed with Prism (version 9.1.2) software (GraphPad Software)  
1060 using one-way analysis of variance (ANOVA) with Bonferroni correction for multiple

1061 comparisons, or unpaired two-tailed Student's t test. Error bars indicate standard errors of the  
1062 means (SEM). Statistical significance is indicated in figures as follows: ns, not significant (P  
1063 >0.05); \*, P < 0.05; \*\*, P < 0.01; \*\*\*, P < 0.001; and \*\*\*\*, P < 0.0001.

#### 1064 ***Authors' contribution***

1065 Conceptualization, J.A.B., A.K., and A.D.; Investigation, A.D., O.C., B.M., J. sP., R. CG.,  
1066 G.M., R.L., D.S., and A.K. Resources, J. sP.; Funding acquisition, J.A.B. and A.K.; Writing  
1067 original draft, J.A.B., A.D., A.K. D.S.; Writing-Review and Editing A.D., D.S., J.A.B. and  
1068 A.K. Supervision, J.A.B., and A.K.

#### 1069 ***Acknowledgements***

1070 We thank the members of the J.A.B. laboratory for their thoughtful discussions and support  
1071 with this project. This work was supported by Biotechnology and Biological Sciences  
1072 Research Council (BBSRC, BB/P006078/1, BB/P020194/1), and Medical Research Council  
1073 (MRC, MR/V032496/1) funds to J.A.B.

#### 1074 ***References***

- 1075 1. Penalva G, Hogberg LD, Weist K, Vlahovic-Palcevski V, Heuer O, Monnet DL, et al. Decreasing  
1076 and stabilising trends of antimicrobial consumption and resistance in Escherichia coli and  
1077 Klebsiella pneumoniae in segmented regression analysis, European Union/European  
1078 Economic Area, 2001 to 2018. *Euro Surveill.* 2019;24(46).
- 1079 2. Giske CG, Monnet DL, Cars O, Carmeli Y, and ReAct-Action on Antibiotic R. Clinical and  
1080 economic impact of common multidrug-resistant gram-negative bacilli. *Antimicrob Agents*  
1081 *Chemother.* 2008;52(3):813-21.
- 1082 3. Malyshev I, and Lyamina S. Imbalance of M1/M2 alveolar macrophages phenotype in  
1083 bronchial asthma (LB506). *The FASEB Journal.* 2014;28:LB506.
- 1084 4. Gleissner CA, Shaked I, Little KM, and Ley K. CXC chemokine ligand 4 induces a unique  
1085 transcriptome in monocyte-derived macrophages. *J Immunol.* 2010;184(9):4810-8.
- 1086 5. Murray PJ, Allen JE, Biswas SK, Fisher EA, Gilroy DW, Goerdt S, et al. Macrophage activation  
1087 and polarization: nomenclature and experimental guidelines. *Immunity.* 2014;41(1):14-20.
- 1088 6. Dolgachev VA, Yu B, Reinke JM, Raghavendran K, and Hemmila MR. Host susceptibility to  
1089 gram-negative pneumonia after lung contusion. *J. Trauma Acute Care Surg.* 2012;72(3):614-  
1090 22.
- 1091 7. Ohama H, Asai A, Ito I, Suzuki S, Kobayashi M, Higuchi K, et al. M2b macrophage elimination  
1092 and improved resistance of mice with chronic alcohol consumption to opportunistic  
1093 infections. *Am. J. Pathol.* 2015;185(2):420-31.

- 1094 8. Tsuchimoto Y, Asai A, Tsuda Y, Ito I, Nishiguchi T, Garcia MC, et al. M2b Monocytes Provoke  
1095 Bacterial Pneumonia and Gut Bacteria-Associated Sepsis in Alcoholics. *J. Immunol.*  
1096 2015;195(11):5169-77.
- 1097 9. Standiford LR, Standiford TJ, Newstead MJ, Zeng X, Ballinger MN, Kovach MA, et al. TLR4-  
1098 dependent GM-CSF protects against lung injury in Gram-negative bacterial pneumonia. *Am.*  
1099 *J. Physiol. - Lung Cell. Mol. Physiol.* 2012;302(5):L447-54.
- 1100 10. Benoit M, Desnues B, and Mege JL. Macrophage polarization in bacterial infections. *J.*  
1101 *Immunol.* 2008;181(6):3733-9.
- 1102 11. Thiriot JD, Martinez-Martinez YB, Endsley JJ, and Torres AG. Hacking the host: exploitation of  
1103 macrophage polarization by intracellular bacterial pathogens. *Pathogens and disease.*  
1104 2020;78(1):ftaa009.
- 1105 12. Bharat A, Bhorade SM, Morales-Nebreda L, McQuattie-Pimentel AC, Soberanes S, Ridge K, et  
1106 al. Flow Cytometry Reveals Similarities Between Lung Macrophages in Humans and Mice.  
1107 *Am J Respir Cell Mol Biol.* 2016;54(1):147-9.
- 1108 13. Gautier EL, Shay T, Miller J, Greter M, Jakubzick C, Ivanov S, et al. Gene-expression profiles  
1109 and transcriptional regulatory pathways that underlie the identity and diversity of mouse  
1110 tissue macrophages. *Nat. Immunol.* 2012;13(11):1118-28.
- 1111 14. Misharin AV, Morales-Nebreda L, Mutlu GM, Budinger GS, and Perlman H. Flow cytometric  
1112 analysis of macrophages and dendritic cell subsets in the mouse lung. *Am. J. Respir. Cell Mol.*  
1113 *Biol.* 2013;49(4):503-10.
- 1114 15. Nassif X, Fournier JM, Arondel J, and Sansonetti PJ. Mucoid phenotype of *Klebsiella*  
1115 *pneumoniae* is a plasmid-encoded virulence factor. *Infect. Immun.* 1989;57(2):546-52.
- 1116 16. Holt KE, Wertheim H, Zadoks RN, Baker S, Whitehouse CA, Dance D, et al. Genomic analysis  
1117 of diversity, population structure, virulence, and antimicrobial resistance in *Klebsiella*  
1118 *pneumoniae*, an urgent threat to public health. *Proc. Natl. Acad. Sci. U.S.A.*  
1119 2015;112(27):E3574-81.
- 1120 17. Lery LM, Frangeul L, Tomas A, Passet V, Almeida AS, Bialek-Davenet S, et al. Comparative  
1121 analysis of *Klebsiella pneumoniae* genomes identifies a phospholipase D family protein as a  
1122 novel virulence factor. *BMC biology.* 2014;12:41-7007-12-41.
- 1123 18. Ivin M, Dumigan A, de Vasconcelos FN, Ebner F, Borroni M, Kavirayani A, et al. Natural killer  
1124 cell-intrinsic type I IFN signaling controls *Klebsiella pneumoniae* growth during lung  
1125 infection. *PLoS pathogens.* 2017;13(11):e1006696.
- 1126 19. Benoist C. Open-source ImmGen: mononuclear phagocytes. *Nat. Immunol.* 2016;17(7):741-  
1127 2.
- 1128 20. Wingender E, Dietze P, Karas H, and Knüppel R. TRANSFAC: a database on transcription  
1129 factors and their DNA binding sites. *Nucleic acids res.* 1996;24(1):238-41.
- 1130 21. Liao X, Sharma N, Kapadia F, Zhou G, Lu Y, Hong H, et al. Krüppel-like factor 4 regulates  
1131 macrophage polarization. *J. Clin. Invest.* 2011;121(7):2736-49.
- 1132 22. Pauleau A-L, Rutschman R, Lang R, Pernis A, Watowich SS, and Murray PJ. Enhancer-  
1133 mediated control of macrophage-specific arginase I expression. *J. Immunol.*  
1134 2004;172(12):7565-73.
- 1135 23. Szanto A, Balint BL, Nagy ZS, Barta E, Dezso B, Pap A, et al. STAT6 transcription factor is a  
1136 facilitator of the nuclear receptor PPARgamma-regulated gene expression in macrophages  
1137 and dendritic cells. *Immunity.* 2010;33(5):699-712.
- 1138 24. Goenka S, and Kaplan MH. Transcriptional regulation by STAT6. *Immunol Res.* 2011;50(1):87-  
1139 96.
- 1140 25. Deleo FR, Chen L, Porcella SF, Martens CA, Kobayashi SD, Porter AR, et al. Molecular  
1141 dissection of the evolution of carbapenem-resistant multilocus sequence type 258 *Klebsiella*  
1142 *pneumoniae*. *Proc. Natl. Acad. Sci. U.S.A.* 2014;111(13):4988-93.

- 1143 26. Lam MMC, Wyres KL, Duchene S, Wick RR, Judd LM, Gan YH, et al. Population genomics of  
1144 hypervirulent *Klebsiella pneumoniae* clonal-group 23 reveals early emergence and rapid  
1145 global dissemination. *Nat Commun.* 2018;9(1):2703.
- 1146 27. Nagashima S, Yokota M, Nakai E, Kuromitsu S, Ohga K, Takeuchi M, et al. Synthesis and  
1147 evaluation of 2-[[2-(4-hydroxyphenyl)-ethyl]amino]pyrimidine-5-carboxamide derivatives as  
1148 novel STAT6 inhibitors. *Bioorg Med Chem.* 2007;15(2):1044-55.
- 1149 28. Cano V, March C, Insua JL, Aguilo N, Llobet E, Moranta D, et al. *Klebsiella pneumoniae*  
1150 survives within macrophages by avoiding delivery to lysosomes. *Cell Microbiol.*  
1151 2015;17:1537-60.
- 1152 29. Ostrowski PP, Fairn GD, Grinstein S, and Johnson DE. Cresyl violet: a superior fluorescent  
1153 lysosomal marker. *Traffic.* 2016;17(12):1313-21.
- 1154 30. Sa-Pessoa J, Przybyszewska K, Vasconcelos FN, Dumigan A, Frank CG, Hopley L, et al.  
1155 *Klebsiella pneumoniae* Reduces SUMOylation To Limit Host Defense Responses. *mBio.*  
1156 2020;11(5).
- 1157 31. O'Neill LA, and Bowie AG. The family of five: TIR-domain-containing adaptors in Toll-like  
1158 receptor signalling. *Nat. Rev. Immunol.* 2007;7(5):353-64.
- 1159 32. Farlik M, Reutterer B, Schindler C, Greten F, Vogl C, Müller M, et al. Nonconventional  
1160 initiation complex assembly by STAT and NF- $\kappa$ B transcription factors regulates nitric oxide  
1161 synthase expression. *Immunity.* 2010;33(1):25-34.
- 1162 33. Saraiva M, and O'Garra A. The regulation of IL-10 production by immune cells. *Nat. Rev.*  
1163 *Immunol.* 2010;10(3):170-81.
- 1164 34. Mayr B, and Montminy M. Transcriptional regulation by the phosphorylation-dependent  
1165 factor CREB. *Nat. Rev. Mol. Cell Biol.* 2001;2(8):599-609.
- 1166 35. Jha AK, Huang SC, Sergushichev A, Lampropoulou V, Ivanova Y, Loginicheva E, et al. Network  
1167 integration of parallel metabolic and transcriptional data reveals metabolic modules that  
1168 regulate macrophage polarization. *Immunity.* 2015;42(3):419-30.
- 1169 36. Biswas SK, and Mantovani A. Orchestration of metabolism by macrophages. *Cell metabolism.*  
1170 2012;15(4):432-7.
- 1171 37. Pålsson-McDermott EM, and O'Neill LA. Targeting immunometabolism as an anti-  
1172 inflammatory strategy. *Cell research.* 2020;30(4):300-14.
- 1173 38. Yang FL, Yang YL, Liao PC, Chou JC, Tsai KC, Yang AS, et al. Structure and immunological  
1174 characterization of the capsular polysaccharide of a pyrogenic liver abscess caused by  
1175 *Klebsiella pneumoniae*: activation of macrophages through Toll-like receptor 4. *J. Biol. Chem.*  
1176 2011;286(24):21041-51.
- 1177 39. Regueiro V, Moranta D, Campos MA, Margareto J, Garmendia J, and Bengoechea JA.  
1178 *Klebsiella pneumoniae* increases the levels of Toll-like receptors 2 and 4 in human airway  
1179 epithelial cells. *Infect. Immun.* 2009;77(2):714-24.
- 1180 40. Llobet E, Tomas JM, and Bengoechea JA. Capsule polysaccharide is a bacterial decoy for  
1181 antimicrobial peptides. *Microbiology.* 2008;154(Pt 12):3877-86.
- 1182 41. Martinez FO, Gordon S, Locati M, and Mantovani A. Transcriptional profiling of the human  
1183 monocyte-to-macrophage differentiation and polarization: new molecules and patterns of  
1184 gene expression. *J Immunol.* 2006;177(10):7303-11.
- 1185 42. Gibbings SL, Thomas SM, Atif SM, McCubbrey AL, Desch AN, Danhorn T, et al. Three Unique  
1186 Interstitial Macrophages in the Murine Lung at Steady State. *Am J Respir Cell Mol Biol.*  
1187 2017;57(1):66-76.
- 1188 43. Chakarov S, Lim HY, Tan L, Lim SY, See P, Lum J, et al. Two distinct interstitial macrophage  
1189 populations coexist across tissues in specific subtissular niches. *Science.* 2019;363(6432).
- 1190 44. Xiong H, Carter RA, Leiner IM, Tang YW, Chen L, Kreiswirth BN, et al. Distinct Contributions of  
1191 Neutrophils and CCR2+ Monocytes to Pulmonary Clearance of Different *Klebsiella*  
1192 *pneumoniae* Strains. *Infect. Immun.* 2015;83(9):3418-27.



- 1193 45. Xiong H, Keith JW, Samilo DW, Carter RA, Leiner IM, and Pamer EG. Innate  
1194 Lymphocyte/Ly6C(hi) Monocyte Crosstalk Promotes Klebsiella Pneumoniae Clearance. *Cell*.  
1195 2016;165(3):679-89.
- 1196 46. Huang L, Nazarova EV, Tan S, Liu Y, and Russell DG. Growth of Mycobacterium tuberculosis  
1197 in vivo segregates with host macrophage metabolism and ontogeny. *J Exp Med*.  
1198 2018;215(4):1135-52.
- 1199 47. Pisu D, Huang L, Narang V, Theriault M, Le-Bury G, Lee B, et al. Single cell analysis of M.  
1200 tuberculosis phenotype and macrophage lineages in the infected lung. *J Exp Med*.  
1201 2021;218(9).
- 1202 48. Dumigan A, Fitzgerald M, Santos JSG, Hamid U, O'Kane CM, McAuley DF, et al. A Porcine Ex  
1203 Vivo Lung Perfusion Model To Investigate Bacterial Pathogenesis. *mBio*. 2019;10(6).
- 1204 49. Fairbairn L, Kapetanovic R, Sester DP, and Hume DA. The mononuclear phagocyte system of  
1205 the pig as a model for understanding human innate immunity and disease. *J. Leukoc. Biol*.  
1206 2011;89(6):855-71.
- 1207 50. Wang Y, and Levy DE. Comparative evolutionary genomics of the STAT family of transcription  
1208 factors. *JAKSTAT*. 2012;1(1):23-33.
- 1209 51. Piazzon MC, Lutfalla G, and Forlenza M. IL10, A Tale of an Evolutionarily Conserved Cytokine  
1210 across Vertebrates. *Crit Rev Immunol*. 2016;36(2):99-129.
- 1211 52. Liu G, Zhang H, Zhao C, and Zhang H. Evolutionary History of the Toll-Like Receptor Gene  
1212 Family across Vertebrates. *Genome Biol Evol*. 2020;12(1):3615-34.
- 1213 53. Arpaia N, Godec J, Lau L, Sivick KE, McLaughlin LM, Jones MB, et al. TLR signaling is required  
1214 for Salmonella typhimurium virulence. *Cell*. 2011;144(5):675-88.
- 1215 54. Pagliuso A, Tham TN, Allemand E, Robertin S, Dupuy B, Bertrand Q, et al. An RNA-Binding  
1216 Protein Secreted by a Bacterial Pathogen Modulates RIG-I Signaling. *Cell Host Microbe*.  
1217 2019;26(6):823-35 e11.
- 1218 55. Frantz R, Teubner L, Schultze T, La Pietra L, Muller C, Gwozdziński K, et al. The secRNome of  
1219 Listeria monocytogenes Harbors Small Noncoding RNAs That Are Potent Inducers of Beta  
1220 Interferon. *mBio*. 2019;10(5).
- 1221 56. Greenberger MJ, Strieter RM, Kunkel SL, Danforth JM, Goodman RE, and Standiford TJ.  
1222 Neutralization of IL-10 increases survival in a murine model of Klebsiella pneumonia. *J*.  
1223 *Immunol*. 1995;155(2):722-9.
- 1224 57. Wen AY, Sakamoto KM, and Miller LS. The role of the transcription factor CREB in immune  
1225 function. *J Immunol*. 2010;185(11):6413-9.
- 1226 58. Puthenveetil A, and Dubey S. Metabolic reprogramming of tumor-associated macrophages.  
1227 *Ann Transl Med*. 2020;8(16):1030.
- 1228 59. Rosenberg G, Yehezkel D, Hoffman D, Mattioli CC, Fremder M, Ben-Arosh H, et al. Host  
1229 succinate is an activation signal for Salmonella virulence during intracellular infection.  
1230 *Science*. 2021;371(6527):400-5.
- 1231 60. Cortes G, Borrell N, de Astorza B, Gomez C, Sauleda J, and Alberti S. Molecular analysis of the  
1232 contribution of the capsular polysaccharide and the lipopolysaccharide O side chain to the  
1233 virulence of Klebsiella pneumoniae in a murine model of pneumonia. *Infect. Immun*.  
1234 2002;70(5):2583-90.
- 1235 61. March C, Cano V, Moranta D, Llobet E, Perez-Gutierrez C, Tomas JM, et al. Role of bacterial  
1236 surface structures on the interaction of Klebsiella pneumoniae with phagocytes. *PloS one*.  
1237 2013;8(2):e56847.
- 1238 62. Evrard B, Balestrino D, Dosgilbert A, Bouya-Gachancard JL, Charbonnel N, Forestier C, et al.  
1239 Roles of capsule and lipopolysaccharide O antigen in interactions of human monocyte-  
1240 derived dendritic cells and Klebsiella pneumoniae. *Infect. Immun*. 2010;78(1):210-9.
- 1241 63. Pan YJ, Lin TL, Hsu CR, and Wang JT. Use of a Dictyostelium model for isolation of genetic loci  
1242 associated with phagocytosis and virulence in Klebsiella pneumoniae. *Infect. Immun*.  
1243 2011;79(3):997-1006.

- 1244 64. Regueiro V, Campos MA, Pons J, Alberti S, and Bengoechea JA. The uptake of a *Klebsiella*  
1245 *pneumoniae* capsule polysaccharide mutant triggers an inflammatory response by human  
1246 airway epithelial cells. *Microbiology*. 2006;152(Pt 2):555-66.
- 1247 65. Bengoechea JA, and Sa Pessoa J. *Klebsiella pneumoniae* infection biology: living to  
1248 counteract host defences. *FEMS Microbiol Rev*. 2019;43(2):123-44.
- 1249 66. Frank CG, Reguerio V, Rother M, Moranta D, Maeurer AP, Garmendia J, et al. *Klebsiella*  
1250 *pneumoniae* targets an EGF receptor-dependent pathway to subvert inflammation. *Cell*  
1251 *Microbiol*. 2013;15(7):1212-33.
- 1252 67. Bartholomew TL, Kidd TJ, Sa Pessoa J, Conde Alvarez R, and Bengoechea JA. 2-Hydroxylation  
1253 of *Acinetobacter baumannii* Lipid A Contributes to Virulence. *Infect Immun*. 2019;87(4).
- 1254 68. Ducas-Mowchun K, De Silva PM, Crisostomo L, Fernando DM, Chao TC, Pelka P, et al. Next  
1255 Generation of Tn7-Based Single-Copy Insertion Elements for Use in Multi- and Pan-Drug-  
1256 Resistant Strains of *Acinetobacter baumannii*. *Appl Environ Microbiol*. 2019;85(11).
- 1257 69. Stuart T, Butler A, Hoffman P, Hafemeister C, Papalexi E, Mauck WM, 3rd, et al.  
1258 Comprehensive Integration of Single-Cell Data. *Cell*. 2019;177(7):1888-902 e21.
- 1259 70. Aran D, Looney AP, Liu L, Wu E, Fong V, Hsu A, et al. Reference-based analysis of lung single-  
1260 cell sequencing reveals a transitional profibrotic macrophage. *Nat Immunol*. 2019;20(2):163-  
1261 72.
- 1262 71. Heng TS, Painter MW, and Immunological Genome Project C. The Immunological Genome  
1263 Project: networks of gene expression in immune cells. *Nat Immunol*. 2008;9(10):1091-4.
- 1264 72. Finak G, McDavid A, Yajima M, Deng J, Gersuk V, Shalek AK, et al. MAST: a flexible statistical  
1265 framework for assessing transcriptional changes and characterizing heterogeneity in single-  
1266 cell RNA sequencing data. *Genome Biol*. 2015;16:278.
- 1267 73. Cao J, Spielmann M, Qiu X, Huang X, Ibrahim DM, Hill AJ, et al. The single-cell transcriptional  
1268 landscape of mammalian organogenesis. *Nature*. 2019;566(7745):496-502.

1269

1270

1271

## 1272 **Figure legends**

1273 **Figure 1. *K. pneumoniae* is associated with interstitial macrophages and alveolar**  
1274 **macrophages in vivo.**

1275 10-12 week old age and sex matched C57BL/6 mice were infected intranasally with mCherry  
1276 tagged Kp52145. After 24 h or 48 h post-infection (n=10/condition) lungs were harvested and  
1277 processed for flow cytometric analysis to assess macrophages populations.

1278 A. % Ly6C+CD11b-CD11c-SiglecF- monocyte (MNs), % Ly6C+CD11b-CD11c+SiglecF+  
1279 alveolar macrophage (AMs), and % Ly6C+CD11b+CD11c+SiglecF- interstitial macrophage  
1280 (IMs) in Kp52145-infected animals compared to PBS controls.

1281 B. Percentage of MN, AM, and IM associated with Kp52145 from infected individual mice.

1282 In all panels, values are presented as the mean  $\pm$  SEM of two independent experiments.  
1283 \*\*\*\*P  $\leq$  0.0001; \*\*\*P  $\leq$  0.001; \*\* P  $\leq$  0.01; ns, P  $>$  0.05 for the indicated comparisons  
1284 determined using One-way ANOVA.

1285 **Figure 2. Analysis of *K. pneumoniae*-induced transcriptome in IMs.**

1286 A. Diagram of the experimental approach to generate the different IMs and AMs samples for  
1287 single-cell RNA sequencing (scRNAseq). C57BL/6 mice (n=17/group) were infected  
1288 intranasally with mCherry tagged Kp52145, after 24 h, lungs were excised, and processed  
1289 for cell sorting. From pooled samples AM and IM populations were sorted from PBS  
1290 controls and infected mice. In the latter group, cells were sorted to separate bystander cells  
1291 and cells with associated bacteria. The viability of each of the samples was determined to be  
1292 higher than 95% before carrying out 10x genomics single cell RNA sequencing.

1293 B. Marker gene detection and differential expression testing was performed in Seurat using  
1294 the MAST package. Higher resolution clustering using uniform manifold approximation and  
1295 projection (UMAP) dimensionality reduction analysis showing selected genes, *cx3cr1*, IM  
1296 marker, and *SiglecF*, AM marker.

1297 C. UMAP of clustering within cells from PBS mock-infected mice (control), bystander and  
1298 Kp52145-associated IMs and AM populations.

1299 D. Network enrichment mapping generated from significantly upregulated genes of IMs with  
1300 associated bacteria. Analysis was performed using the g:SCS method for multiple testing  
1301 correction (gProflier), the Reactome database as a data source, and the default settings for  
1302 the other parameters in gProflier. Results were exported to Cytoscape and visualized using  
1303 the AutoAnnotate plug.

1304 E. Network enrichment mapping generated from significantly upregulated genes of  
1305 bystander IMs. Analysis was performed using the g:SCS method for multiple testing  
1306 correction (gProflier), the Reactome database as a data source, and the default settings for  
1307 the other parameters in gProflier. Results were exported to Cytoscape and visualized using  
1308 the AutoAnnoate application

1309 **Figure 3. Single-cell trajectory analysis of IMs from non-infected to infected cells.**

1310 A. Monocle analysis to determine the temporal pattern of gene expression over pseudotime  
1311 in bystander and Kp52145-associated IMs from infected animals compared to PBS controls.  
1312 Monocle analysis revealed 7 modules of genes showing similar pattern of expression.

1313 B. Heat map showing relative expression of the 7 modules found in IMs.

1314 C. Pathway analysis of modules 3 and 4 corresponding to Kp52145-infected IMs. Analysis  
1315 was performed using the g:SCS method for multiple testing correction, the Reactome  
1316 database as a data source, and the default settings for the other parameters in G:profiler.

1317 D. STRING database was used to predict protein-protein interactions using the clustering  
1318 algorithm MCL with default parameters using as data source the genes within modules 3 and  
1319 4.

1320 E. Pathway analysis of module 6 corresponding to bystander IMs. Analysis was performed  
1321 using the g:SCS method for multiple testing correction, the Reactome database as a data  
1322 source, and the default settings for the other parameters in G:profiler.

1323 F. Changes over pseudotime of selected top expressed genes within the modules 3, 4 and 6.

1324 **Figure 4. *K. pneumoniae* skews macrophage polarization towards a singular state**  
1325 **termed M(Kp).**

1326 A. Heat map presents relative expression of the indicated genes between IMs from non-  
1327 infected mice (control), and bystander and Kp52145-associated IMs from infected mice.  
1328 Selected genes are related to M1 and M2 macrophage polarisation.

1329

1330 Analysis by flow cytometry of the levels of M(Kp) markers expressed by cells from PBS  
1331 mock infected mice (black dots), and by cells from infected mice (blue dots) with and without  
1332 associated Kp52145.

1333 B. Percentage of positive cells for iNOS.

1334 C. Percentage of positive cells for Arg1.

1335 D. Percentage of positive cells for Fizz1.

1336 E. Percentage of positive cells for CD136.

1337 Values in panel B-E are presented as the mean  $\pm$  SEM whereby each dot represents an  
1338 individual animal. \*\*\*\*P  $\leq$  0.0001; \*\*\*P  $\leq$  0.001; \*\*P  $\leq$  0.01; \*P  $\leq$  0.05; ns, P > 0.05 for the

1339 indicated comparisons using one way-ANOVA with Bonferroni contrast for multiple  
1340 comparisons test.

1341 **Figure 5. *K. pneumoniae*-induced M(Kp) polarization is STAT6 dependent.**

1342 A. Immunoblot analysis of phospho-STAT6 (pSTAT6) and tubulin levels in lysates from  
1343 non-infected (ni) and infected wild-type iBMDMs for 60 or 120 min. After 1 h contact,  
1344 medium replaced with medium containing gentamycin (100 µg/ml) to kill extracellular  
1345 bacteria.

1346 B. Immunoblot analysis of phospho-STAT6 (pSTAT6) and tubulin levels in lysates from  
1347 non-infected (ni) and infected with different *K. pneumoniae* strains, Kp52145, NJST258-1,  
1348 NJST258-2, or SHG10, for 60 min.

1349 C. *klf4* mRNA levels were assessed by qPCR in wild-type iBMDMs infected with Kp52145  
1350 for 1, 3 or 5 h. Immunoblot analysis of Klf4 and tubulin levels in lysates from non-infected  
1351 (ni) and infected wild-type iBMDMs for 60 or 120 min.

1352 D. *arg1* mRNA levels were assessed by qPCR in wild-type and *stat6*<sup>-/-</sup> iBMDMs non-infected  
1353 (ni) or infected with Kp52145 for 1, 3 or 5 h. Immunoblot analysis of Arg1 and tubulin levels  
1354 in lysates from non-infected (ni) and infected wild-type and *stat6*<sup>-/-</sup> iBMDMs for 60 or 120  
1355 min.

1356 E. *il10* mRNA levels were assessed by qPCR in wild-type (WT) and *stat6*<sup>-/-</sup> iBMDMs non-  
1357 infected (ni) or infected with Kp52145 for 1, 3 or 5 h.

1358 F. *klf4* mRNA levels were assessed by qPCR in wild-type (WT) and *stat6*<sup>-/-</sup> iBMDMs non-  
1359 infected (ni) or infected with Kp52145 for 1, 3 or 5 h.

1360 G. *pparg* mRNA levels were assessed by qPCR in wild-type (WT) and *stat6*<sup>-/-</sup> iBMDMs non-  
1361 infected (ni) or infected with Kp52145 for 1, 3 or 5 h.

1362 H. *nos2* mRNA levels were assessed by qPCR in wild-type (WT) and *stat6*<sup>-/-</sup> iBMDMs non-  
1363 infected (ni) or infected with Kp52145 for 1, 3 or 5 h.

1364 I. *tnfa* mRNA levels were assessed by qPCR in wild-type (WT) and *stat6*<sup>-/-</sup> iBMDMs non-  
1365 infected (ni) or infected with Kp52145 for 1, 3 or 5 h.

1366 J. *il12* mRNA levels were assessed by qPCR in wild-type (WT) and *stat6*<sup>-/-</sup> iBMDMs non-  
1367 infected (ni) or infected with Kp52145 for 1, 3 or 5 h.

1368 K. *il6* mRNA levels were assessed by qPCR in wild-type (WT) and *stat6*<sup>-/-</sup> iBMDMs non-  
1369 infected (ni) or infected with Kp52145 for 1, 3 or 5 h.

1370 L. *isg15* mRNA levels were assessed by qPCR in wild-type (WT) and *stat6*<sup>-/-</sup> iBMDMs non-  
1371 infected (ni) or infected with Kp52145 for 1, 3 or 5 h.

1372 M. Percentage of wild-type (WT) and *stat6*<sup>-/-</sup> iBMDMs with and without associated Kp52145  
1373 positive for Arg1 1, 3 or 5 h post infection. Kp52145 was tagged with mCherry.

1374 N. Percentage of wild-type (WT) and *stat6*<sup>-/-</sup> iBMDMs with and without associated Kp52145  
1375 positive for CD206 1, 3 or 5 h post infection. Kp52145 was tagged with mCherry.

1376 O. Percentage of wild-type (WT) and *stat6*<sup>-/-</sup> iBMDMs with and without associated Kp52145  
1377 positive for MHC-II 1, 3 or 5 h post infection. Kp52145 was tagged with mCherry.

1378 For all infections, after 1 h contact, medium replaced with medium containing gentamycin  
1379 (100 µg/ml) to kill extracellular bacteria. qPCR and flow cytometry values are presented as  
1380 the mean ± SEM of three independent experiments measured in duplicate. Images are  
1381 representative of three independent experiments. \*\*\*\*P ≤ 0.0001; \*\*\*P ≤ 0.001; \*\*P ≤ 0.01;  
1382 \*P ≤ 0.05; ns, P > 0.05 for the indicated comparisons using one way-ANOVA with  
1383 Bonferroni contrast for multiple comparisons test.

1384 **Figure 6. STAT6 promotes *K. pneumoniae* infection.**

1385 A. Kp52145 adhesion to wild-type (WT) and *stat6*<sup>-/-</sup> iBMDMs. Cells were infected with  
1386 Kp52145 for 30 min, washed, cell lysed with saponin, and bacteria quantified after serial  
1387 dilution followed by plating on LB agar plates.

1388 B. Phagocytosis of Kp52145 by wild-type (WT) and *stat6*<sup>-/-</sup> iBMDMs. Cells were infected for  
1389 30 min, wells were washed, and it was added medium containing gentamicin (100 µg/ml) to  
1390 kill extracellular bacteria. After 30 min, cells were washed, cell lysed with saponin, and  
1391 bacteria quantified after serial dilution followed by plating on LB agar plates.

1392 C. Kp52145 intracellular survival in wild-type (WT) and *stat6*<sup>-/-</sup> 5 h after addition of  
1393 gentamycin (30 min of contact). Results are expressed as % of survival (CFUs at 5 h versus  
1394 30 min in *stat6*<sup>-/-</sup> cells normalized to the results obtained in wild-type macrophages set to  
1395 100%).

1396 D. Immunofluorescence confocal microscopy of the colocalization of Kp52145 harbouring  
1397 pFPV25.1Cm, and cresyl violet dye in wild-type (WT) and *stat6*<sup>-/-</sup> macrophages. The images



1398 were taken 90 min post infection. Images are representative of duplicate coverslips of three  
1399 independent experiments.

1400 E. Percentage of Kp52145 harbouring pFPV25.1Cm co-localization with cresyl violet over a  
1401 time course. Wild-type (WT) and *stat6*<sup>-/-</sup> macrophages were infected; coverslips were fixed  
1402 and stained at the indicated times. Values are given as mean percentage of Kp52145 co-  
1403 localizing with the marker  $\pm$  SEM. The number of infected cells counted per time in three  
1404 independent experiments are indicated in the figure.

1405 F. C56BL/6 mice were treated 24 h prior to infection with the STAT6 inhibitor AS1517499  
1406 (10mg/kg in 200  $\mu$ L volume by i.p) and 6 h post infection (5 mg/kg in 30  $\mu$ L volume  
1407 intranasally) or vehicle control DMSO. Bacterial burden was established by serial dilutions of  
1408 lung homogenates on *Salmonella-Shigella* agar. Each dot represents one animal.

1409 G. Bacterial dissemination assessed by quantifying CFUs in the spleens from infected mice  
1410 treated with AS1517499 or vehicle control DMSO. Each dot represents one animal.

1411 H. *arg1* mRNA levels were assessed by qPCR in the lungs of non-infected or infected wild-  
1412 type mice for 24 h treated with the STAT6 inhibitor AS1517499 or DMSO vehicle control.  
1413 Each dot represents different mice.

1414 I. *il10* mRNA levels were assessed by qPCR in the lungs of non-infected or infected wild-  
1415 type mice for 24 h treated with the STAT6 inhibitor AS1517499 or DMSO vehicle control.  
1416 Each dot represents different mice.

1417 J. *pparg* mRNA levels were assessed by qPCR in the lungs of non-infected or infected wild-  
1418 type mice for 24 h treated with the STAT6 inhibitor AS1517499 or DMSO vehicle control.  
1419 Each dot represents different mice.

1420 Values are presented as the mean  $\pm$  SEM of three independent experiments measured in  
1421 duplicate. In panels A, B, C, E, F and G, unpaired t test was used to determine statistical  
1422 significance. In panels H, I and J, statistical analysis were carried out using one-way ANOVA  
1423 with Bonferroni contrast for multiple comparisons test. \*\*\*\*P  $\leq$  0.0001; \*\*\*P  $\leq$  0.001; \*\* P  
1424  $\leq$  0.01; ns, P > 0.05 for the indicated comparisons determined using unpaired t test.  
1425 \*\*\*\*P  $\leq$  0.0001; \*\*\*P  $\leq$  0.001; \*\* P  $\leq$  0.01; \*P  $\leq$  0.05; ns, P > 0.05 for the indicated  
1426 comparisons.

1427 **Figure 7. *K. pneumoniae*-induced M (Kp) polarisation is dependent on TLR signalling.**

1428 A. Immunoblot analysis of phospho-STAT6 (pSTAT6) and tubulin levels in lysates from  
1429 non-infected (ni) and infected wild-type (WT), *tlr2*<sup>-/-</sup>, *tlr4*<sup>-/-</sup> and *tlr2/4*<sup>-/-</sup> iBMDMs for 60 or  
1430 120 min.

1431 B. Immunoblot analysis of Arg1 and tubulin levels in lysates from non-infected (ni) and  
1432 infected wild-type (WT), *tlr2*<sup>-/-</sup>, *tlr4*<sup>-/-</sup> and *tlr2/4*<sup>-/-</sup> iBMDMs for 60 or 120 min.

1433 C. *arg1* mRNA levels were assessed by qPCR in wild-type (WT) and *tlr2*<sup>-/-</sup>, *tlr4*<sup>-/-</sup> and *tlr2/4*<sup>-/-</sup>  
1434 iBMDMs non-infected (ni) or infected with Kp52145 for 1, 3 or 5 h.

1435 D. *fizz1* mRNA levels were assessed by qPCR in wild-type (WT) and *tlr2*<sup>-/-</sup>, *tlr4*<sup>-/-</sup> and *tlr2/4*<sup>-/-</sup>  
1436 iBMDMs non-infected (ni) or infected with Kp52145 for 1, 3 or 5 h.

1437 E. *il10* mRNA levels were assessed by qPCR in wild-type (WT) and *tlr2*<sup>-/-</sup>, *tlr4*<sup>-/-</sup> and *tlr2/4*<sup>-/-</sup>  
1438 iBMDMs non-infected (ni) or infected with Kp52145 for 1, 3 or 5 h.

1439 F. *nos2* mRNA levels were assessed by qPCR in wild-type (WT) and *tlr2*<sup>-/-</sup>, *tlr4*<sup>-/-</sup> and *tlr2/4*<sup>-/-</sup>  
1440 iBMDMs non-infected (ni) or infected with Kp52145 for 1, 3 or 5 h.

1441 G. *isg15* mRNA levels were assessed by qPCR in wild-type (WT) and *tlr2*<sup>-/-</sup>, *tlr4*<sup>-/-</sup> and *tlr2/4*  
1442 <sup>-/-</sup> iBMDMs non-infected (ni) or infected with Kp52145 for 1, 3 or 5 h.

1443 H. *mx1* mRNA levels were assessed by qPCR in wild-type (WT) and *tlr2*<sup>-/-</sup>, *tlr4*<sup>-/-</sup> and *tlr2/4*<sup>-/-</sup>  
1444 iBMDMs non-infected (ni) or infected with Kp52145 for 1, 3 or 5 h.

1445 I. *pparg* mRNA levels were assessed by qPCR in wild-type (WT) and *tlr2*<sup>-/-</sup>, *tlr4*<sup>-/-</sup> and *tlr2/4*  
1446 <sup>-/-</sup> iBMDMs non-infected (ni) or infected with Kp52145 for 1, 3 or 5 h.

1447 For all infections, after 1 h contact, medium replaced with medium containing gentamycin  
1448 (100 µg/ml) to kill extracellular bacteria. Error bars are presented as the mean ± SEM of three  
1449 independent experiments in duplicate. Images are representative of three independent  
1450 experiments. \*\*\*\*P ≤ 0.0001; \*\*\*P ≤ 0.001; \*\*P ≤ 0.01; \*P ≤ 0.05; ns, P > 0.05 for the  
1451 indicated comparisons using one way-ANOVA with Bonferroni contrast for multiple  
1452 comparisons test.

1453 **Figure 8. *K. pneumoniae*-induced M (Kp) polarisation is dependent on the TLR**  
1454 **adaptors MyD88, TRAM and TRIF.**

1455 A. Immunoblot analysis of phospho-STAT6 (pSTAT6) and tubulin levels in lysates from  
1456 non-infected (ni) and infected wild-type (WT), *myd88*<sup>-/-</sup>, *tram/trif*<sup>-/-</sup> for 60 or 120 min.

1457 B. Immunoblot analysis of Arg1 and tubulin levels in lysates from non-infected (ni) and  
1458 infected wild-type (WT), *myd88*<sup>-/-</sup>, *tram/trif*<sup>-/-</sup> for 60 or 120 min.

1459 C. *arg1* mRNA levels were assessed by qPCR in wild-type (WT), *myd88*<sup>-/-</sup>, *tram/trif*<sup>-/-</sup> non-  
1460 infected (ni) or infected with Kp52145 for 1, 3 or 5 h.

1461 D. *ill10* mRNA levels were assessed by qPCR in wild-type (WT), *myd88*<sup>-/-</sup>, *tram/trif*<sup>-/-</sup> non-  
1462 infected (ni) or infected with Kp52145 for 1, 3 or 5 h.  
1463 E. *pparg* mRNA levels were assessed by qPCR in wild-type (WT), *myd88*<sup>-/-</sup>, *tram/trif*<sup>-/-</sup> non-  
1464 infected (ni) or infected with Kp52145 for 1, 3 or 5 h.  
1465 F. *fizz1* mRNA levels were assessed by qPCR in wild-type (WT), *myd88*<sup>-/-</sup>, *tram/trif*<sup>-/-</sup> non-  
1466 infected (ni) or infected with Kp52145 for 1, 3 or 5 h.  
1467 G. *isg15* mRNA levels were assessed by qPCR in wild-type (WT), *myd88*<sup>-/-</sup>, *tram/trif*<sup>-/-</sup> non-  
1468 infected (ni) or infected with Kp52145 for 1, 3 or 5 h.  
1469 H. *mx1* mRNA levels were assessed by qPCR in wild-type (WT), *myd88*<sup>-/-</sup>, *tram/trif*<sup>-/-</sup> non-  
1470 infected (ni) or infected with Kp52145 for 1, 3 or 5 h.  
1471 I. *nos2* mRNA levels were assessed by qPCR in wild-type (WT), *myd88*<sup>-/-</sup>, *tram/trif*<sup>-/-</sup> non-  
1472 infected (ni) or infected with Kp52145 for 1, 3 or 5 h.  
1473 For all infections, after 1 h contact, medium replaced with medium containing gentamycin  
1474 (100 µg/ml) to kill extracellular bacteria. Error bars are presented as the mean ± SEM of three  
1475 independent experiments in duplicate. Images are representative of three independent  
1476 experiments. \*\*\*\*P ≤ 0.0001; \*\*\*P ≤ 0.001; \*\*P ≤ 0.01; \*P ≤ 0.05; ns, P > 0.05 for the  
1477 indicated comparisons using one way-ANOVA with Bonferroni contrast for multiple  
1478 comparisons test.

1479

1480 **Figure 9. *K. pneumoniae* exploits type I IFN signalling to induce M(Kp) polarisation.**

1481 A. Immunoblot analysis of phospho-STAT6 (pSTAT6) and tubulin levels in lysates from  
1482 non-infected (ni) and infected wild-type (WT), or *ifnar1*<sup>-/-</sup> for 60 or 120 min.  
1483 B. Immunoblot analysis of Arg1 and tubulin levels in lysates from non-infected (ni) and  
1484 infected wild-type (WT), or *ifnar1*<sup>-/-</sup> for 60 or 120 min. *arg1* mRNA levels were assessed by  
1485 qPCR in wild-type (WT), *irf3*<sup>-/-</sup>, *ifnar1*<sup>-/-</sup> non-infected (ni) or infected with Kp52145 for 1, 3  
1486 or 5 h.  
1487 C. *nos2* mRNA levels were assessed by qPCR in wild-type (WT), *irf3*<sup>-/-</sup>, *ifnar1*<sup>-/-</sup> non-  
1488 infected (ni) or infected with Kp52145 for 1, 3 or 5 h.  
1489 D. *pparg* mRNA levels were assessed by qPCR in wild-type (WT), *irf3*<sup>-/-</sup>, *ifnar1*<sup>-/-</sup> non-  
1490 infected (ni) or infected with Kp52145 for 1, 3 or 5 h.  
1491 E. *fizz1* mRNA levels were assessed by qPCR in wild-type (WT), *irf3*<sup>-/-</sup>, *ifnar1*<sup>-/-</sup> non-  
1492 infected (ni) or infected with Kp52145 for 1, 3 or 5 h.  
1493 F. *ill10* mRNA levels were assessed by qPCR in wild-type (WT), *irf3*<sup>-/-</sup>, *ifnar1*<sup>-/-</sup> non-infected  
1494 (ni) or infected with Kp52145 for 1, 3 or 5 h.

1495 G. Percentage of wild-type (WT) and *ifnar1*<sup>-/-</sup> iBMDMs with and without associated  
1496 Kp52145 positive for Arg1 1, 3 or 5 h post infection. Kp52145 was tagged with mCherry.

1497 H. Percentage of wild-type (WT) and *ifnar1*<sup>-/-</sup> iBMDMs with and without associated  
1498 Kp52145 positive for CD206 1, 3 or 5 h post infection. Kp52145 was tagged with mCherry.

1499 I. Percentage of wild-type (WT) and *ifnar1*<sup>-/-</sup> iBMDMs with and without associated Kp52145  
1500 positive for MHCII 1, 3 or 5 h post infection. Kp52145 was tagged with mCherry.

1501 J. Immunoblot analysis of phospho-STAT6 (pSTAT6) and tubulin levels in lysates from non-  
1502 infected (ni) and infected wild-type (WT), or *irf3*<sup>-/-</sup> for 60 or 120 min.

1503 K. Immunoblot analysis of Arg1 and tubulin levels in lysates from non-infected (ni) and  
1504 infected wild-type (WT), or *irf3*<sup>-/-</sup> for 60 or 120 min.

1505 For all infections, after 1 h contact, medium replaced with medium containing gentamycin  
1506 (100 µg/ml) to kill extracellular bacteria. Error bars are presented as the mean ± SEM of three  
1507 independent experiments in duplicate. Images are representative of three independent  
1508 experiments. \*\*\*\*P ≤ 0.0001; \*\*\*P ≤ 0.001; \*\*P ≤ 0.01; \*P ≤ 0.05; ns, P > 0.05 for the  
1509 indicated comparisons using one way-ANOVA with Bonferroni contrast for multiple  
1510 comparisons test.

1511 **Figure 10. *K. pneumoniae*-induced M(Kp) polarisation is dependent on IL10.**

1512 A. Immunoblot analysis of phospho-CREB (pCREB) and tubulin levels in lysates from non-  
1513 infected (ni) and infected wild-type (WT), or *tlr4*<sup>-/-</sup> for 60 or 120 min.

1514 B. Immunoblot analysis of phospho-CREB (pCREB) and tubulin levels in lysates from non-  
1515 infected (ni) and infected wild-type (WT), or *myd88*<sup>-/-</sup> for 60 or 120 min.

1516 C. *il0* mRNA levels were assessed by qPCR in iBMDMs transfected with All Stars siRNA  
1517 control (AS), or CREB siRNA (CREBsi) non-infected (ni) or infected with Kp52145 for 3 h.  
1518 After 1 h contact, the medium was replaced with medium containing gentamicin (100 µg/ml)  
1519 to kill extracellular bacteria.

1520 D. Immunoblot analysis of phospho-STAT6 (pSTAT6) and tubulin levels in lysates from  
1521 non-infected (ni) and infected wild-type (WT), or *il10*<sup>-/-</sup> for 60 or 120 min.

1522 E. *arg1* mRNA levels were assessed by qPCR in wild-type (WT), *il10*<sup>-/-</sup> non-infected (ni) or  
1523 infected with Kp52145 for 1, 3 or 5 h. Immunoblot analysis of Arg1 and tubulin levels in  
1524 lysates from non-infected (ni) and infected wild-type (WT), or *il10*<sup>-/-</sup> for 60 or 120 min.

1525 F. *pparg* mRNA levels were assessed by qPCR in wild-type (WT), *il10*<sup>-/-</sup> non-infected (ni) or  
1526 infected with Kp52145 for 1, 3 or 5 h.

1527 G. *fizz1* mRNA levels were assessed by qPCR in wild-type (WT), *il10*<sup>-/-</sup> non-infected (ni) or  
1528 infected with Kp52145 for 1, 3 or 5 h.

- 1529 H. *nos2* mRNA levels were assessed by qPCR in wild-type (WT), *il10*<sup>-/-</sup> non-infected (ni) or  
1530 infected with Kp52145 for 1, 3 or 5 h.
- 1531 I. *tnfa* mRNA levels were assessed by qPCR in wild-type (WT), *il10*<sup>-/-</sup> non-infected (ni) or  
1532 infected with Kp52145 for 1, 3 or 5 h.
- 1533 J. *mx1* mRNA levels were assessed by qPCR in wild-type (WT), *il10*<sup>-/-</sup> non-infected (ni) or  
1534 infected with Kp52145 for 1, 3 or 5 h.
- 1535 K. *isg15* mRNA levels were assessed by qPCR in wild-type (WT), *il10*<sup>-/-</sup> non-infected (ni) or  
1536 infected with Kp52145 for 1, 3 or 5 h.
- 1537 L. Percentage of wild-type (WT) and *il10*<sup>-/-</sup> iBMDMs with and without associated Kp52145  
1538 positive for Arg1 1, 3 or 5 h post infection. Kp52145 was tagged with mCherry.
- 1539 M. Percentage of wild-type (WT) and *il10*<sup>-/-</sup> iBMDMs with and without associated Kp52145  
1540 positive for CD206 1, 3 or 5 h post infection. Kp52145 was tagged with mCherry.
- 1541 N. Percentage of wild-type (WT) and *il10*<sup>-/-</sup> iBMDMs with and without associated Kp52145  
1542 positive for MHCII 1, 3 or 5 h post infection. Kp52145 was tagged with mCherry.
- 1543 O. Kp52145 adhesion to wild-type (WT) and *il10*<sup>-/-</sup> iBMDMs. Cells were infected with  
1544 Kp52145 for 30 min, washed, cell lysed with saponin, and bacteria quantified after serial  
1545 dilution followed by plating on LB agar plates.
- 1546 P. Phagocytosis of Kp52145 by wild-type (WT) and *il10*<sup>-/-</sup> iBMDMs. Cells were infected for  
1547 30 min, wells were washed, and it was added medium containing gentamicin (100 µg/ml) to  
1548 kill extracellular bacteria. After 30 min, cells were washed, cell lysed with saponin, and  
1549 bacteria quantified after serial dilution followed by plating on LB agar plates.
- 1550 Q. Kp52145 intracellular survival in wild-type (WT) and *il10*<sup>-/-</sup> 5 h after addition of  
1551 gentamycin (30 min of contact). Results are expressed as % of survival (CFUs at 5 h versus  
1552 30 min in *stat6*<sup>-/-</sup> cells normalized to the results obtained in wild-type macrophages set to  
1553 100%).
- 1554 R. Immunofluorescence confocal microscopy of the colocalization of Kp52145 harbouring  
1555 pFPV25.1Cm, and cresyl violet dye in wild-type (WT) and *il10*<sup>-/-</sup> macrophages. The images  
1556 were taken 90 min post infection. Images are representative of duplicate coverslips of three  
1557 independent experiments.
- 1558 S. Percentage of Kp52145 harbouring pFPV25.1Cm co-localization with cresyl violet over a  
1559 time course. Wild-type (WT) and *il10*<sup>-/-</sup> macrophages were infected; coverslips were fixed  
1560 and stained at the indicated times. Values are given as mean percentage of Kp52145 co-

1561 localizing with the marker  $\square \pm \square$  SEM. The number of infected cells counted per time in three  
1562 independent experiments are indicated in the figure.

1563 For all infections, after 1 h contact, medium replaced with medium containing gentamycin  
1564 (100  $\mu\text{g/ml}$ ) to kill extracellular bacteria. Error bars are presented as the mean  $\pm$  SEM of three  
1565 independent experiments in duplicate. Images are representative of three independent  
1566 experiments. In panels O, P, and Q unpaired t test was used to determine statistical  
1567 significance. In all the other panels, statistical analysis were carried out using one-way  
1568 ANOVA with Bonferroni contrast for multiple comparisons test. \*\*\*\*P  $\leq$  0.0001; \*\*\*P  $\leq$   
1569 0.001; \*\*P  $\leq$  0.01; \*P  $\leq$  0.05; ns, P  $>$  0.05 for the indicated comparisons.

1570 **Figure 11. Glycolysis characterizes *K. pneumoniae*-induced M(Kp) polarisation.**

1571 A. Dot Plot analysis of the expression levels of genes related to fatty acid oxidation (FAO)  
1572 and glycolysis from the scRNAseq data set of PBS-infected IMs (control), and bystander and  
1573 Kp52145-associated IMs. Dot size reflects percentage of cells in a cluster expressing each  
1574 gene; dot colour intensity reflects expression level as indicated on legend.

1575 B. Extracellular acidification rate (ECAR, in mpH/min) of non-infected (ni) and Kp52145-  
1576 infected iBMDMs (Kp52145) measured using Mito-stress test kit and the Seahorse XF  
1577 analyser. When indicated oligomycin (2.5  $\mu\text{M}$ ), FCCP (2  $\mu\text{M}$ ), antimycin and roteanone (0.5  
1578  $\mu\text{M}$ ) were added to the cells.

1579 C. Oxygen consumption rates (OCR, in pMoles/min) of non-infected (ni) and Kp52145-  
1580 infected iBMDMs (Kp52145) measured using Mito-stress test kit and the Seahorse XF  
1581 analyser. When indicated oligomycin (2.5  $\mu\text{M}$ ), FCCP (2  $\mu\text{M}$ ), antimycin and roteanone (0.5  
1582  $\mu\text{M}$ ) were added to the cells.

1583 D. Basal respiration of non-infected (ni) and Kp52145-infected iBMDMs.

1584 E. Maximal respiration of non-infected (ni) and Kp52145-infected iBMDMs.

1585 F. Spare respiratory capacity of non-infected (ni) and Kp52145-infected iBMDMs.

1586 G. ATP production by non-infected (ni) and Kp52145-infected iBMDMs.

1587 H. Non mitochondrial O<sub>2</sub> consumption by non-infected (ni) and Kp52145-infected iBMDMs.

1588 I. Kp52145 intracellular survival in wild-type iBMDMs 5 h after addition of gentamycin (30  
1589 min of contact). Results are expressed as % of survival (CFUs at 5 h versus 30 min in *stat6*<sup>-/-</sup>



1590 cells normalized to the results obtained in wild-type macrophages set to 100%). Cells were  
1591 treated with DMSO vehicle, or 2-deoxyglucose (2DG, 3  $\mu$ M), oligomycin (3  $\mu$ M), etomoxir  
1592 (50  $\mu$ M) 2 h before infection and maintained thought.

1593 J. Immunofluorescence confocal microscopy of the colocalization of Kp52145 harbouring  
1594 pFPV25.1Cm, and cresyl violet dye in wild-type macrophages treated with DMSO vehicle  
1595 solution (control) or 2DG. The images were taken 90 min post infection. Images are  
1596 representative of duplicate coverslips of three independent experiments.

1597 K. Percentage of Kp52145 harbouring pFPV25.1Cm co-localization with cresyl violet over a  
1598 time course. Wild-type iBMDMs treated with DMSO vehicle solution (control) or 2DG. were  
1599 infected; coverslips were fixed and stained at the indicated times. Values are given as mean  
1600 percentage of Kp52145 co-localizing with the marker  $\pm$  SEM. The number of infected cells  
1601 counted per time in three independent experiments are indicated in the figure.

1602 Error bars are presented as the mean  $\pm$  SEM of three independent experiments in duplicate.  
1603 Images are representative of three independent experiments. In panels D, E, F, G, H, and K  
1604 unpaired t test was used to determine statistical significance. In all the other panels, statistical  
1605 analysis were carried out using one-way ANOVA with Bonferroni contrast for multiple  
1606 comparisons test. \*\*\*\*P  $\leq$  0.0001; \*\*\*P  $\leq$  0.001; \*\*P  $\leq$  0.01; \*P  $\leq$  0.05; ns, P > 0.05 for the  
1607 indicated comparisons.

1608 **Figure 12. *K. pneumoniae*-governed M(Kp) is dependent on the capsule polysaccharide.**

1609 A. Immunoblot analysis of phospho-STAT6 (pSTAT6) and tubulin levels in lysates from  
1610 wild-type macrophages non-infected (ni), or infected with Kp52145 or the LPS O-  
1611 polysaccharide mutant, strain 52145- $\Delta$ glf, for 60 or 120 min.

1612 B. Percentage of wild-type macrophages with and without associated Kp52145 or 52145- $\Delta$ glf  
1613 positive for CD206 5 h post infection. Bacteria were tagged with mCherry.

1614 C. Immunoblot analysis of phospho-STAT6 (pSTAT6) and tubulin levels in lysates from  
1615 wild-type macrophages non-infected (ni), or infected with Kp52145 or the CPS mutant, strain  
1616 52145- $\Delta$ wca<sub>K2</sub>, for 60 or 120 min.

1617 D. *arg1* mRNA levels were assessed by qPCR in wild-type macrophages non-infected (ni) or  
1618 infected Kp52145 or the CPS mutant, strain 52145- $\Delta$ wca<sub>K2</sub>, for 1, 3 or 5 h.

1619 E. Percentage of wild-type macrophages with and without associated Kp52145 or 52145-  
1620  $\Delta wca_{K2}$  positive for Arg1 5 h post infection. Bacteria were tagged with mCherry.

1621 F. Percentage of wild-type macrophages with and without associated Kp52145 or 52145-  
1622  $\Delta wca_{K2}$  positive for CD206 5 h post infection. Bacteria were tagged with mCherry.

1623 G. Percentage of wild-type macrophages with and without associated Kp52145 or 52145-  
1624  $\Delta wca_{K2}$  positive for MHCII 5 h post infection. Bacteria were tagged with mCherry.

1625 For all infections, after 1 h contact, medium replaced with medium containing gentamycin  
1626 (100  $\mu$ g/ml) to kill extracellular bacteria. Error bars are presented as the mean  $\pm$  SEM of three  
1627 independent experiments in duplicate or triplicate. Images are representative of three  
1628 independent experiments. Statistical analysis were carried out using one-way ANOVA with  
1629 Bonferroni contrast for multiple comparisons test. \*\*\*\*P  $\leq$  0.0001; \*\*\*P  $\leq$  0.001; \*P  $\leq$  0.05;  
1630 ns, P > 0.05 for the indicated comparisons.

1631 **Figure 13. *K. pneumoniae* induces M(Kp) polarization in human macrophages.**

1632 A. *arg1* mRNA levels were assessed by qPCR in hM-CSF-treated PBMCs from 6 donors  
1633 non-infected (ni) or infected Kp52145 for 1, 3 or 5 h.

1634 B. *il10* mRNA levels were assessed by qPCR in M-CSF-treated PBMCs from 6 donors non-  
1635 infected (ni) or infected Kp52145 for 1, 3 or 5 h.

1636 C. *chi3l* mRNA levels were assessed by qPCR in hM-CSF-treated PBMCs from 6 donors  
1637 non-infected (ni) or infected Kp52145 for 1, 3 or 5 h.

1638 D. *pparg* mRNA levels were assessed by qPCR in hM-CSF-treated PBMCs from 6 donors  
1639 non-infected (ni) or infected Kp52145 for 1, 3 or 5 h.

1640 E. *mrc1* mRNA levels were assessed by qPCR in hM-CSF-treated PBMCs from 6 donors  
1641 non-infected (ni) or infected Kp52145 for 1, 3 or 5 h.

1642 F. *nos2* mRNA levels were assessed by qPCR in hM-CSF-treated PBMCs from 6 donors  
1643 non-infected (ni) or infected Kp52145 for 1, 3 or 5 h.

1644 G. *isg56* mRNA levels were assessed by qPCR in hM-CSF-treated PBMCs from 6 donors  
1645 non-infected (ni) or infected Kp52145 for 1, 3 or 5 h.

1646 H. *illrn* mRNA levels were assessed by qPCR in hM-CSF-treated PBMCs from 6 donors  
1647 non-infected (ni) or infected Kp52145 for 1, 3 or 5 h.

1648 I. *ido* mRNA levels were assessed by qPCR in hM-CSF-treated PBMCs from 6 donors non-  
1649 infected (ni) or infected Kp52145 for 1, 3 or 5 h.

1650 J. Immunoblot analysis of phospho-STAT6 (pSTAT6) and tubulin levels in lysates from  
1651 PMA-treated THP-1 macrophages non-infected (ni), or infected with Kp52145 for 60 or 120  
1652 min

1653 K. *argl* mRNA levels were assessed by qPCR in PMA-treated THP-1 macrophages non-  
1654 infected (ni) or infected Kp52145 for 1, 3 or 5 h and treated with the STAT6 inhibitor  
1655 AS1517499 or DMSO vehicle control.

1656 L. *il10* mRNA levels were assessed by qPCR in PMA-treated THP-1 macrophages non-  
1657 infected (ni) or infected Kp52145 for 1, 3 or 5 h and treated with the STAT6 inhibitor  
1658 AS1517499 or DMSO vehicle control.

1659 M. *nos2* mRNA levels were assessed by qPCR in PMA-treated THP-1 macrophages non-  
1660 infected (ni) or infected Kp52145 for 1, 3 or 5 h and treated with the STAT6 inhibitor  
1661 AS1517499 or DMSO vehicle control.

1662 N. *isg56* mRNA levels were assessed by qPCR in PMA-treated THP-1 macrophages non-  
1663 infected (ni) or infected Kp52145 for 1, 3 or 5 h and treated with the STAT6 inhibitor  
1664 AS1517499 or DMSO vehicle control.

1665 O. *ido* mRNA levels were assessed by qPCR in PMA-treated THP-1 macrophages non-  
1666 infected (ni) or infected Kp52145 for 1, 3 or 5 h and treated with the STAT6 inhibitor  
1667 AS1517499 or DMSO vehicle control.

1668 P. *argl* mRNA levels were assessed by qPCR in PMA-treated THP-1 macrophages non-  
1669 infected (ni) or infected Kp52145 for 1, 3 or 5 h and treated with IFNAR1 blocking antibody  
1670 or isotype control.

1671 Q. *ido* mRNA levels were assessed by qPCR in PMA-treated THP-1 macrophages non-  
1672 infected (ni) or infected Kp52145 for 1, 3 or 5 h and treated with IFNAR1 blocking antibody  
1673 or isotype control.

1674 R. *arg1* mRNA levels were assessed by qPCR in PMA-treated THP-1 macrophages non-  
1675 infected (ni) or infected Kp52145 for 1, 3 or 5 h and treated with IL10 blocking antibody or  
1676 isotype control.

1677 S. *ido* mRNA levels were assessed by qPCR in PMA-treated THP-1 macrophages non-  
1678 infected (ni) or infected Kp52145 for 1, 3 or 5 h and treated with IL10 blocking antibody or  
1679 isotype control.

1680 T. Immunoblot analysis of phospho-STAT6 (pSTAT6) and tubulin levels in lysates from  
1681 PMA-treated THP-1 macrophages non-infected (ni), or infected with Kp52145 or the CPS  
1682 mutant, strain 52145- $\Delta wca_{K2}$ , for 60 or 120 min.

1683 U. Percentage of PMA-treated THP-1 macrophages with and without associated Kp52145 or  
1684 52145- $\Delta wca_{K2}$  positive for Arg1 5 h post infection. Bacteria were tagged with mCherry.

1685 V. Percentage of PMA-treated THP-1 macrophages with and without associated Kp52145 or  
1686 52145- $\Delta wca_{K2}$  positive for CD206 5 h post infection. Bacteria were tagged with mCherry.

1687 For all infections, after 1 h contact, medium replaced with medium containing gentamycin  
1688 (100  $\mu$ g/ml) to kill extracellular bacteria. Error bars are presented as the mean  $\pm$  SEM of three  
1689 independent experiments in duplicate. Images are representative of three independent  
1690 experiments. Statistical analysis were carried out using one-way ANOVA with Bonferroni  
1691 contrast for multiple comparisons test. \*\*\*\*P  $\leq$  0.0001; \*\*\*P  $\leq$  0.001; \*\*P  $\leq$  0.01; \*P  $\leq$  0.05;  
1692 ns, P > 0.05 for the indicated comparisons.

1693

1694

1695

1696

1697

1698

1699 *Supplementary figure legends*

1700 **Figure S1. Flow cytometric analysis of myeloid subsets in lungs of *K. pneumoniae*-**  
1701 **infected mice.**

1702 Gating strategy utilised to identify CD11b+CD11c-SiglecF- monocytes (MN),  
1703 CD11b+CD11c+SiglecF- interstitial macrophages (IMs) and CD11b-CD11c+SiglecF+ tissue  
1704 resident alveolar macrophages (AMs). Kp52145 was tagged with mCherry to allow the  
1705 identification of macrophages with associated bacteria and bystander cells. This gating  
1706 strategy was utilised also for FACS sorting of these populations for scRNAseq.

1707 **Figure S2. Network enrichment mapping of significantly downregulated genes of IMs.**

1708 Analysis was performed using the g:SCS method for multiple testing correction (gProflier),  
1709 the Reactome database as a data source, and the default settings for the other parameters in  
1710 gProflier. Results were exported to Cytoscape and visualized using the AutoAnnotate plug.

1711 A. Kp52145-infected IMs.

1712 B. Bystander IMs.

1713 **Figure S3. Network enrichment mapping of significantly upregulated genes of infected**  
1714 **AMs.**

1715 Analysis was performed using the g:SCS method for multiple testing correction (gProflier),  
1716 the Reactome database as a data source, and the default settings for the other parameters in  
1717 gProflier. Results were exported to Cytoscape and visualized using the AutoAnnotate plug.

1718 **Figure S4. Trajectory analysis of AMs from PBS-mock infected mice, and *K.***  
1719 ***pneumoniae* infected mice.**

1720 Monocle analysis did not reveal any clear trajectory in AMs from non-infected, or infected  
1721 mice.

1722 **Figure S5. Network enrichment mapping of significantly upregulated pathways within**  
1723 **modules 1 and 7 of *K. pneumoniae*-infected IMs.**

1724 Analysis was performed using the g:SCS method for multiple testing correction (gProflier),  
1725 the Reactome database as a data source, and the default settings for the other parameters in  
1726 gProflier. Results were exported to Cytoscape and visualized using the AutoAnnotate plug.

1727 **Figure S6. Expression of macrophage polarisation markers in bystander and *K.***  
1728 ***pneumoniae*-infected AMs.**

1729 Dot Plot analysis of the expression levels of genes related to M1 and M2 polarisation from  
1730 the scRNAseq data set of PBS-infected AMs cells (control), and bystander and Kp52145-  
1731 associated AM. Dot size reflects percentage of cells in a cluster expressing each gene; dot  
1732 colour intensity reflects expression level as indicated on legend.

1733 **Figure S7. *K. pneumoniae* induces M(Kp) polarisation in immortalized BMDMs.**

1734 A. *arg1* mRNA levels were assessed by qPCR in wild-type iBMDMs non-infected (ni) or  
1735 infected with Kp52145 for 1, 3 or 5 h. Immunoblot analysis of Arg1 and tubulin levels in  
1736 lysates from non-infected (ni) and infected wild-type cells with Kp52145 for 60 or 120 min.

1737 B. *fizz1* mRNA levels were assessed by qPCR in wild-type iBMDMs non-infected (ni) or  
1738 infected with Kp52145 for 1, 3 or 5 h. Immunoblot analysis of Fizz1 and tubulin levels in  
1739 lysates from non-infected (ni) and infected wild-type cells with Kp52145 for 60 or 120 min.

1740 C. *pparg* mRNA levels were assessed by qPCR in wild-type iBMDMs non-infected (ni) or  
1741 infected with Kp52145 for 1, 3 or 5 h.

1742 D. *nos2* mRNA levels were assessed by qPCR in wild-type iBMDMs non-infected (ni) or  
1743 infected with Kp52145 for 1, 3 or 5 h.

1744 E. *il12* mRNA levels were assessed by qPCR in wild-type iBMDMs non-infected (ni) or  
1745 infected with Kp52145 for 1, 3 or 5 h.

1746 F. *il6* mRNA levels were assessed by qPCR in wild-type iBMDMs non-infected (ni) or  
1747 infected with Kp52145 for 1, 3 or 5 h.

1748 G. *tnfa* mRNA levels were assessed by qPCR in wild-type iBMDMs non-infected (ni) or  
1749 infected with Kp52145 for 1, 3 or 5 h.

1750 H. *il10* mRNA levels were assessed by qPCR in wild-type iBMDMs non-infected (ni) or  
1751 infected with Kp52145 for 1, 3 or 5 h.

1752 I. Immunoblot analysis of phospho-STAT3 (pSTAT3) and tubulin levels in lysates from non-  
1753 infected (ni) and infected wild-type cells with Kp52145 for 60 or 120 min.



1754 For all infections, after 1 h contact, medium replaced with medium containing gentamycin  
1755 (100 µg/ml) to kill extracellular bacteria. Error bars are presented as the mean ± SEM of three  
1756 independent experiments in duplicate. Images are representative of three independent  
1757 experiments. Statistical analysis were carried out using one-way ANOVA with Bonferroni  
1758 contrast for multiple comparisons test. \*\*\*\*P ≤ 0.0001; \*\*P ≤ 0.01; \*P ≤ 0.05; ns, P > 0.05  
1759 for the indicated comparisons.

1760 **Figure S8. *K. pneumoniae*-induced M(Kp) polarisation is STAT6-dependent.**

1761 A. *arg1* mRNA levels were assessed by qPCR in wild-type iBMDMs non-infected (ni) or  
1762 infected with Kp52145 for 1, 3 or 5 h treated with STAT6 inhibitor AS1517499 or vehicle  
1763 control.

1764 B. *il10* mRNA levels were assessed by qPCR in wild-type iBMDMs non-infected (ni) or  
1765 infected with Kp52145 for 1, 3 or 5 h treated with STAT6 inhibitor AS1517499 or vehicle  
1766 control.

1767 C. *fizz1* mRNA levels were assessed by qPCR in wild-type iBMDMs non-infected (ni) or  
1768 infected with Kp52145 for 1, 3 or 5 h treated with STAT6 inhibitor AS1517499 or vehicle  
1769 control.

1770 D. *nos2* mRNA levels were assessed by qPCR in wild-type iBMDMs non-infected (ni) or  
1771 infected with Kp52145 for 1, 3 or 5 h treated with STAT6 inhibitor AS1517499 or vehicle  
1772 control.

1773 E. *il12* mRNA levels were assessed by qPCR in wild-type iBMDMs non-infected (ni) or  
1774 infected with Kp52145 for 1, 3 or 5 h treated with STAT6 inhibitor AS1517499 or vehicle  
1775 control.

1776 F. *isg15* mRNA levels were assessed by qPCR in wild-type iBMDMs non-infected (ni) or  
1777 infected with Kp52145 for 1, 3 or 5 h treated with STAT6 inhibitor AS1517499 or vehicle  
1778 control.

1779 For all infections, after 1 h contact, medium replaced with medium containing gentamycin  
1780 (100 µg/ml) to kill extracellular bacteria. Error bars are presented as the mean ± SEM of three  
1781 independent experiments in duplicate. Statistical analysis were carried out using one-way

1782 ANOVA with Bonferroni contrast for multiple comparisons test. \*\*\*\*P  $\leq$  0.0001; \*\*\*P  $\leq$   
1783 0.001; \*\*P  $\leq$  0.01; \*P  $\leq$  0.05; ns, P > 0.05 for the indicated comparisons.

1784 **Figure S9. Neither IL10 nor type I IFN activate STAT6.**

1785 A. Immunoblot analysis of phospho-STAT6 (pSTAT6) and tubulin levels in lysates from  
1786 non-infected (ni) and cells treated with recombinant IL10 (250  $\mu$ g/ml), recombinant IFN $\beta$   
1787 (1000 units/ml) or both for 3 h.

1788 B. Immunoblot analysis of Arg1 and tubulin levels in lysates from non-infected (ni) and cells  
1789 treated with recombinant IL10 (250  $\mu$ g/ml), recombinant IFN $\beta$  (1000 units/ml) or both for 3  
1790 h.

1791 Images are representative of three independent experiments.

1792 **Figure S10. Knockdown efficiency of CREB in iBMDMs using siRNA.**

1793 Efficiency of transfection of CREB siRNA (siCREB) in wild-type macrophages. mRNA  
1794 levels were assessed 16 h post transfection as fold change against control non-silencing  
1795 agents AllStars (siAS). Values are presented as the mean  $\pm$  SEM of three independent  
1796 experiments measured in duplicate. \*\*P  $\leq$  0.01 unpaired t test.

1797

1798 **Figure S11. STAT6 governed M(Kp) metabolism.**

1799 A. Extracellular acidification rate (ECAR, in mpH/min) of non-infected (ni) and Kp52145-  
1800 infected iBMDMS (Kp52145) treated with DMSO vehicle control or the STAT6 inhibitor  
1801 AS1517499 measured using Mito-stress test kit and the Seahorse XF analyser. When  
1802 indicated oligomycin (2.5  $\mu$ M), FCCP (2  $\mu$ M), antimycin and rotenone (0.5  $\mu$ M) were added  
1803 to the cells.

1804 B. Oxygen consumption rates (OCR, in pMoles/min) of non-infected (ni) and Kp52145-  
1805 infected iBMDMS (Kp52145) treated with DMSO vehicle control or the STAT6 inhibitor  
1806 AS1517499 measured using Mito-stress test kit and the Seahorse XF analyser. When  
1807 indicated oligomycin (2.5  $\mu$ M), FCCP (2  $\mu$ M), antimycin and rotenone (0.5  $\mu$ M) were added  
1808 to the cells.

1809 For each measurement, the standard error of the mean (SEM) of eight individual wells in  
1810 three independent experiments is presented.

1811 **Figure S12. Upregulation of genes related to glycolysis in AMs following infection.**

1812 Dot Plot analysis of the expression levels of genes related to fatty acid oxidation (FAO) and  
1813 glycolysis from the scRNAseq data set of PBS-infected AMs (control), and bystander and  
1814 Kp52145-associated AMs. Dot size reflects percentage of cells in a cluster expressing each  
1815 gene; dot colour intensity reflects expression level as indicated on legend.

1816 **Figure S13. Effect of inhibition of host metabolism on *K. pneumoniae*-macrophage  
1817 interface.**

1818 A. Growth kinetics of Kp52145 cultures in LB containing the glycolysis inhibitor 2-  
1819 doxyglucose (2DG, 3  $\mu$ M), the FAO inhibitors oligomycin (1  $\mu$ M) or etomoxir (50  $\mu$ M), or  
1820 DMSO vehicle control. Values are presented as the mean  $\pm$  SEM of three independent  
1821 experiments measured in triplicate

1822 B. Adhesion of Kp52145 to iBMDMs treated with DMSO vehicle control or the glycolysis  
1823 inhibitor 2-doxyglucose (2DG, 3  $\mu$ M), the FAO inhibitors oligomycin (1  $\mu$ M) or etomoxir (50  
1824  $\mu$ M). Inhibitors were added 2 h before and maintained throughout.

1825 C. Phagocytosis of Kp52145 by iBMDMs treated with DMSO vehicle control or the  
1826 glycolysis inhibitor 2-doxyglucose (2DG, 3  $\mu$ M), the FAO inhibitors oligomycin (1  $\mu$ M) or  
1827 etomoxir (50  $\mu$ M). Inhibitors were added 2 h before and maintained throughout.

1828 D. Activation of NF- $\kappa$ B signalling measured by quantifying SEAP secreted to the  
1829 supernatants of Raw-Blue cells (InvivoGen) following infection with Kp52145. Cells treated  
1830 with DMSO, 2DG (3  $\mu$ M), oligomycin (1  $\mu$ M) or etomoxir (50  $\mu$ M) 2 h before infection and  
1831 maintained throughout experiment.

1832 E. Activation of Irf3 measured by quantifying secreted Lucia luciferase to the supernatants of  
1833 Raw-Lucia ISG cells (InvivoGen) following infection with Kp52145. Cells treated with  
1834 DMSO, 2DG (3  $\mu$ M), oligomycin (1  $\mu$ M) or etomoxir (50  $\mu$ M) 2 h before infection and  
1835 maintained throughout experiment.

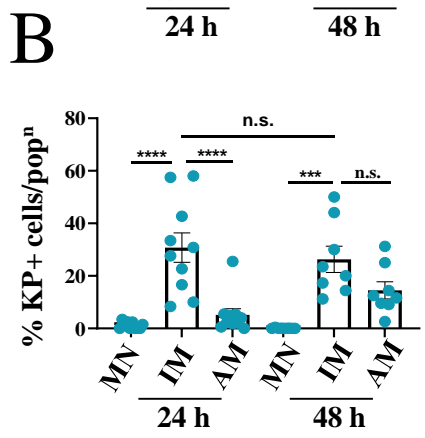
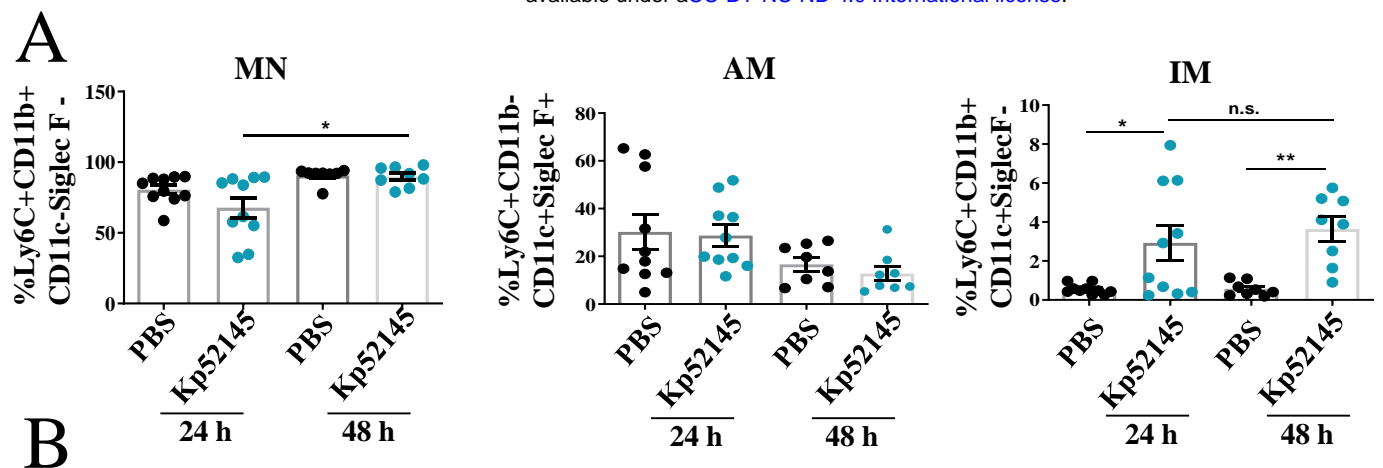
1836 For all infections, after 1 h contact, medium replaced with medium containing gentamycin  
1837 (100  $\mu$ g/ml) to kill extracellular bacteria. Error bars are presented as the mean  $\pm$  SEM of three  
1838 independent experiments in duplicate. Statistical analysis were carried out using one-way

1839 ANOVA with Bonferroni contrast for multiple comparisons test. \*\*\*\* $P \leq 0.0001$ ; ns,  $P >$

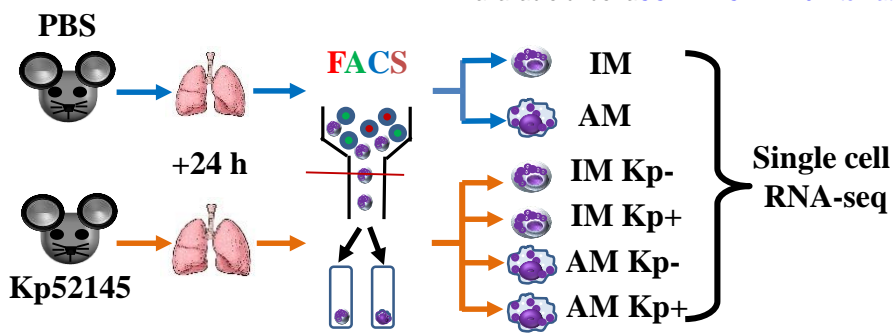
1840 0.05 for the indicated comparisons.

1841

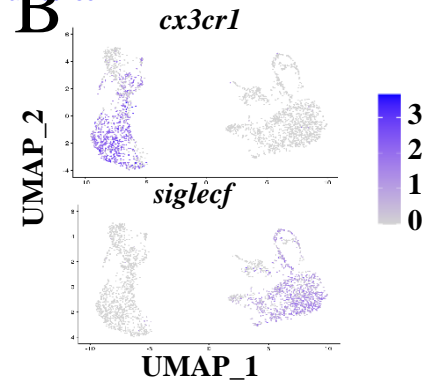
1842



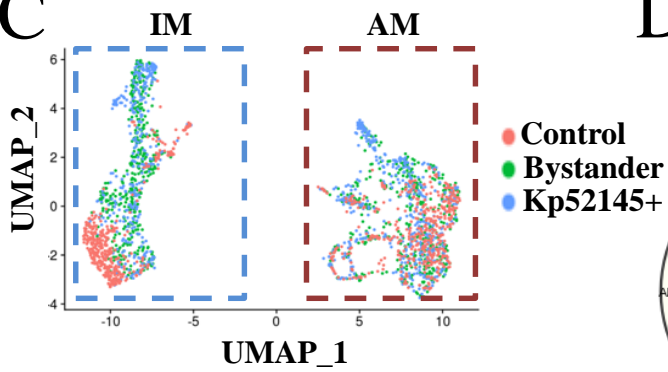
**A**



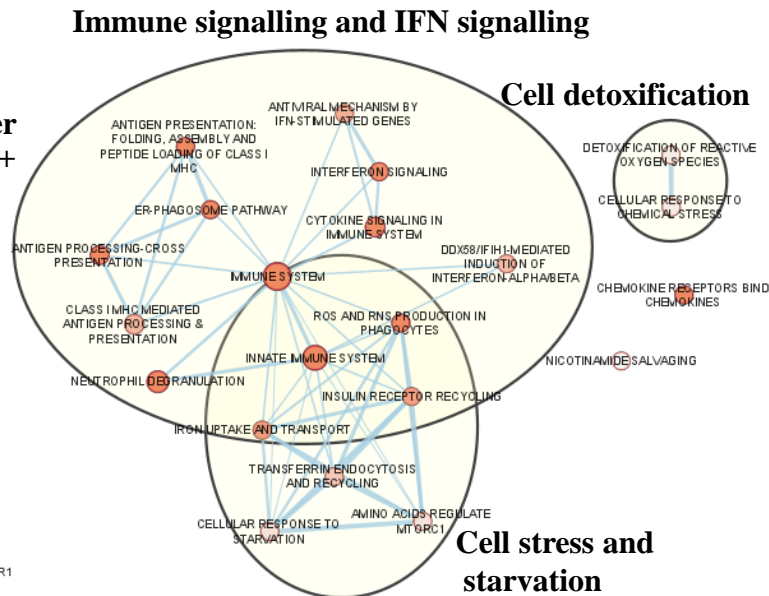
**B**



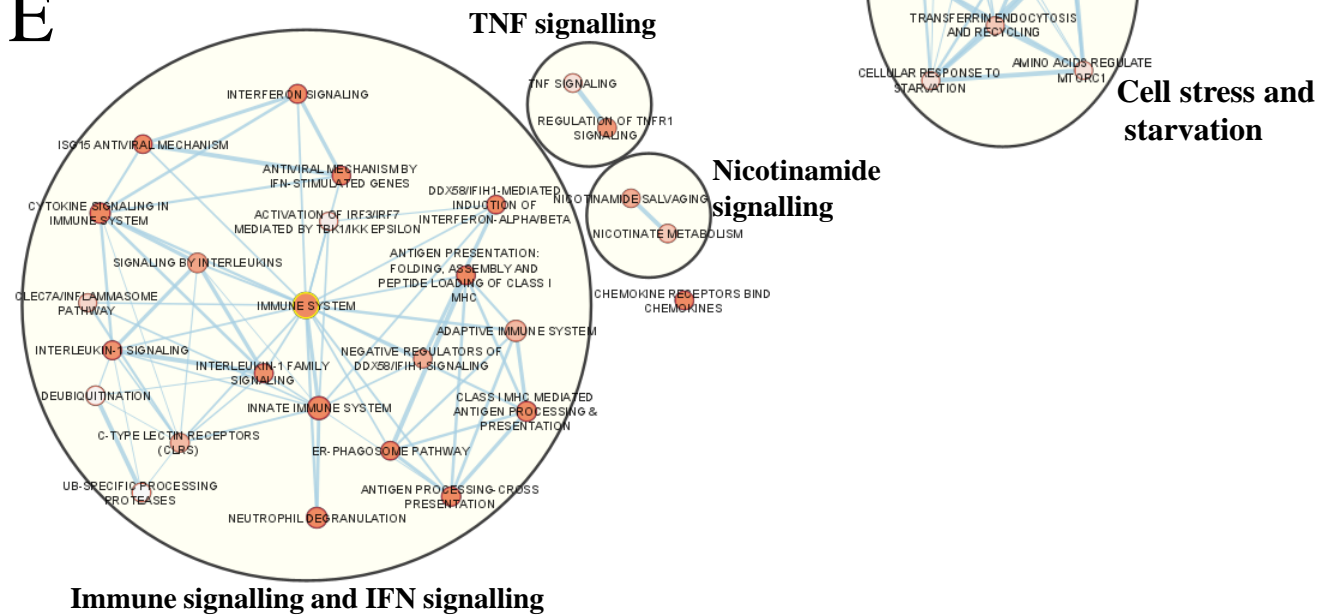
**C**



**D**



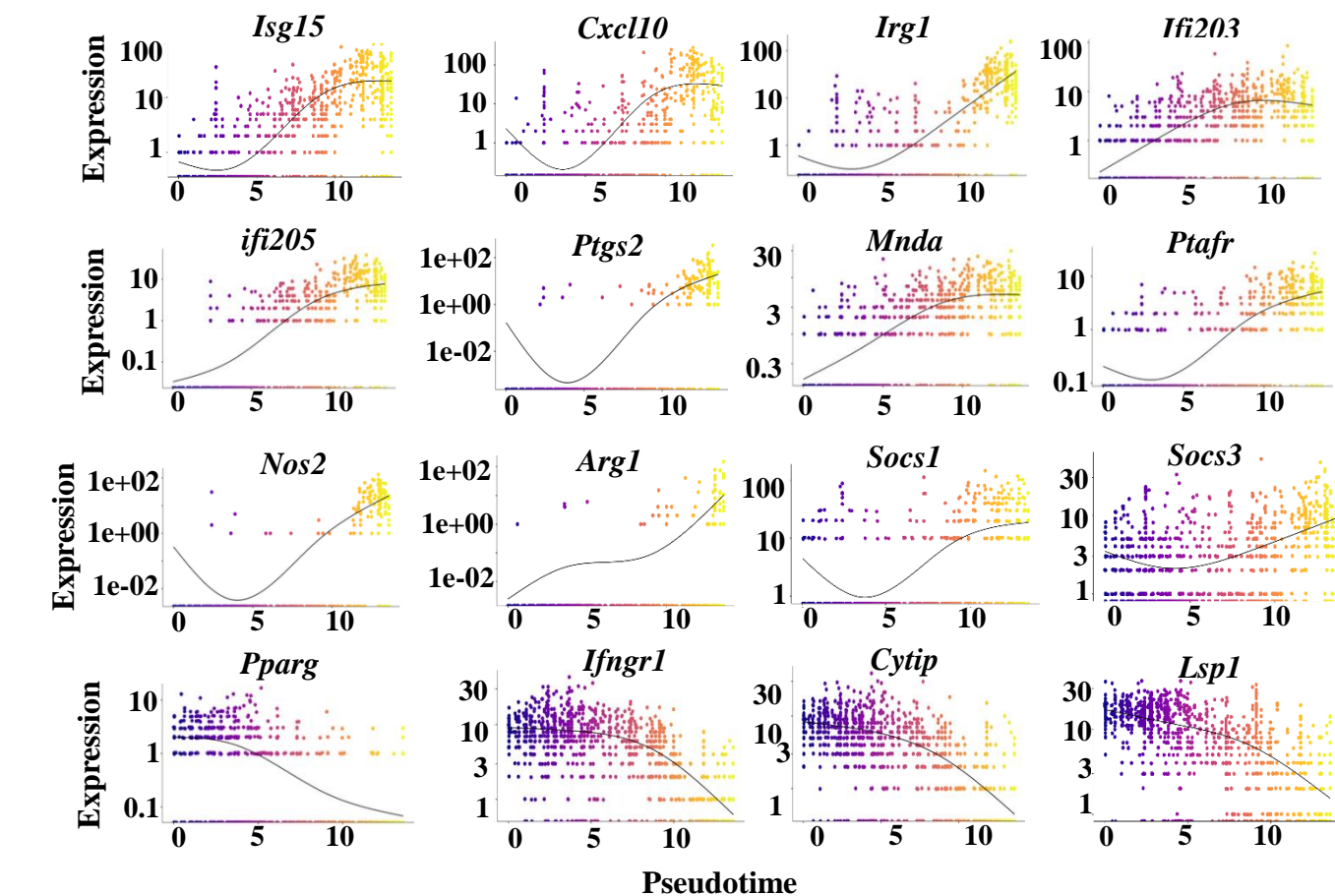
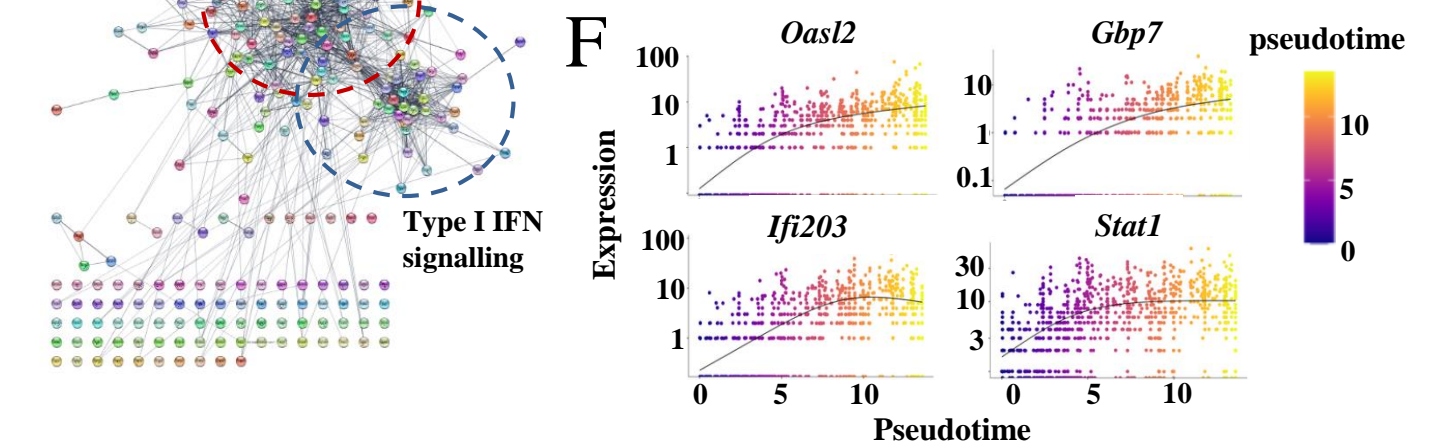
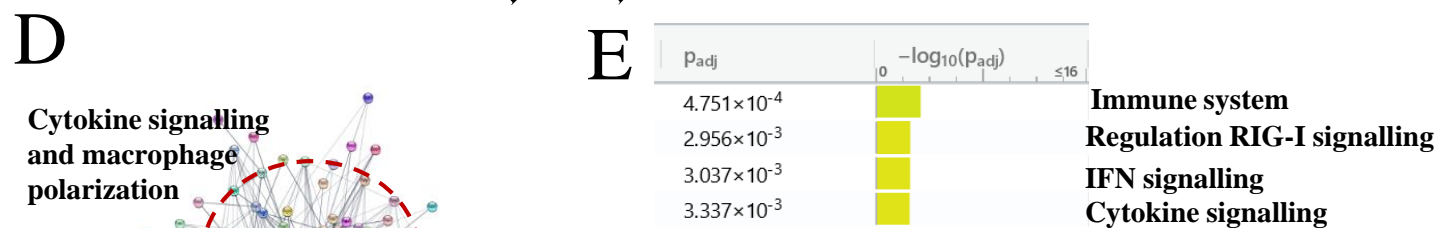
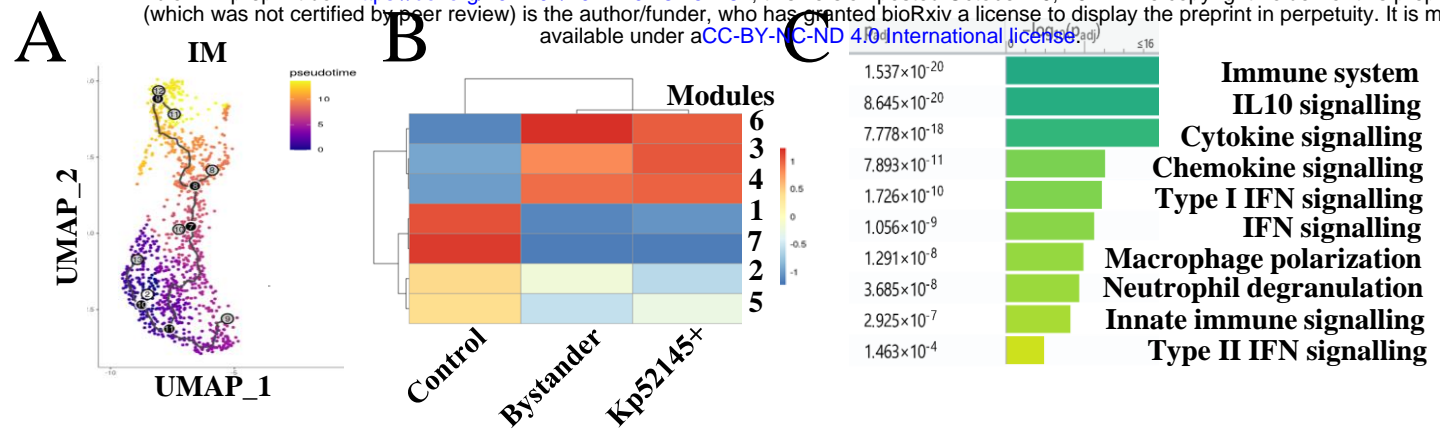
**E**

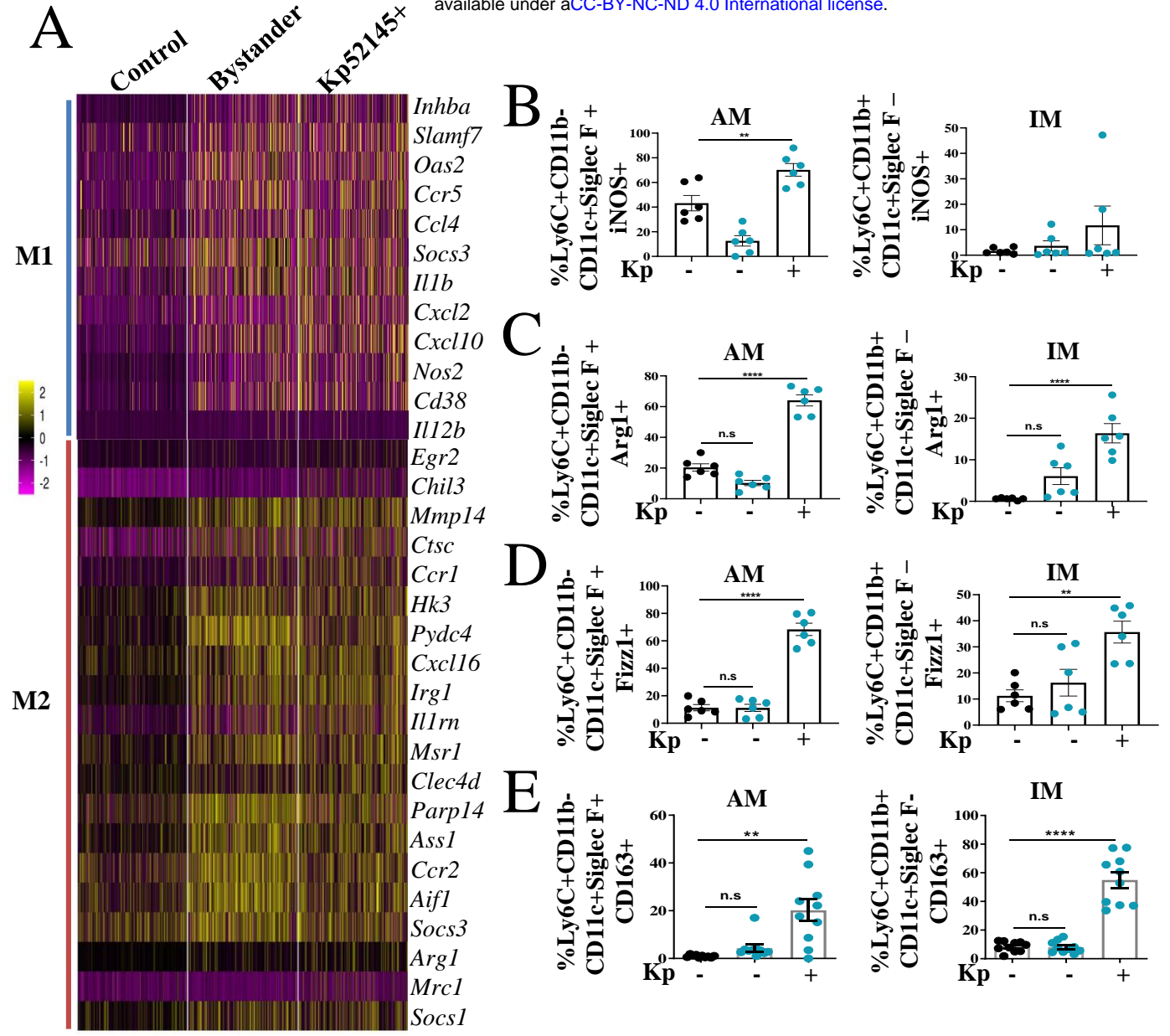


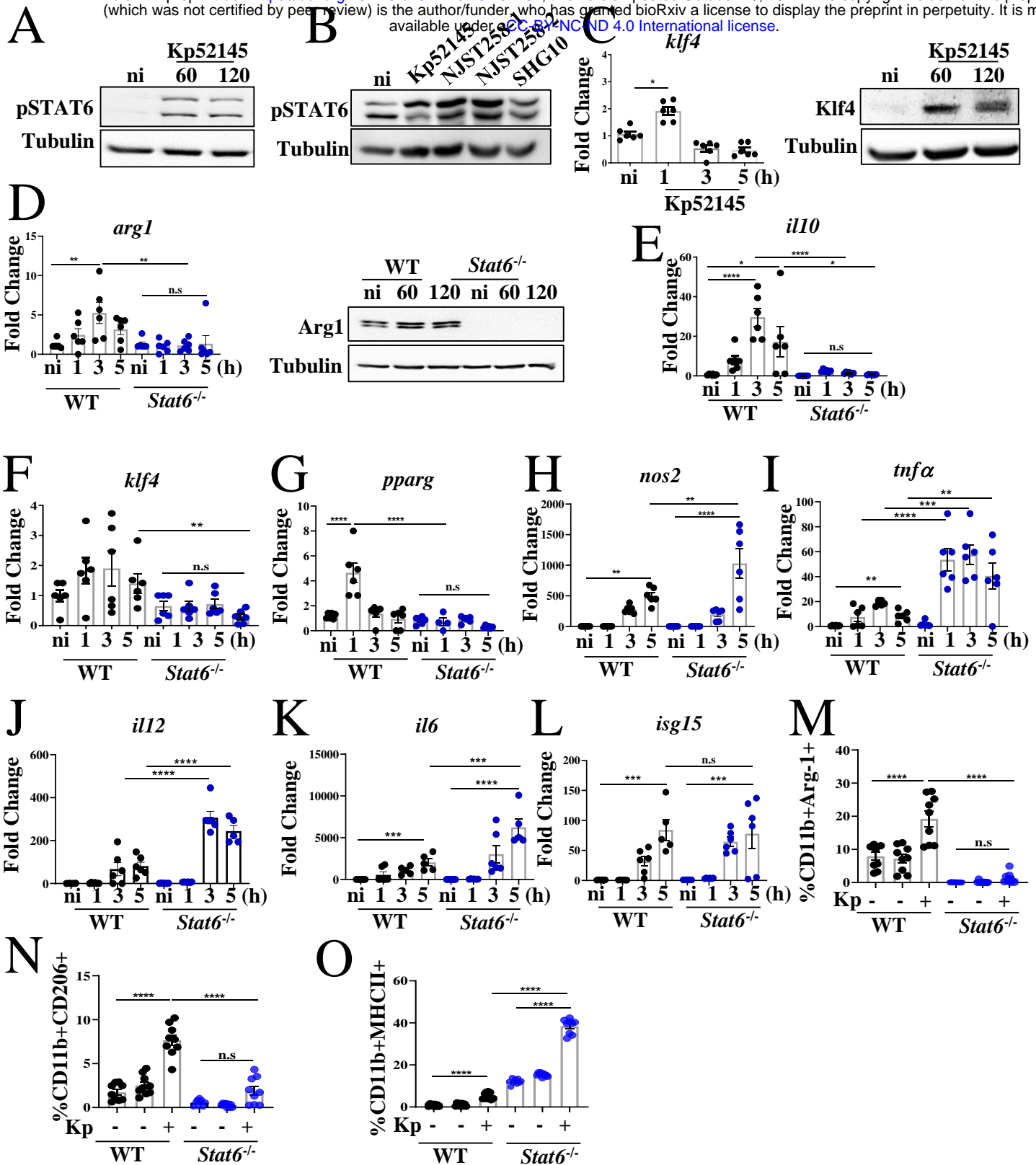
**Nicotinamide signalling**

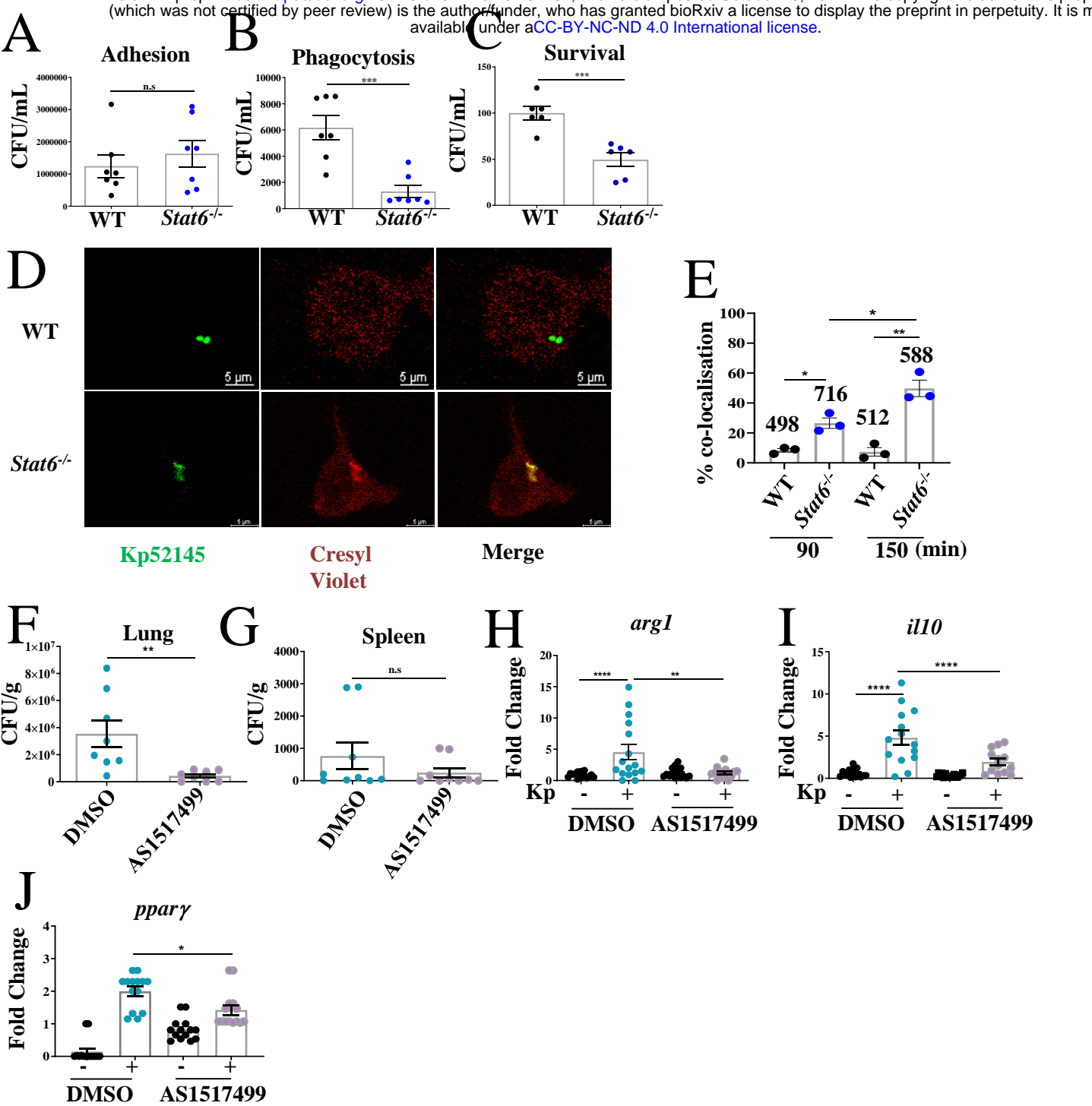
**Immune signalling and IFN signalling**

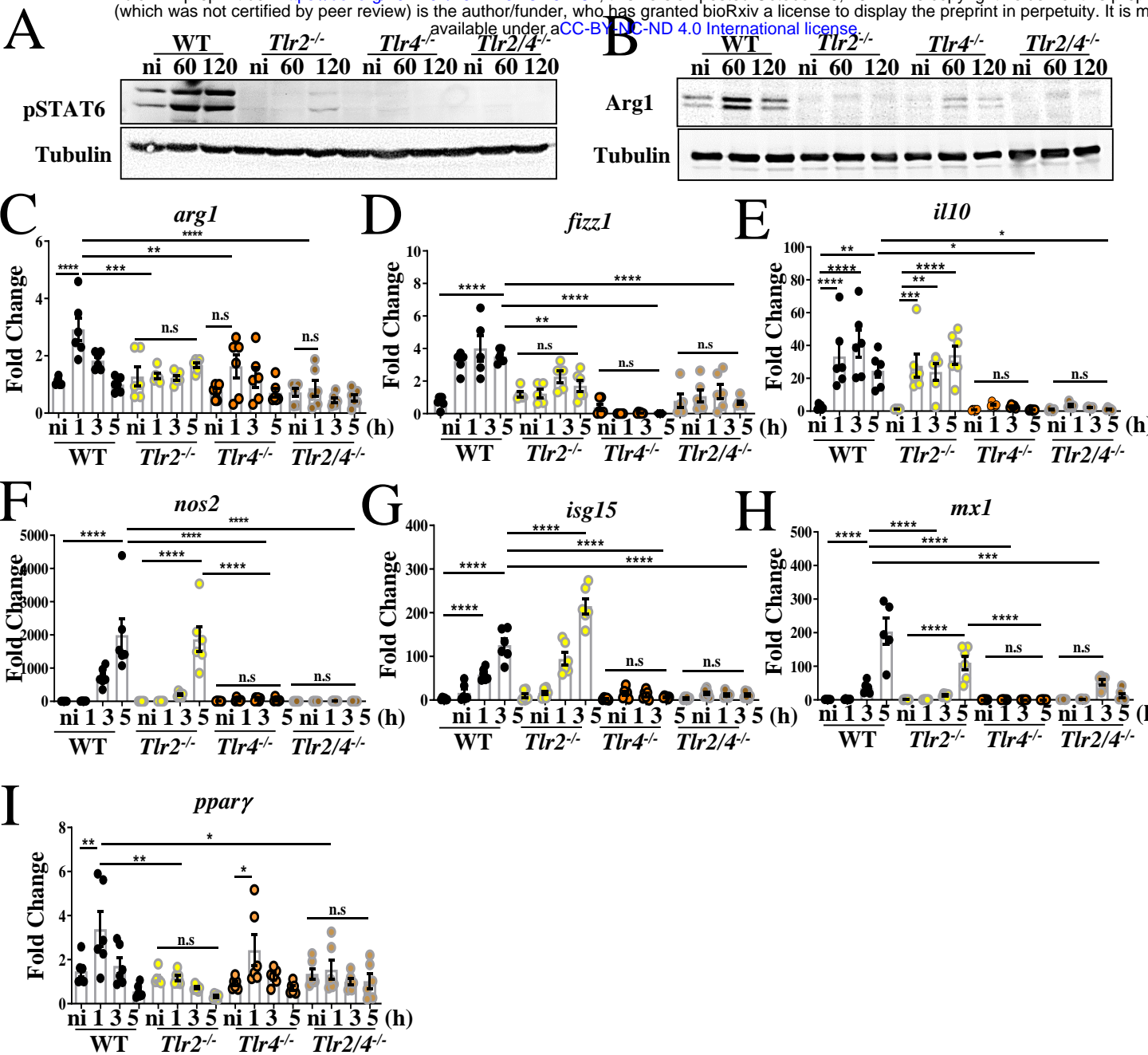


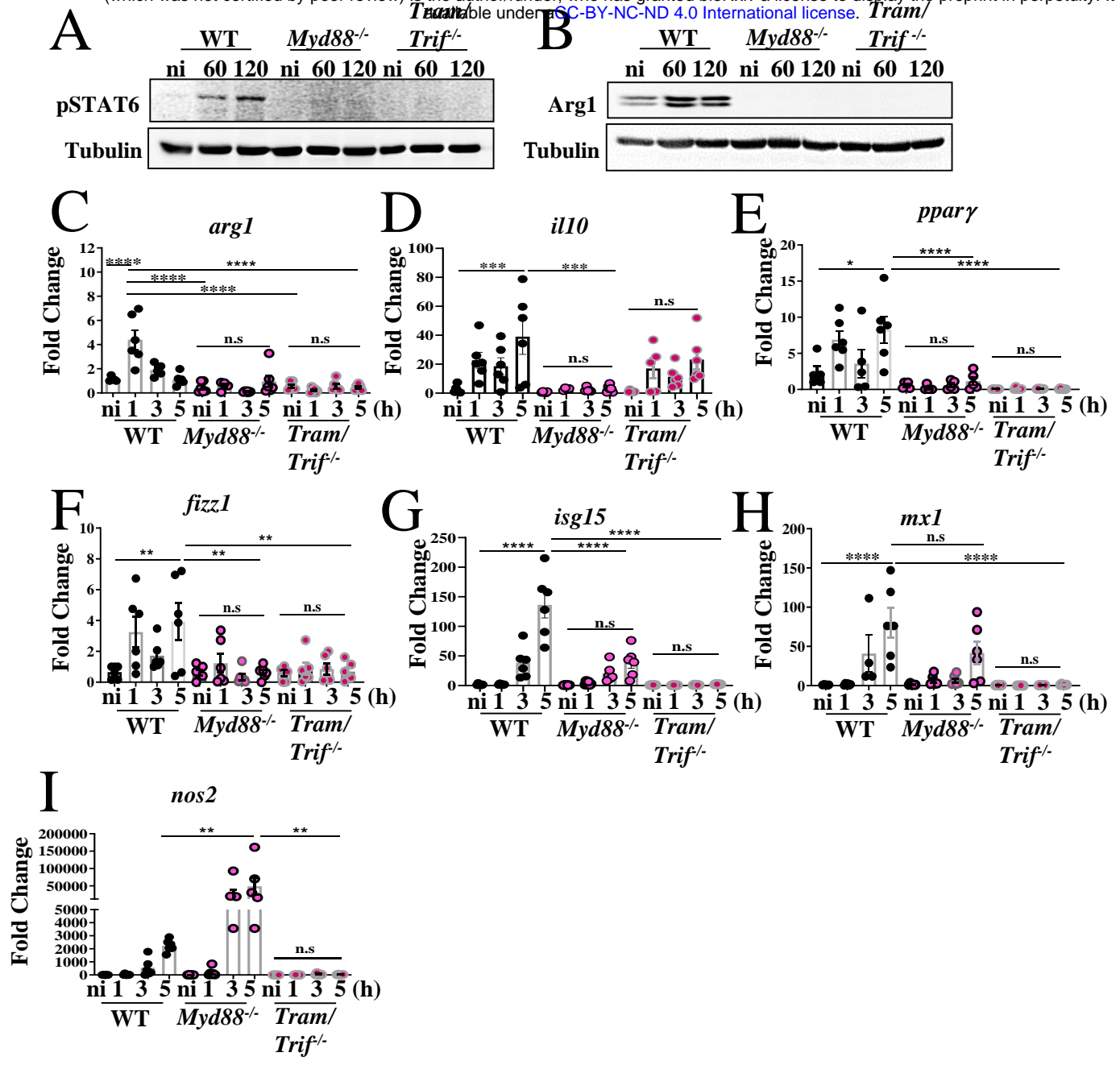




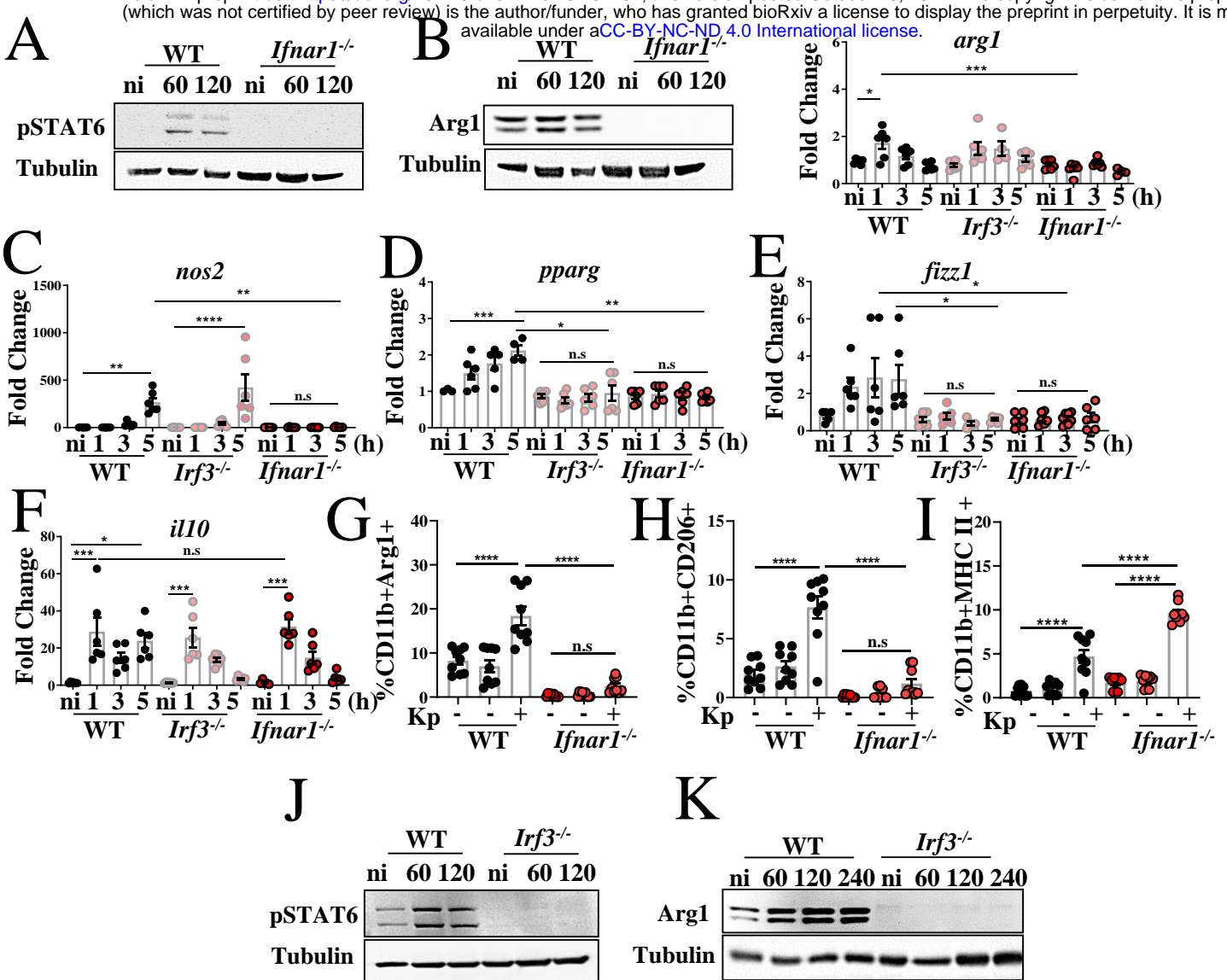




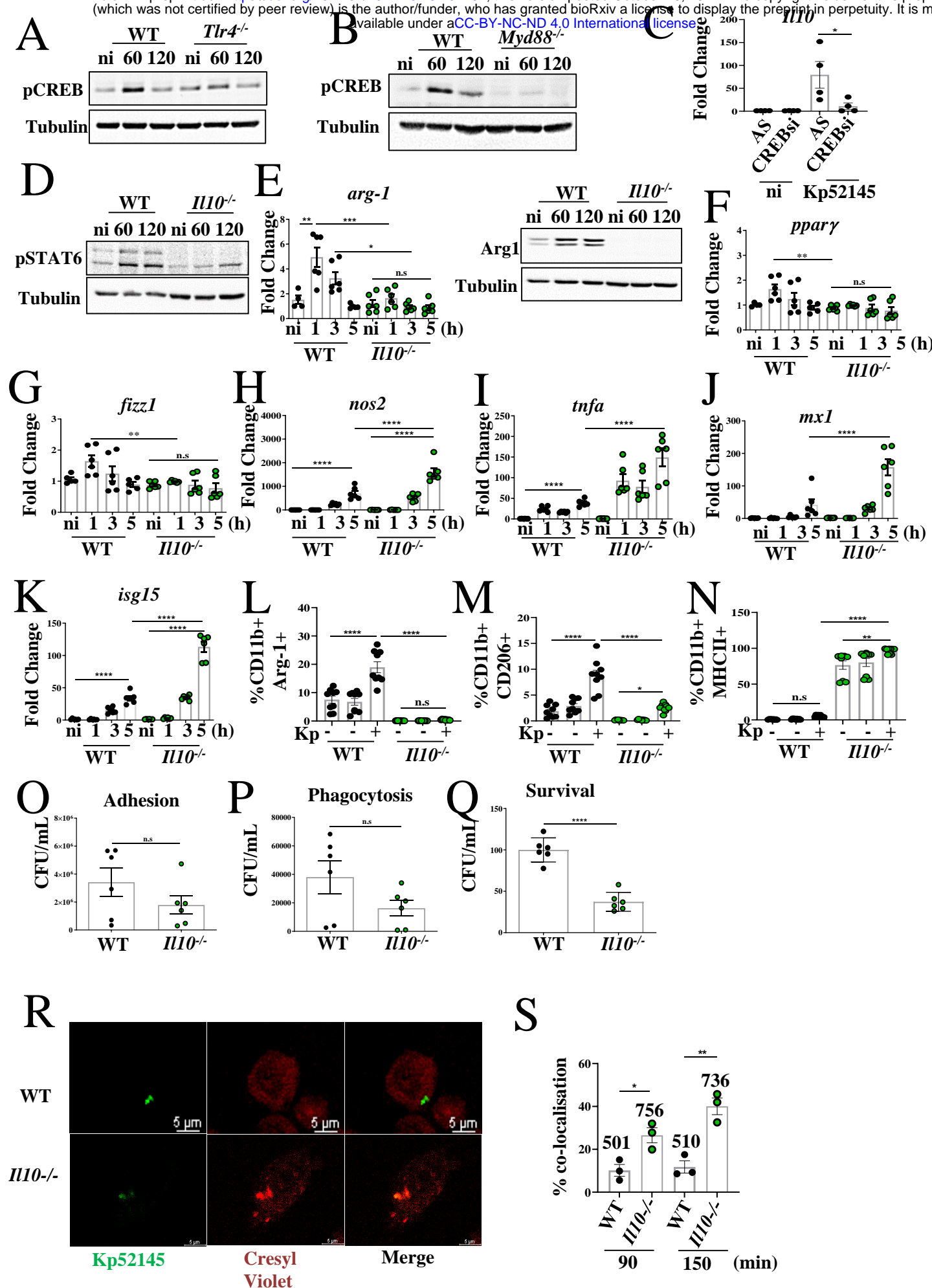




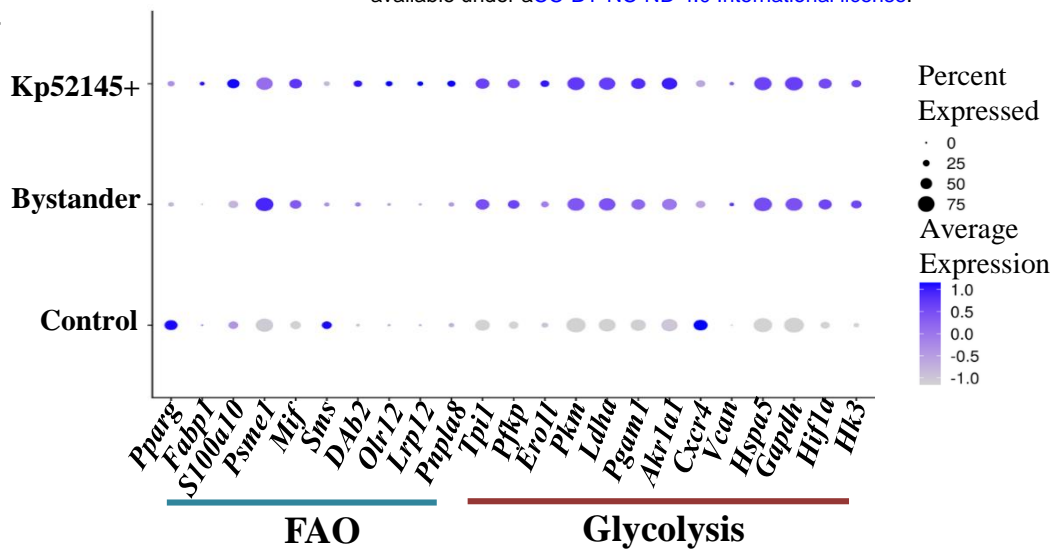




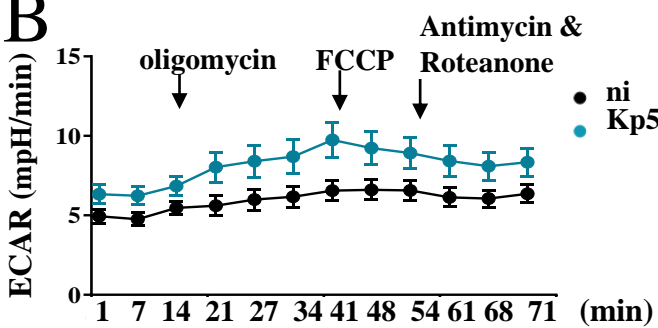




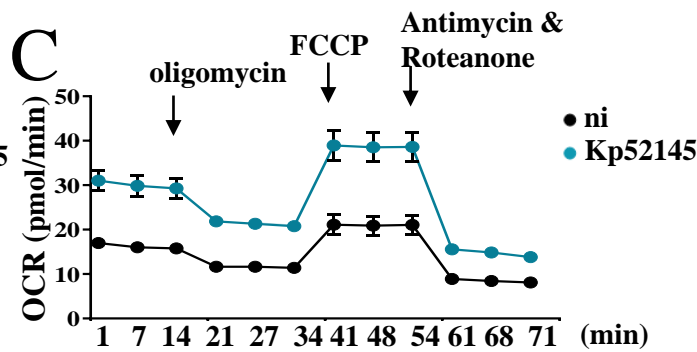
**A**



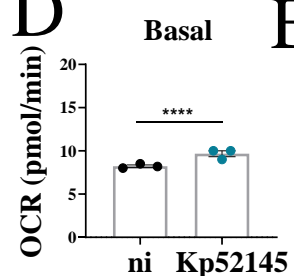
**B**



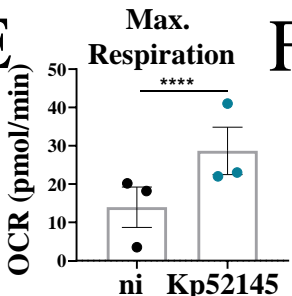
**C**



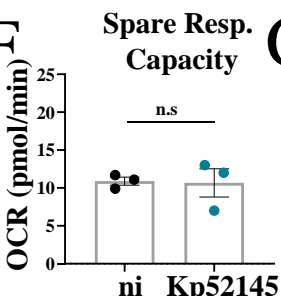
**D**



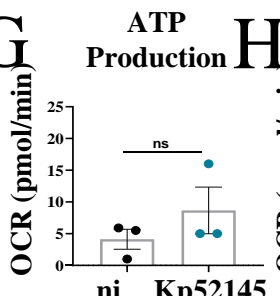
**E**



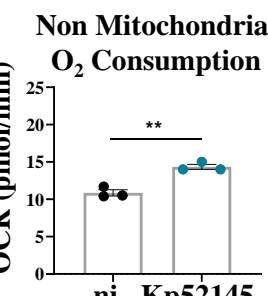
**F**



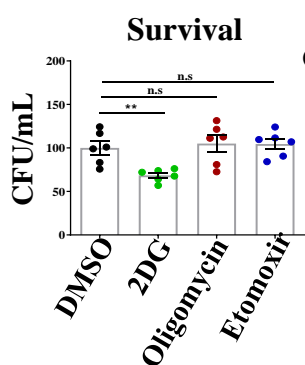
**G**



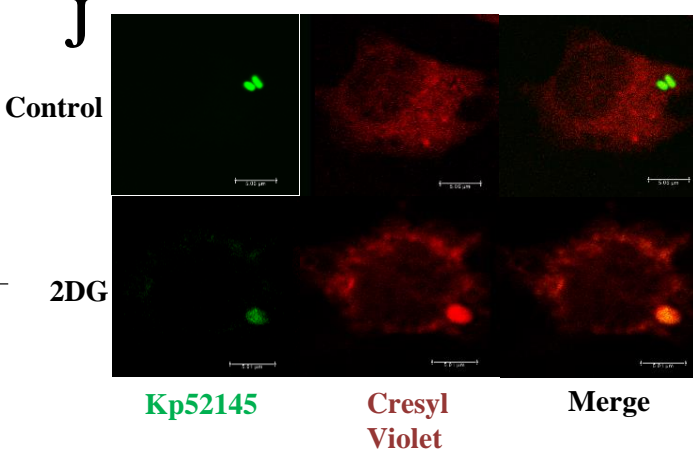
**H**



**I**



**J**



**K**

